AN AUTOMATED INSTRUMENT FOR THE QUANTITATION OF ATMOSPHERIC CARBONYLS: MEASUREMENTS AND INTERPRETATION IN SOUTHERN ONTARIO

Mauro Aiello

A thesis submitted to the Faculty of Graduate Studies in partial fulfillment of the requirements for the degree of

Doctor of Philosophy

Graduate Programme in Chemistry
York University
Toronto, Ontario

December 2003

Your file Votre référence
ISBN: 0-612-99134-2
Our file Notre référence
ISBN: 0-612-99134-2

ABSTRACT

An automated instrument for *in-situ* analysis of low molecular weight atmospheric carbonyl species has been developed. Adaptation of the DNPH silica cartridge method using an online derivatization and injection technique allowed coupling of an air sampling system to a micro-HPLC chromatographic system. Cycle times of 2 hours were obtained. Detection limits of 89 pptV, 54 pptV, 54 pptV and 39 pptV were obtained for formaldehyde, acetaldehyde, acetone, and glyoxal during field use. Detection limits for other carbonyls are estimated to be approximately 50 pptV. Experiments performed to determine the carbonyl collection efficiencies using the automated system confirmed complete recoveries of several carbonyl species.

Field measurements using a manually operated version of the technique were made as part of a field study in the summer of 1999 at an urban site in Hamilton Ontario. The technique successfully measured several important carbonyl species, showing reasonable results for many species of interest. Glyoxal concentrations during a tropospheric ozone episode, with winds from the southwest, were higher than what could be accounted for from known gas phase hydrocarbon chemistry, indicating the possibility of unknown sources.

In the summer of 2000 the automated instrument was used as part of a field study at an agricultural site in Simcoe, Ontario, located ~70 km southwest of Hamilton. Glyoxal concentrations measured were again found to be significantly above what could be accounted for by known gas phase hydrocarbon oxidation chemistry. Possible mechanisms for the formation of glyoxal have been proposed. The contribution of formaldehyde, acetaldehyde and glyoxal to the daytime $HO^{\cdot}$ radical source have been estimated to be 13.6%, 0.8% and 6.9% at midday, and somewhat enhanced during the early morning and late evening. Daytime formaldehyde sources from isoprene, methane, alkenes, acetaldehyde and alkanes are estimated as 42.5%, 23.9%, 21.6%, 11.3% and 0.6% respectively, assuming sources other than hydrocarbons and acetaldehyde to be insignificant. The alkene contribution was found to be dominated by $HO^{\cdot}$ chemistry (~ 87%), with a minor contribution from alkene reactions with ozone (~13%). Acetaldehyde sources are estimated as 19%, 64%, and 17% for the alkanes, $HO^{\cdot}$ with alkenes, and O_3 with alkenes respectively. Alkenes represent a combined contribution of 81% of the total acetaldehyde production. Acetone was found to have a major source in i-butene and 2-methyl-2-butene despite their low levels of ~20 pptV. Propane represents only ~12% of the total acetone production and is therefore a relatively small source of acetone production at this site.

Table of Contents

List of Figures

List of Tables

1. INTRODUCTION

Understanding the chemistry of the atmosphere is a challenging endeavor, which must be pursued for the well being of all living things. The fundamental understanding of atmospheric processes is investigated in two ways. It is necessary to perform laboratory investigations to obtain kinetic and mechanistic information regarding atmospheric processes. It is also important to then apply that understanding to the real atmosphere through field measurements. While laboratory investigations are often carried out under 'ideal' conditions to study the mechanisms and reaction kinetics of interest, field investigations rely on the real processes at work in the atmosphere to provide insight into atmospheric chemistry. The interpretation of these processes is complicated by the fact that in general multiple processes are occurring simultaneously in the real atmosphere. The analysis and computer based modeling of the results obtained from field studies, then, requires adequate kinetic and mechanistic knowledge, obtained through laboratory studies, for the interpretation of the results to be accurate. In turn, the field measurements are useful, as a guide to new areas of needed laboratory investigations.

It is important to understand the limitations of field investigations, and the inherent uncertainty associated with such studies. The information collected at one site may not be representative of atmospheric conditions at other locations, since the meteorology, geography and emission influences will be different for different

locations. Many field studies over various locations, times of year, and conditions are needed, so that a more complete understanding can be obtained. The development of robust and useful measurement techniques is vital to this task, so that reliable measurements can be routinely made.

1.1. Importance of Carbonyl Compounds to Tropospheric Chemistry

The importance of oxygenated hydrocarbons to the atmosphere is becoming increasingly understood (Lary and Shalcross, 2000). The relative amount of reactive carbon present in the troposphere as oxygenated species can be significant (Goldan *et al*, 1995). However since the commonly used methods for hydrocarbon analysis do not allow reliable quantification of many oxygenated compounds, the information available for many species is somewhat lacking compared to hydrocarbons, despite their importance (Goldan *et al*, 1995). Carbonyl compounds are emitted to the atmosphere by various sources, including biogenic emissions (Kesselmeier and Staudt, 1999), and various anthropogenic activities, including vehicle exhaust (Fraser *et al*, 1998; Grosjean *et. al.* 2001) and industrial emissions. More importantly however, carbonyls are the first 'stable' products formed in the oxidation of tropospheric hydrocarbons (Kotzias *et al*, in Helas *et al*, 1997). As such, carbonyl measurements, along with the measurement of their parent hydrocarbons, can yield information about the relative importance of various oxidation processes occurring in the atmosphere. Specifically, they can be used to test the current experimental

information, and determine whether unknown sources or sinks may exist which are not currently known. The overall goal then is to be able to accurately predict the important processes in the atmosphere through various models. Carbonyls also play a significant role in atmospheric chemistry through their photolysis yielding radicals, which are the main driving force behind atmospheric oxidation. Carbonyls then are central to tropospheric chemistry, since they are products of oxidation, and through their radical source, a contributor to oxidation. A good understanding of the chemistry of the atmosphere then relies on reliable carbonyl measurements, collected on reasonably fast time-scales, in various locations, and under various conditions, so that a complete picture of these processes can be had.

1.2. Atmospheric Oxidants

Oxidation in the atmosphere is initiated for the most part by three species. These are the hydroxyl radical ($HO^{\cdot}$), nitrate radical (NO_3) and ozone (O_3) (Atkinson, 1990). The major sources of these species will be briefly discussed.

1.2.1. $HO^{\cdot}$ Formation

The major source of $HO^{\cdot}$ is in general photolysis of O_3 to $O(^1D)$, followed by reaction with H_2O, as shown in the following reactions (Atkinson, 2000).

$$O_3 + h\nu\ (\lambda \leq 335\ nm) \rightarrow O(^1D) + O_2 \qquad (R1)$$

$$O(^1D) + H_2O \rightarrow \mathbf{2HO^{\cdot}} \qquad (R2)$$

$$O(^1D) + M \rightarrow O(^3P) + M \qquad (R3)$$

At the earth's surface at 298K and 50% relative humidity, only ~10% of the O_3 photolysis to yield $O(^1D)$ results in the formation of $HO^{\cdot}$, through R2, due to the competitive deactivation of $O(^1D)$ by air (M) in R3 (Atkinson, 2000). Aldehyde photolysis can also be a significant source of $HO^{\cdot}$. The following mechanism shows the major pathway for $HO^{\cdot}$ production from formaldehyde (HCHO) photolysis. This mechanism dominates in all but the most remote locations where NO concentrations are too low (Finlayson-Pitts and Pitts, 2000).

$$HCHO + h\nu\ (\lambda<370\ nm) \rightarrow HCO^{\cdot} + H^{\cdot} \qquad (R4)$$

$$H^{\cdot} + O_2 + M \rightarrow HO_2^{\cdot} + M \qquad (R5)$$

$$HCO^{\cdot} + O_2 \rightarrow HO_2^{\cdot} + CO \qquad (R6)$$

$$2HO_2^{\cdot} + 2NO \rightarrow 2\mathbf{HO^{\cdot}} + 2NO_2 \qquad (R7)$$

The net reaction is then:

$$HCHO + h\nu + 2O_2 + 2NO \rightarrow CO + 2\ \mathbf{HO^{\cdot}} + \mathbf{2\ NO_2} \qquad (R8)$$

Other somewhat less significant sources of $HO^{\cdot}$ include photolysis of HONO, and reactions of O_3 and NO_3 with alkenes, although these can be quite important at times (Finlayson-Pitts and Pitts, 2000).

1.2.2. Nitrate Radical Formation

The NO_3 radical is formed via reaction of NO_2 with O_3 to yield NO_3 and O_2. NO_3 is photolysed during the day very quickly, so that its concentration is higher at night. Levels are generally less than a few parts per trillion (ppt) in remote areas, and

several hundred ppt in urban areas at night (Finlayson-Pitts and Pitts, 2000). Although nitrate radical initiated chemistry can be significant at times, reactions of most hydrocarbons with nitrate radicals are generally less important than those with hydroxyl radicals, and ozone. Nitrate chemistry then need only be considered under certain specific conditions for specific compounds where its effects can be significant.

1.2.3. Ozone Formation

The formation of ozone in the troposphere has been a subject of much research in recent years. The known adverse health effects caused by ozone on most living things has created a need for the understanding of the processes involved in the formation of ground level ozone. The formation of ozone under tropospheric conditions proceeds by the following mechanism (Finlayson-Pitts and Pitts, 2000),

$$NO_2 + h\nu\ (\lambda < 430\ nm) \rightarrow NO + O \qquad (R9)$$

$$O + O_2 + M \rightarrow O_3 + M \qquad (R10)$$

NO can react with O_3 to regenerate NO_2,

$$O_3 + NO \rightarrow NO_2 + O_2 \qquad (R11)$$

The role of organics in the troposphere, as will be discussed in section 1.3.1, is to increase the number of NO to NO_2 conversions, and thus the total amount of O_3 at steady state.

1.3. Sources of Atmospheric Carbonyls

The sources of atmospheric carbonyls are quite varied, and are of course highly dependent on time of year and region. Sources of many carbonyls include atmospheric oxidation of hydrocarbons (Altshuller, 1993), direct emissions from biogenic sources (Kotzias *et al*, 1997; Isidorov *et al*, 1985; Kesselmeier *et al*, 1997; Kirstine *et al*, 1998), vehicle exhaust (Fraser *et al*, 1998), and other combustion sources. The following sections give an overview of some of the oxidation sources of atmospheric carbonyls, since these sources are the atmospherically interesting ones with respect to understanding processes in the atmosphere.

1.3.1. Hydrocarbon Oxidation in the Troposphere

The formation of a carbonyl in the troposphere from hydroxyl initiated oxidation of an aliphatic hydrocarbon is shown in Figure 1. Once formed in the troposphere, the carbonyl compounds can photolyse to produce radicals, or be oxidized further by radicals, to continue converting NO to NO_2, and so continue the formation of ozone, until completely oxidized, or removed by some other mechanism. This mechanism only shows the pathways which are important in a 'high NO_x' environment, defined as the NO_x level at which the above mechanism dominates over peroxy-peroxy self reactions. This is estimated to be at a NO_x level of ~10 to 50 ppt (Finlayson-Pitts and Pitts, 2000). In general, a high NO_x environment is found in all

but the most remote areas, where there is little influence from anthropogenic emissions. The work presented here will generally assume a high NO_x environment.

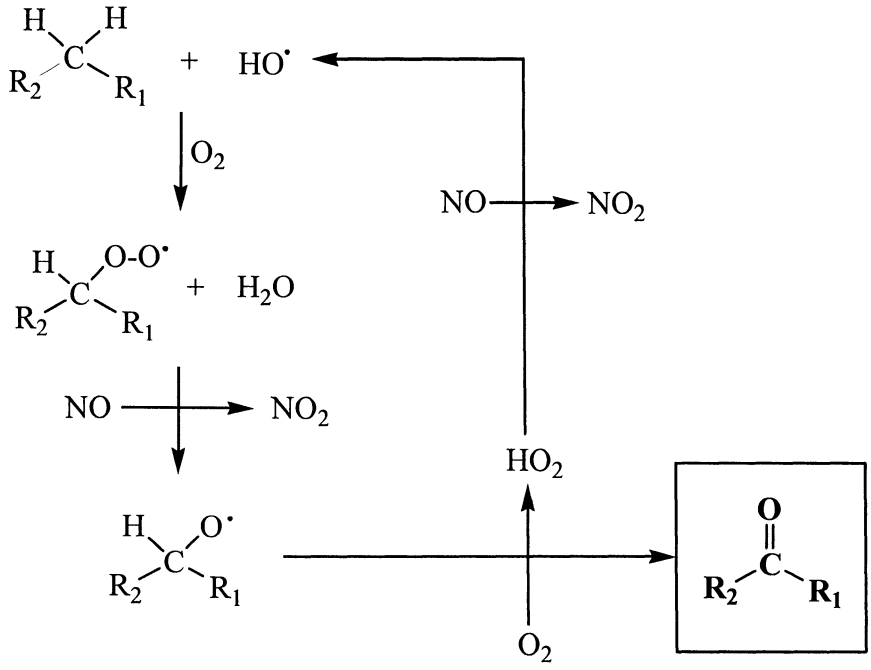

Figure 1. Hydroxyl initiated tropospheric oxidation of a hydrocarbon to produce a carbonyl.

The oxidation of alkenes in the atmosphere can occur by reactions with both hydroxyl radical, and ozone. The major pathway for the hydroxyl radical reaction is by addition to the double bond, with a minor contribution by H atom abstraction. The addition reaction is shown in Figure 2. The β-hydroxyalkylperoxy radicals formed decompose via two different channels, labeled A and B in Figure 2. The importance of each channel is dependant on the nature of the hydrocarbon, with smaller

hydrocarbons ($\leq C_4$) favouring decomposition via channel B (Atkinson, 1990). A third channel also exists, but has been omitted here, where larger hydrocarbons ($\geq C_5$) can isomerize before reaction with O_2. Reaction via channel A, proceeds by the same mechanism as the alkylperoxy radicals formed via the hydroxyl-alkane reaction

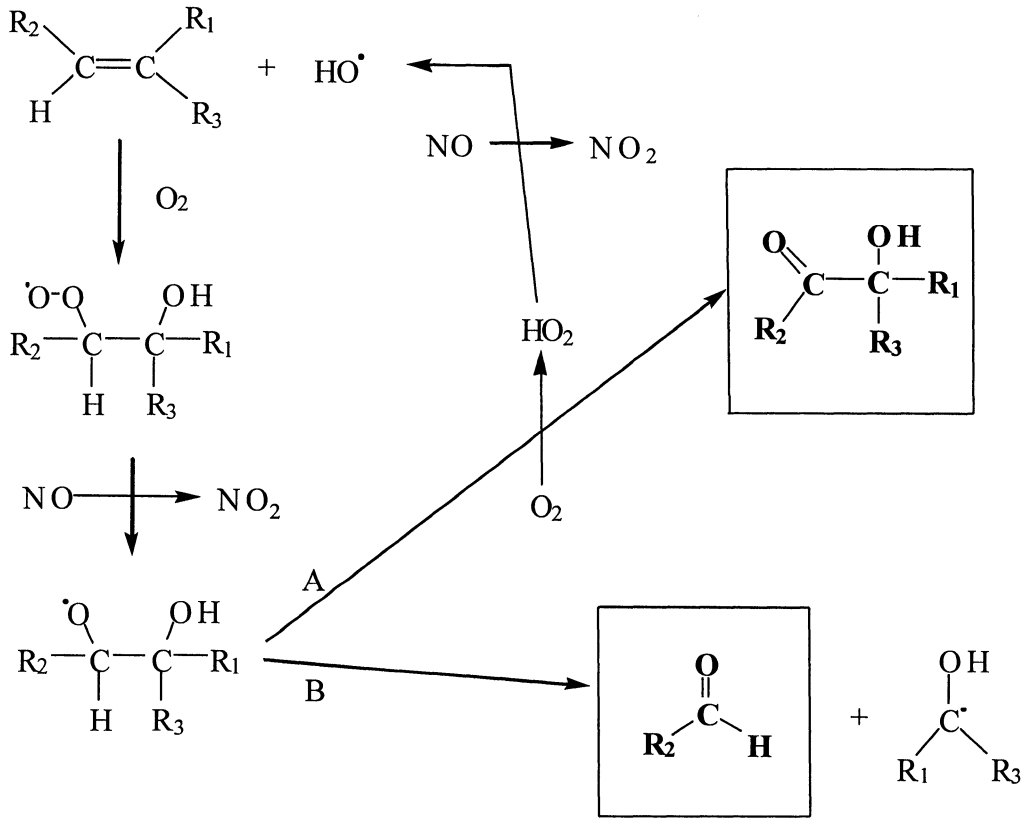

Figure 2. Hydroxyl initiated oxidation of an alkene via addition to the double bond.

shown in Figure 1. Under most conditions they will oxidize NO to NO_2, followed by H atom abstraction by O_2 to form HO_2, yielding a carbonyl product. The β-hydroxyalkylperoxy radicals can decompose via channel B to yield a carbonyl

product and a β–hydroxy-alkyl radical, which will also react with O_2 to yield a carbonyl product, as shown in Figure 3.

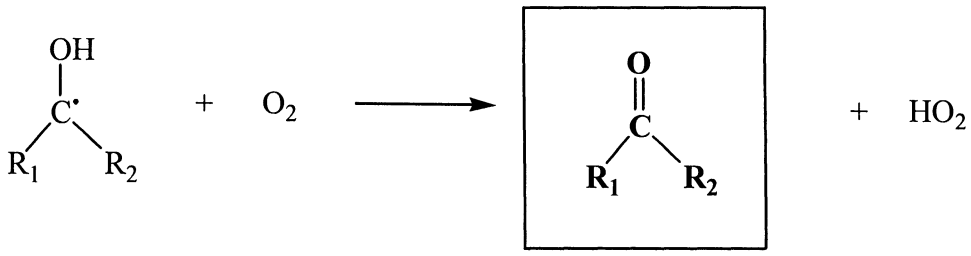

Figure 3. β–hydroxy-alkyl radical reaction with O_2 to form a carbonyl.

Ozone reaction with alkenes occurs via addition of ozone to the double bond to form an unstable molozonide, which decomposes to yield a carbonyl, and a Criegee intermediate, as shown in Figure 4. The carbonyl produced depends on the parent alkene and the substituent groups bonded to the alkene moiety. The Criegee intermediate can then decompose by various pathways to form other products, including carbonyls and hydroxyl radicals (Atkinson, 2000).

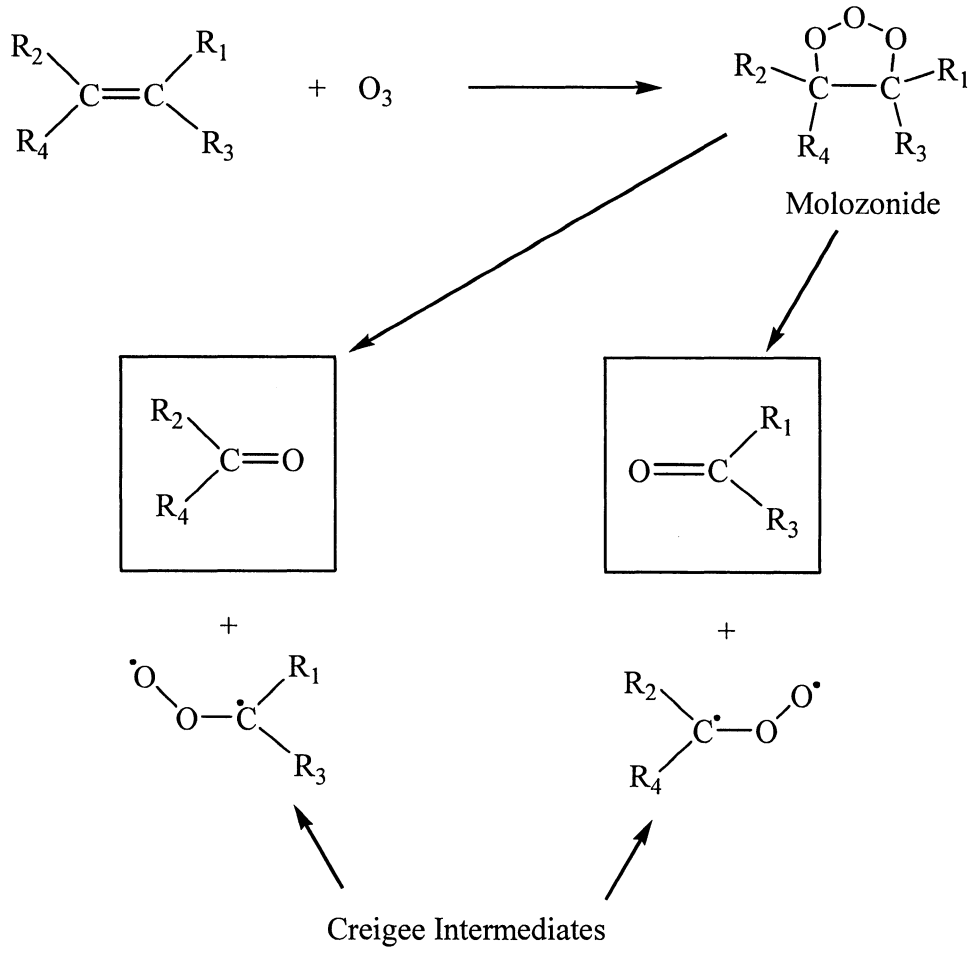

Figure 4. Ozone reaction with alkenes to form carbonyls and Criegee intermediates.

1.3.2. Aromatic Hydrocarbon Oxidation

Several aromatic hydrocarbons are present in significant quantities in gasoline vapour, and vehicle exhaust (Fraser *et al*, 1998), and therefore represent a significant emission to the atmosphere, especially in urban areas. Measurements of the oxidation

products of these compounds then, along with measurements of the precursor hydrocarbons can be useful to the understanding of the oxidation processes involved. The most significant atmospheric oxidation process for the aromatics is reaction with HO·. Reactions of aromatics with both nitrate radicals, and ozone are too slow to be significant in the atmosphere (Atkinson, 1990). The oxidation of aromatic hydrocarbons results in the formation of several product species, some of which are carbonyls (Yu *et al*, 1997). These reaction pathways remain a field of study, however several researchers have experimentally determined the product yields from the most important aromatics. These products are listed in Table 7, section 4.1.1. The reaction of HO· with an aromatic hydrocarbon can proceed either by abstraction of a hydrogen atom from the alkyl groups, if any, or by addition to the aromatic ring (Carlier *et al*, 1986). If addition to the aromatic ring occurs, then the aromatic ring will open, resulting in the formation of various ring opening products. These include the di-carbonyl products, glyoxal and methylglyoxal. If the reaction occurs at an alkyl group, then the carbonyl product formed can be predicted using the scheme shown in Figure 1. For toluene, this will result in the formation of benzaldehyde, as shown in Figure 5.

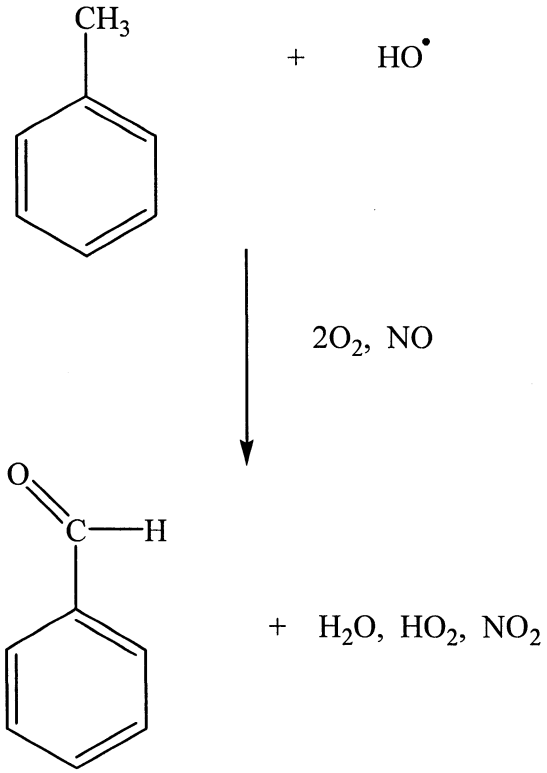

Figure 5. Formation of benzaldehyde from toluene via atmospheric hydroxyl reaction.

1.4. Atmospheric Carbonyl Removal Processes

The removal of carbonyls from the atmosphere occurs through several processes. The main gas phase removal processes for aliphatic carbonyls are photolysis and reaction with the hydroxyl radical. The reaction rates and corresponding estimated lifetimes of several species have been tabulated and are presented in Table 1.

1.4.1. Photolysis of Carbonyls

The photolysis of carbonyls is an important process since it results in the formation of radicals, which drive atmospheric chemistry. The products of the photolysis of formaldehyde are shown below.

$$HCHO + h\nu \rightarrow HCO^{\cdot} + H^{\cdot} \quad \text{(R12)}$$

$$\rightarrow CO + H_2 \quad \text{(R13)}$$

The hydrogen radical ($H^{\cdot}$) and the formyl radical ($HCO^{\cdot}$) formed can then react with O_2 to form $HO_2^{\cdot}$, which can oxidize NO to NO_2, and form $HO^{\cdot}$. The photolysis of formaldehyde to produce CO and H_2 does not produce any radicals directly, and is therefore referred to as a molecular channel. This serves as a sink for formaldehyde, but not as a source of radicals. The photolysis process happens quickly enough under tropospheric conditions to be both a significant sink for aldehydes, and a significant source of hydroxyl radicals. The rates of photolysis for ketones tend to be slower than aldehydes, and therefore less important as ketone sinks and radical sources. The photolysis rates for both the molecular and radical channels are wavelength dependant, and therefore dependant on solar zenith angle. Photolysis rates must then be evaluated for each carbonyl species for each reaction channel, as a function of time of day and location. Representative photolysis rates are given in Table 1. Some photolysis rates evaluated as a function of solar zenith angle are shown in Figure 51.

1.4.2. Hydroxyl Reactions

The removal of carbonyls from the atmosphere via reaction with $HO^{\cdot}$ occurs at reasonably fast rates, as shown in Table 1. The dominant mechanism for the reaction of aldehydes with hydroxyl radical is via abstraction of the aldehyde hydrogen, followed by addition to O_2, and reaction with NO or NO_2, (Atkinson, 2000). The oxidation of acetaldehyde is shown below:

$$CH_3CHO + HO^{\cdot} \rightarrow H_2O + CH_3C^{\cdot}O \quad \text{(R14)}$$

$$CH_3C^{\cdot}O + O_2 \rightarrow CH_3COOO \quad \text{(R15)}$$

$$CH_3COOO + NO \rightarrow CH_3COO + NO_2 \quad \text{(R16)}$$

or, CH_3COOO can react with NO_2 to form peroxyacetyl nitrate (PAN):

$$CH_3COOO + NO_2 \rightarrow CH_3COOONO_2 \quad \text{(R17)}$$

CH_3COO formed in the reaction with NO, decomposes to form a methyl radical ($CH_3^{\cdot}$) and CO_2. The methyl radical then reacts to form formaldehyde as in Figure 1. The reaction of hydroxyl radical with a ketone proceeds via reaction similar to an alkane, resulting in the formation of an RO_2 type of radical, which can then react with NO to form NO_2. The relative importance of these processes depends on several factors including NO and NO_2 levels.

	HO Rate Constant ($\times 10^{12}$) (cm^3/molecule/s)[a]	HO Lifetime (hours)	Photolysis Rate Constant ($\times 10^5$) (s^{-1})[b]	Photolysis Lifetime (hours)	Atmospheric Lifetime (hours)
Formaldehyde	9.20	6.04	6.05	4.59	2.61
Acetaldehyde	16.0	3.47	0.303	91.8	3.35
Acetone	0.220	253	0.0352	788	191
Propanal	0.200	2.78	1.30	21.4	2.46
Benzaldehyde	12.9*	4.31*			
Glyoxal	11.0	5.05	7.88	3.52	2.08
Methylglyoxal	17.2	3.23*	11.1	2.50	1.41

Table 1. Photolysis and Hydroxyl radical (HO) reaction rates, and estimated lifetimes. Hydroxyl lifetimes are based on an assumed [HO] of 5×10^6 molecules/cm^3. Photolysis rates assume a solar zenith angle of 45°. (a) Finlayson-Pitts and Pitts (2000) ; (b) Jenkin *et al*, 1997; * Atkinson, (1994).

1.5. Overview of Past Carbonyl Measurements

Atmospheric carbonyl measurements have been made in the past by several researchers in various locations, ranging from the arctic (Biesenthal *et al*, 1997) to remote tropical locations (Mackay *et al*, 1996; Heikes *et. al.*, 1992), using significantly different methods ranging from liquid chromatography (Smith *et al*, 1989) to satellite based measurements (Chance *et al*, 2000). The need for measurements continues, as the understanding of processes continues to grow, and the importance of various compounds becomes clearer. A collection of past measurements has been compiled, and is listed in Table 2. This is not intended to be an exhaustive list of all measurements made and methods used. Several different techniques are included to illustrate the wide range of methods used. Much of the

carbonyl data collected has been with 2,4 dinitrophenylhydrazine (DNPH) derivatization in one of its many variations. This is largely due to the method's convenience and ease of field operation with a minimum of equipment. Derivatization methods such as the DNPH method remain the only ones capable of quantifying a range of carbonyls *including* formaldehyde. Although DNPH is the most commonly used, other derivatizing agents exist for sensitive detection, for example Houdier *et al*, 2000, and Mopper *et al*, 1983, describe fluorescent carbonyl derivatives used to quantify carbonyls. Methods such as gas chromatography with mass selective detection (GC/MS), (Possanzini *et al*, 2000; Biesenthal *et al*, 1998), are able to quantify a range of carbonyls very well, without derivatization, but are not able to quantify formaldehyde. Use of derivatization combined with GC/MS has been used effectively by several researchers, and is a method capable of quantifying formaldehyde as well as other carbonyls (Le Lacheur *et al*, 1993; Spaulding *et al*, 1999). There also exist methods capable of quantifying formaldehyde very well such as Tunable Diode Laser (TDL), (Heikes *et al*, 1996; Gilpin *et al*, 1997) and Differential Optical Absorption Spectroscopy (DOAS), (Cardenas *et al*, 2000), but these are unable to quantify many other important atmospheric carbonyl species. Since both formaldehyde and acetaldehyde are important to atmospheric chemistry, methods capable of quantifying these two species, as well as others are advantageous, and their development and improvement remains an important field of instrument development.

Reference	Location	Environment	Time	Method	Observed Levels (ppbV)	Detection Limit(pptV)	Compound	Sampling Time	Sample Volume (L)
Anderson *et al*, 1996	Denver, CO, USA	Urban	Nov, Dec, Jan	DNPH, Silica HPLC-UV	3.9		formaldehyde		
					1.6		acetaldehyde		
			Mar, Apr, May		2.3		formaldehyde		
					1.0		acetaldehyde		
			Jun, Jul, Aug		2.7		formaldehyde		
					1.4		acetaldehyde		
Apel, E.C. *et al*, 1998	Nashville, USA.	Rural-forest	June-July	DNPH, Silica	1-32	100	formaldehyde	3 hours	180
				HPLC-UV	0.2-6.5		acetaldehyde		
					1-16		acetone		
					dl-0.5		propanal		
				DNPH, C18		<400	C1 to C3	3 hours	144
				HPLC-UV					
Chance *et al*, 2000	Southeastern USA		July	Satellite	4-6	~400	formaldehyde	NA	NA
Christensen *et al*, 2000	Denmark	Semi-Rural	May, Jun, Jul	DNPH, Silica	1.2	200	formaldehyde	4 hour, 12 hour	240, 720
				HPLC-UV	0.8	100	acetaldehyde		
					1.9	100	acetone		
Fried *et al*, 1997	Boulder Colorado	Mountain	Aug-Sept	TDLAS	~1.2		formaldehyde		
Goldan *et al*, 1995	Southeastern USA	Rural	Jun, Jul	Cryogenic trapping, GC-FID	1.3	NR	acetaldehyde	9 min	0.9
					4.2	NR	acetone		
Goldstein and Schade, 2000	California, USA	Rural	Jul-Oct	Cryogenic Sampling GC-FID	1-8	NR	acetone	20 min	0.4
Grosjean, D., 1982	Los Angeles, USA	Urban	Sept-Oct	Microimpingers, DNPH	8-48	2000	formaldehyde	1 hour	60
				HPLC-UV	3-38		acetaldehyde		
					0-14		propanal		
					0-1		benzaldhyde		
Grosjean, E. *et al*, 1996b	Southern California, USA	Urban	Sept	DNPH, C18	5.3	480	formaldehyde	4 hours	~180
				HPLC-UV	4	710	acetaldehyde		
					1.6	320	acetone		
					0.79	130	propanal		
					0.22	70	benzaldhyde		
					0.78	30	glyoxal		
					1.04	60	methylglyoxal		

Table 2. Overview of past carbonyl measurements and methods used.

Reference	Location	Environment	Time	Method	Observed Levels (ppbV)	Detection Limit (pptV)	Compound	Sampling Time	Sample Volume (L)
Heikes, B. *et al*, 1996	Mauna Loa Observatory, Hawaii	Remote	4 times during year	TDL	~0.2	25	formaldehyde	30 min	NA
				Coil collection, immobilized enzyme-fluorescence		80	formaldehyde	30-45 min	NA
				Aqueous coil scrubber, DNPH derivatization, HPLC-UV		10	formaldehyde	10 min	20
				DNPH, Florisil Cartridge		50	formaldehyde	5 to 9 hours	150 to 270
				Coil collection, enzyme-fluorescence		90	formaldehyde	15 min	NA
Kesselmeier, J. *et al*, 2000	Balbina, Amizonia	Remote forest	March-April	DNPH, C18	0.5-3	NR	formaldehyde	1-2 hours	~30-80
				HPLC-UV	0-1	NR	acetaldehyde		
Kleindienst, T.E. *et al*, 1998	Laboratory Experiments			DNPH, Silica		~130	formaldehyde	3 hours	180
				DNPH, C18		~170	formaldehyde	3 hours	180
Lee, Y. *et al*, 1995	Southeastern USA	Rural-forest	July-Aug	DNPH, C18	0.66	NR	acetaldehyde	1 hour	42
				HPLC-UV	1.8	NR	acetone		
				Aqueous coil scrubber, DNPH derivatization	3.4	15	formaldehyde	7 min	17
				HPLC-UV	0.06	10	glyoxal		
					0.06	5	methylglyoxal		
Lee, Y. *et al*, 1996	Nova Scotia, Canada	Aircraft	Aug	Aqueous coil scrubber, DNPH derivatization	0.7-5	15	formaldehyde		
				HPLC-UV	0.14	15	glyoxal		
					0.23	15	methylglyoxal		
Lee, Y. *et al*, 1998	Middle Tennessee, USA	Aircraft	June-July	Aqueous coil scrubber, DNPH derivatization	3.9		formaldehyde	5 min	10
				HPLC-UV	0.1		glyoxal		
					0.23		methylglyoxal		
Leibrock and Slemr, 1997	Garmisch-Partenkirchen, Germany	Rural	Jul, Aug	Cryogenic Sampling	0.8	~25	acetaldehyde	~5 min	1
				2D-GC, FID, MS	1.7	~25	acetone		
Lowe, D. C. *et al*, 1983	Julich, Germany	Continental - nonurban	Jan-Feb	Rotating Glass Ring Packed Sampler, DNPH	0.3	10	formaldehyde	1 hour	2000
	West Coast of Ireland	Coastal	April	HPLC-UV	0.25	10	formaldehyde		
	Atlantic Ocean	Ocean Cruise	Oct-Nov		0.23	10	formaldehyde		

Table 2 continued.

Reference	Location	Environment	Time	Method	Observed Levels (ppbV)	Detection Limit (pptV)	Compound	Sampling Time	Sample Volume (L)
Mackay *et al*, 1996	Mauna Loa Observatory, Hawaii	Remote	Oct, Jan-Feb	TDL	~0.2	25	formaldehyde	30 min	
Neitzert, V *et al*, 1981	Mainz, Germany		July-Oct	Cryogenic trapping, DNPH derivatization	0.7-5.1	125	formaldehyde	70-90 min	~70-90
	Deuselbach, Germany	Rural mountains	Nov	GC-ECD	0.4-3.8	125	formaldehyde		
	Cape Point, South Africa		Dec		0.2-1.0	125	formaldehyde		
Nondek, L. *et al*,1992	Niwot Ridge, USA.	rural-forest	June	DNSH, Direct injection	0.4-1.2	100	formaldehyde	1.5 hours	1
				HPLC-fluoresence	0.3-0.7	100	acetaldehyde		
Possanzini *et al*,1996	Rome, Italy.	urban	June-July	DNPH, Silica	17	NR	formaldehyde	1 hour	60
				HPLC-UV	9.3	NR	acetaldehyde		
					1.8	NR	acetone		
					6.8	NR	propanal		
					0.7	NR	Benzaldehyde		
	Rome, Italy.	urban	Jan-Mar	DNPH, Silica	11.2	NR	formaldehyde	1 hour	60
				HPLC-UV	4.6	NR	acetaldehyde		
					0.9	NR	acetone		
					4.4	NR	propanal		
					0.5	NR	Benzaldehyde		
Possanzini *et al*,2000	Montelibretti, Italy	sub-urban	June	Carbon trap/DNPH-Silica	4.2	125	formaldehyde	8 hours	160
				GC-MS/HPLC-UV	2.7	125	acetaldehyde		
					2.4	125	acetone		
					0.11	125	propanal		
	Burriana, Spain	Orange orchard	June	Carbon trap and DNPH-Silica train	4.5	1000	formaldehyde	2 hours	20
				GC-MS/HPLC-UV	4.2	23	acetaldehyde		
					4.6	17	acetone		
					<MDL	25	propanal		
Shepson, P.B. *et al*, 1991	Central Ontario, Canada	Rural	July-August	DNPH, Silica	1.7	150	formaldehyde	3 hours	540
				HPLC-UV	0.5	100	acetaldehyde		
					1.7	NR	acetone		
Singh *et al*, 1995	Aircraft-Pacific Ocean	Remote	Feb, Mar	GC-Reduction Gas Detector	0.4	10	acetone	Real time	0.175
Slemr, J. *et al*, 1996	Southern Germany	Rural	Sept	DNPH, Silica	1	250	formaldehyde	1 hour	NR
				HPLC-UV	0.7		acetaldehyde		
					2.6		acetone		

Table 2 continued.

Reference	Location	Environment	Time	Method	Observed Levels (ppbV)	Detection Limit (pptV)	Compound	Sampling Time	Sample Volume (L)
Smith *et al*, 1989	Laboratory Experiments			DNPH, Impingers HPLC-UV		1000	C1 to C4 carbonyls	NR	
Solberg, S. *et al*, 2001	Europe	Rural	All Year	DNPH, Silica, HPLC-UV	0.3-3	NR	formaldehyde	8 hours	750
Swarin, S. *et al*, 1983	Vehicle Exhaust Experiments			Impingers-fluoresecent azine derivatizing agent HPLC, fluorescence		6000 4500 600 150	formaldehyde acetaldehyde acrolien benzaldehyde	20 min	20
Tanner and Meng, 1984	Northeastern USA	Coastal	1 year	DNPH, Impingers HPLC-UV	7.5 2.9	1000 1000	formaldehyde acetaldehyde	1 hour	30
Viskari *et al*, 2000	Eastern Finland	Highway	May, Jul, Jan	DNPH, Silica HPLC-UV	1-30	200 800	formaldehyde acetaldehyde	~12 hours	~100

Table 2 continued.

1.6. Project Overview

The task of quantifying carbonyl compounds in air can be a challenging one. At typical ambient gas phase concentrations of low ppbV or less, it is necessary to perform some type of sample preconcentration if one is to use a chromatographic technique. The carbonyls from a large volume of air must be collected and trapped in a small volume so that traditional analytical detectors can reliably quantify their concentrations. Once collected, the carbonyls must be separated from each other so that they may be quantified individually. Generally this is done using some type of chromatographic technique. The methods used for sample preconcentration and separation are closely linked, and must therefore be compatible with each other and the detection method.

Some carbonyls can be fairly unstable, and can decompose upon heating. Problem compounds include the dicarbonyls glyoxal and methyl-glyoxal, which decompose to formaldehyde and acetaldehyde respectively (Saito *et al*, 1984; Steacie *et al*, 1935). Thus, any method involving cryogenic trapping followed by thermal desorption can create negative artifacts for glyoxal and methyl glyoxal, while creating positive artifacts for both formaldehyde and acetaldehyde. By converting the carbonyl analytes to stable derivatives and using a solvent extraction procedure to prepare the analytes for analysis, these thermal instability problems can be overcome.

One of the main goals for this project was to develop an automated system to collect atmospheric carbonyl samples *in situ* with a reasonable cycle time, for various

carbonyls, including formaldehyde, with reasonable detection limits. The method used to achieve these goals was based on the widely used DNPH coated packed cartridge method, with separation and detection by micro-HPLC with UV absorbance detection (described in section 2.1). The DNPH method is appropriate for the quantification of carbonyls since it allows the collection of large integrated sample volumes with the formation of stable carbonyl derivatives (2,4-dinitrophenylhydrazones), with significant UV absorbance. While the DNPH method is generally robust, and a reasonably 'universal' method for carbonyls, it suffers certain shortcomings. These sometimes include poor detection limits for several important species, which are limited by high and variable blank values, poor temporal resolution, and manual sample preparation. Also, the separation of several important carbonyls can be difficult using HPLC separation.

The other goal in this project was to use the instrument to collect carbonyl samples in the field, and investigate the possible sources and sinks of measured species. This was achieved by making measurements during field studies using the automated instrument once developed. Several carbonyl species remain poorly characterized and measurements in various locations and under differing conditions are needed to determine their relative role in the overall atmospheric process. Care must be taken in general not to underestimate the importance of species that are not routinely measured, or to assume that model calculations can be used to simply estimate levels of species which have been difficult to measure.

1.6.1. Improvements in Separations

The separation of several atmospherically important carbonyl derivatives has been somewhat difficult using high performance liquid chromatography (HPLC). Improvements in recent years in liquid phase separations have been in the direction of miniaturization. In HPLC this has been through the use of smaller column particle sizes, giving significant improvements in separation power, although the minimum practical size for particles is limited by the requirement for increased pressures to achieve the required flow rates. The development of liquid phase separation methods such as capillary electrophoresis (CE) and capillary electro-chromatography (CEC) has greatly improved the achievable liquid phase separation power. These small volume techniques however require miniaturized injection and detection methods (Yang, 1981), which have not been developed to the same extent as the separation methods themselves. Adaptation of conventional derivatization techniques to these newer, more powerful separation methods, requires significant development work to achieve improvements in both separation and detection limits. Development of an automated instrument based on a small volume method such as micro-HPLC is simply the first step toward the goal of developing an automated CE or CEC system for automated carbonyl analysis using DNPH, or any other derivatizing agent.

1.6.2. The DNPH Method

The usefulness of DNPH derivatization for the purpose of improved UV absorbance detection of carbonyls has been known for some time (e.g. Carey *et al*, 1972). The evolution of the DNPH method has been relatively slow over the last several years. The method began its history as a liquid extraction method, where sample air was bubbled through a solution of acidified DNPH in acetonitrile (Papa and Turner, 1972a; Papa and Turner, 1972b; Kuwata et al, 1979), using an impinger. Detection of the hydrazones as the 2,4-dinitrophenylhydrazonate anion is also possible in alkaline solution, (for example Dasgupta *et al*, 1994), although much less common. The carbonyls in the air would react with DNPH, forming hydrazone derivatives, which would then remain in solution. Although simple, this method proved to be quite useful for atmospheric applications, where little or no information had previously been available. The method however lacked convenience, required significant manual operation, and required large sample volumes, typically hundreds of liters of air (for example Lowe *et. al.*, 1981). The detection limits were often poor for atmospheric work, since contamination of the DNPH solutions is inevitable over time, and in the exposure before and after sampling.

A significant improvement in the method was made with the use of packed cartridges as a sampling medium. The packed cartridges are coated with an acidified DNPH solution and allowed to dry, leaving behind a DNPH coating on the particles (Tejada, 1986). The cartridges could then be packaged and sent to field sites of

interest, where samples could be taken by pulling air through them using a pump. Typically mass flow controllers are used to regulate the flow rate and allow the volume of air to be quantified. Various packing materials have been used including silica gel (Tejada, 1986), glass beads (Grosjean and Fung, 1982), octadecylsilane (C_{18}) bonded silica gel (Kuntz *et al*, 1980), and Florisil (Lipari and Swarin, 1985). The two most popular ones remain silica, and C_{18} silanized silica. Silica is a hydrophilic medium, while C_{18} is hydrophobic, however these materials do not differ significantly in their effectiveness for the DNPH method. The cartridges have been commercially available for some time as a polymeric cartridge, with the media of choice contained within. The use of the cartridges over impingers allowed greater portability and convenience. The problem of contamination before and after sampling however remains a problem (Slemr *et al*, 1996). Also, large sampling volumes (and long times) are required to overcome the poor detection limits often achieved using this method.

The concentration detection limits (C_{dl}), are in general defined as 3 times the standard deviation of the blank concentration level (σ_{bl}).

$$C_{dl} = 3\sigma_{bl} \qquad \text{Equation 1}$$

These detection limits are often determined using multiple cartridges, which are treated as samples in every way with the exception of sampling. This is a reasonable blank determination, but usually leads to highly variable blank values, and in turn high detection limits. There are several possibilities for the high variability in blank

determinations. The first possibility is the significant manual handling required for loading, sampling, extraction and injection. Exposure to laboratory air, which can be highly polluted with carbonyls, during the extraction and injection is most likely the cause of this variability, with conditions being somewhat different for each blank cartridge extraction, and also different for each sample. The second reason is simply the use of multiple cartridges. Since many cartridges are used, the possibility of differences between cartridges increases. The level of contamination may be different between cartridges, since the packing material will be slightly different, and may have slightly different histories. Also, since the amount of time an individual cartridge spends between loading, sampling, and analysis must be significantly different, this will create differences in the way individual cartridges have been treated. Third, the polymeric casing used in the commercially available cartridges creates the possibility for external contamination via diffusion through the case, or possibly from the case material itself. Lastly, it has been determined that the packing material itself can be contaminated with carbonyls, making the often long cycle time for cartridges worrisome (e.g. Arlander *et al*, 1995a and 1995b, where cartridges were coated nearly 7 weeks before analysis).

The development of the methodology used in this project had these problems in mind at each stage of the design. The concept of design, was to eliminate as many possible differences between individual samples, and individual blanks. At the same time, elimination of the manual extraction procedure would be necessary. Also,

ideally the cartridge casing would be made of a non-porous material such as stainless steel or fused silica, and a single cartridge would be used for all samples. The use of a single cartridge essentially required *in situ* operation of the instrument, and so the obvious solution would be to automate the instrument. The determination of blanks as part of the overall sampling scheme, using the same cartridge continuously creates the desired result. That is, complete elimination of the extraction step, samples analysed immediately after sampling, blanks determined using the same cartridge as that used for sampling, which results in the most significant advantage of all, the determination of well defined blank values, with a low variability.

2. EXPERIMENTAL

2.1. Measurement Technique

Carbonyls are known to react universally with DNPH to form hydrazone derivatives. The reaction between a general carbonyl and DNPH is shown below in Figure 6:

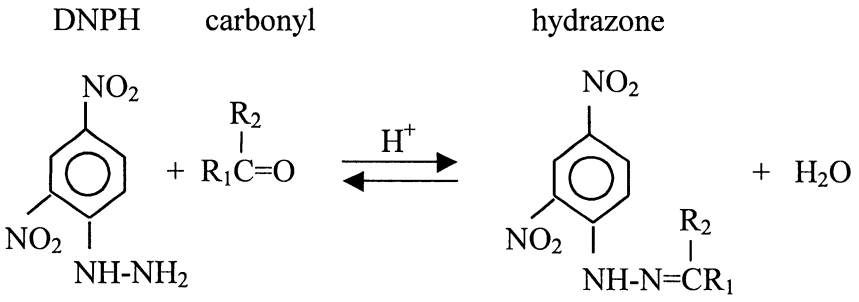

Figure 6. General reaction between a carbonyl and DNPH to form a hydrazone.

The formed hydrazones are relatively stable, non-volatile and strongly absorbing in the UV. Also, the hydrazone derivatives can be uniquely identified with their parent carbonyl, and can be separated from each other using liquid chromatography. The quantification of atmospheric carbonyls using DNPH is based on five main steps. First the carbonyls in ambient air must come in contact with the DNPH to allow the derivatization reaction to occur. Generally this is done by taking a cartridge which is packed with some type of absorbent packing material, filling it with

DNPH solution and blowing out the excess to leave behind a coating of DNPH on the packing material (for example: Grosjean and Fung, 1982; Lipari and Swarin, 1985; Kleindienst *et al*, 1998). Second, sample air can then be drawn through the cartridge using a pump, so that the carbonyls in the sample air can be converted to hydrazones. Third, the hydrazones must be extracted from the cartridge using an appropriate solvent. Fourth, the hydrazones are separated using liquid chromatography, and lastly, the separated hydrazones are detected using UV-absorbance detection.

The instrument used in this project for the purpose of separating the hydrazones was a micro-HPLC operated at flow rates of 50 μL/min with a 1 mm I.D. packed column. The volume of each component in the overall system, and the sampling method used must be appropriate for this separation system. The injection volume should be ≤10% of the peak volume so that the peak width is not adversely affected (Skoog and Leary, 1992). For a peak width of 10 seconds at a flow rate of 50 μL/min, a peak's volume is 8.3 μL. The injection volume should therefore be ≤ 0.8μL. This requires that either the entire sample is injected in a volume of 0.8 μL or less, or that some method of injection is used which does not contribute to band broadening. The detection volume must also be 0.8 μL or less so that peak widths are not adversely affected. A small volume flow cell specific to the instrument was designed and is discussed in section 2.2.3.2.

The instrument went through major changes over the course of the project, with development always targeted towards an automated instrument. An instrument

was successfully automated and deployed in the field to collect ambient data, and is described in section 2.4. The automation of the DNPH technique was achieved by combining the sampling step, the extraction step and the injection step into one component, with the overall method referred to as 'direct injection'. This method is described in section 2.1.1.

2.1.1. Direct Injection

The direct injection method is based on the manual system developed by Nondek *et al* (1991, 1992) and also described by Rodier, 1993. In their system, the carbonyls in sample air were converted to fluorescent DNSH derivatives on a packed cartridge. The cartridge was then manually filled with water and connected as the sample loop in the HPLC injector. The analytes in the sample were then injected, separated by HPLC, and detected by fluorescence. The direct injection method in principle could also be applied to the DNPH method with the significant advantage of allowing the instrument to be automated. In this project, various media for use in the direct injection method were explored, and are described in section 2.2.2. The basic system for all sampling methods used in this project is shown in Figure 7.

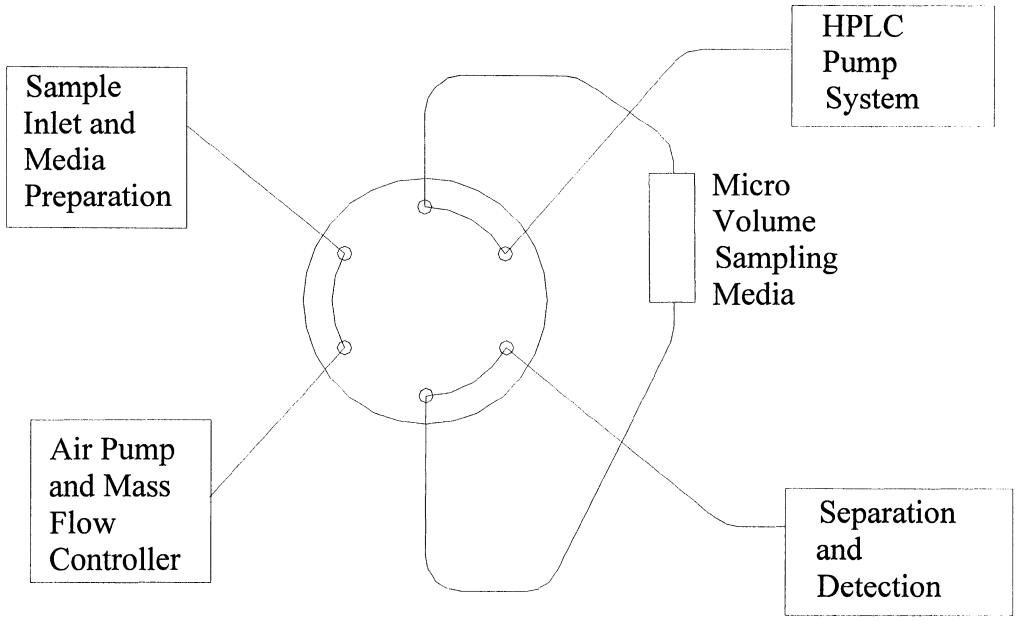

Figure 7. Direct Injection Method Schematic with the HPLC injection valve in inject position.

Using the direct injection method, a sampling medium is connected as the sample loop in the injector of the HPLC system. DNPH is coated onto the sampling medium by filling it with an acidified DNPH solution, and then blowing out the excess solution leaving behind a coating of DNPH. Sample air is then drawn through the sample loop so that carbonyls can come in contact with the DNPH and be trapped as hydrazones. After sampling is complete, the sample loop must be filled with liquid to avoid air bubbles entering the HPLC system. The injector valve can then be switched to the inject position allowing the HPLC solvents to transfer the entire contents of the sample loop to the column for analysis.

Using the direct injection method, the analytes transferred to the column from the sample loop must be contained in as narrow a band as possible. This can be accomplished in two different ways. One way is to simply make the volume of the injection small. The other is to use the technique referred to as 'peak compression' discussed in section 2.1.2. Making the volume of the injection small imposes restrictions on the volume of the sampling medium (~0.8 μL for an 8 μL peak). This volume limit can be met using an open tubular capillary. The experiments performed to test the use of a capillary for sampling, and the results are discussed in section 2.2.2.1.

Regardless of the sampling method used, the method of direct injection has several advantages over conventional cartridge extraction methods. The most important advantage is that it allows the automation of the instrument, which in general results in an improvement in the precision of a method. With direct injection, the extraction step has been completely eliminated. This is advantageous since excess handling is often the primary cause of sample contamination in an analytical method (Slemr *et al*, 1996). Also, the entire contents of the cartridge are injected for analysis, which eliminates any dilution of samples, and eliminates any uncertainty in the completeness of the extraction. A disadvantage of most cartridge methods is that they often involve multiple cartridges for field sampling. This creates the possibility for variability from one cartridge to another. With the direct injection method, one cartridge is used continuously, eliminating any cartridge to cartridge variability which

may exist. This should significantly improve the sample to sample reproducibility of the method. Another advantage is that collection of blanks using the same cartridge and the same method, for both sample and blank, allows a well defined blank value to be obtained. The variability in the blank value determines the sample detection limit for the method (generally 3σ), and a well defined blank obtained using an automated instrument is ideal for obtaining blanks with a low variability. Also, it is expected that with continued use, any contamination of the packing material that may be present initially will be removed via reaction with the DNPH coating solution. For the reasons listed above, significant effort went into the development of an automated direct injection method.

2.1.2. Peak compression

Peak compression simply refers to a process by which the volume that an analyte occupies on the head of the separation column, is smaller than the volume the analyte occupied in the injector's sample loop; in essence this represents a type of preconcentration step. The volume of a packed cartridge is usually larger than what is acceptable for the injection process. The method of peak compression allows large volumes for the sampling medium without affecting the widths of analyte peaks. The following section describes the peak compression process. The velocity at which a component migrates in a packed column can be described using the following equation:

$$v_i = \frac{v_c}{1 + K'_{eq}\frac{V_s}{V_m}} \qquad \text{Equation 2}$$

where v_i is the migration velocity of component i, v_c is the velocity of the mobile phase, K'_{eq} is the equilibrium constant relating the distribution of the concentration of component i between the mobile and stationary phases, and V_s and V_m are the volume of the stationary phase and mobile phase respectively. K'_{eq} is, in general, different for each analyte, and is a function of both mobile phase composition, and the nature of the stationary phase. Since hydrazones are relatively hydrophobic, they will have a high value of K'_{eq} on a hydrophobic stationary phase, and therefore a low migration velocity. For the same reason, hydrazones will have a high migration velocity on a hydrophilic stationary phase. The nature of the mobile phase has the opposite effect on the migration velocity. A more hydrophilic mobile phase, causes the migration velocity of a hydrazone to be lower. These properties can be used to select an appropriate packing material and solvent composition to allow an injected analyte peak to be compressed at the head of the separation column.

The separation column used to separate the hydrazones, was packed with C_{18} silanized silica particles. The C_{18} stationary phase is hydrophobic, and so the hydrazone analytes are well retained. A useful sampling medium, which allows peak compression, is one which is more hydrophilic than the C_{18}. The materials which were explored for this application were a C_4 silanized silica packing, and a pure silica packing material, both of which are more hydrophilic than C_{18}. These are discussed

in sections 2.2.2.2 and 2.2.2.3. The solvent composition at the time of injection must be hydrophilic, and so the cartridge was filled with water before injection, and the solvent composition delivered by the pumps at the time of injection was 80% water with 20% organic solvent, usually acetonitrile. This high water fraction effectively transferred the analytes to the head of the separation column, without affecting the peak widths.

2.1.3. Chromatography

Separation of the hydrazones into individual peaks using HPLC can be a difficult task, and is a significant limitation of the DNPH method. HPLC in general is not as efficient as other separation techniques. A typical capillary gas chromatographic (GC) column achieves separations with ~100,000 theoretical plates. A typical HPLC column achieves ~10,000 to 20,000 theoretical plates (Skoog and Leary, 1992). This significant difference in resolution between the two methods makes gas chromatography more attractive as a separation method. Typical GC separations require elevated temperatures for effective separations of polar analytes such as carbonyls. This makes GC problematic for the separation of thermally unstable carbonyls such as glyoxal and methylglyoxal, or for carbonyls which can readily polymerize such as formaldehyde. Also, injection methods for GC tend to involve elevated temperatures, which would result in the thermal decomposition of these di-carbonlys before injection. The decomposition products for these compounds

include other carbonyls such as formaldehyde (Steacie *et al*, 1935; Saito *et al* 1984), so that methods where thermally unstable di-carbonyls are not the analytes, could suffer from positive artifacts as well. Care must be taken to ensure that excess heat is not used on the sampling lines for gas phase C_1 and C_2 carbonyl analysis techniques. Sampling using DNPH as a derivatizing agent followed by HPLC analysis eliminates any possibility of thermal decomposition of carbonyl analytes. The sacrifice made is the poorer separation efficiency with HPLC.

The efficiency of separations in packed column HPLC depends on several factors. Optimization of the separation is made with these factors in mind. Perhaps the most important single factor affecting the efficiency of an HPLC column is the diameter of the packing material (D_p). The effect of D_p on the efficiency of a separation can be predicted using the Van Deempter equation given below (Poole and Poole, 1997). The height equivalent of a theoretical plate (H) can be given by:

$$H = 2\lambda D_p + (2\gamma D_m)\frac{1}{u} + CD_p^2 u \qquad \text{Equation 3}$$

where H is the height equivalent of a theoretical plate, λ and γ are constants which vary with the quality of the packing, D_m is the diffusion coefficient of the analyte in the mobile phase, C is a constant, u is the velocity of the mobile phase, and D_p is the diameter of the packing material. It is obvious that decreasing the diameter of the packing material in general results in a decrease in the height equivalent of a

theoretical plate, which gives improved separations. This effect is due to a reduction in the time required for an analyte molecule to diffuse between particles. The minimum particle size commonly available for C_{18} packing has a diameter of 3 μm. Another way to increase the number of theoretical plates is to simply use a longer column. The longest column commercially available with a 1mm I.D. and 3 μm diameter packing is 25 cm long. Columns of this type were used throughout the project, and will be discussed as they pertain to each study. The limit to the length of the column is determined by the pressure drop created by the packing material, and the physical pressure limit which the pumping system can deliver. Smaller packing material creates a larger pressure drop for a given flow rate and solvent composition, and longer columns give a higher pressure drop as well. Because of the injection method used in this system (section 2.1.2), the solvent composition with the highest viscosity is at the beginning of a separation and is 80% water, 20% organic. A pressure of ~5000 to 6000 psi is required for this solvent composition with this column at a flow rate of 50 μL/min. This pressure is close to the upper limit of what an HPLC can deliver, and so smaller packing or longer columns are not useable for a 1 mm I.D. column at 50 μL/min.

For a given column, the most efficient separations can be obtained using a gradient solvent program. This simply means that the composition of the mobile phase changes over the course of a separation. For the reversed phase C_{18} packed HPLC column used in this project, the solvent composition changes gradually from a

polar solvent to a less polar solvent as the separation proceeds. The quality of a separation can be altered by changing the rate at which the solvent composition changes over the course of a run. Separations of particular interest can be targeted, and gradient programs can be developed to improve separations for particular analytes. Usually this results in poorer separations for other analytes, and often longer separation times. A compromise must be made between analysis time, the analytes of greatest interest, and adequate separations.

2.1.4. UV Absorbance Detection

The hydrazone analytes absorb light in the 330 to 500 nm range (Grosjean E and Grosjean D., 1995), and their strong absorbance coefficients makes them easily detectable using an absorbance detector. For low analyte concentrations, the absorbance is given according to Beer-Lambert's law:

$$A = \varepsilon c l = \log_{10} \frac{I_0}{I} \qquad \text{Equation 4}$$

where A is the absorbance, ε is the absorbance coefficient, c is the concentration of an analyte, and l is the path length of the detector. To detect an analyte, light is allowed to pass through a flow cell, that contains the analyte. The analyte absorbs light, so that the exiting light intensity (I) is lower than the entering light (I_o). The log of the ratio of entering light to exiting light at a given wavelength is the absorbance signal. It is obvious that the absorbance signal is proportional to the

path length, and therefore increasing the path length of a detector results in a linear increase in absorbance for a given analyte. For an HPLC absorbance detector, the limitation is that the volume of the flow cell of the detector should be <5% of the volume of a peak. For an 8 μL peak this gives an upper limit to the detector volume of 0.4 μL. The detector flow cell should be built to be as long as possible, without exceeding the volume limits. This can only be done by minimizing the cross sectional area of the flow cell. A flow cell was constructed for the purpose of absorbance detection for the micro-HPLC system with both a long path length, and a small volume. The detector system is described in section 2.2.3.

2.2. Instrument Development

2.2.1. Micro-HPLC Pumping System

The pumping system was based on a Micro-tech Scientific Ultra Plus pumping system. This system was used throughout the project. It includes 2 Ultra Plus Micro-Pump modules, a Dyna-Mix Plus solvent mixing module, and an Ultra Plus Pump Controller. The system was designed to deliver 2 separate solvents at different flow rates to allow the use of gradient solvent programming for optimizing separations. One pump delivered water, and the other delivered an organic solvent, generally acetonitrile or a tetrahydrofuran-acetonitrile mixture. For an organic solvent mixture, the pure solvents had to be mixed manually and placed in the reservoir for the organic solvent pump. Each Micro-Pump module consisted of a reciprocating piston pump driven by a stepper motor. The piston is 1/16" O.D. zirconium oxide rod. The small diameter of the piston allows the flow rate to be controlled precisely. The volume the piston displaces is proportional to the volume delivered, and so a longer distance is traveled with a smaller diameter piston, giving better flow rate control (Microtech Scientific quotes <0.5% at 100 μL/min). This accuracy is required for micro-HPLC since the flow rate precision greatly affects the gradient reproducibility, and in turn the retention time reproducibility for analyte peaks. The Micro-Tech Scientific system did not perform adequately and required significant modification. The

following describes the nature of the problem, how it was solved, and the method used to check and calibrate the flow rates delivered by the pumps.

2.2.1.1.Inlet Check Valves

The measurement of low flow rates in the 1 μL/min range can be difficult to perform, but it was necessary to ensure that the desired flow rates were in fact being delivered. The method used was to simply measure the time a solvent took to flow through a known length of fused silica capillary of know I.D. When the pump flow rates were measured, it became obvious that there was a problem with the flows. Flows were generally about 10% or less of the desired flow rate. The nature of the problem was eventually tracked down to a faulty inlet check valve design, and could only be fixed by changing the check valve system.

The check valves use a ball and seat design which is very similar in design to those used in typical analytical HPLC systems. Although they are effective valves at the higher flow rates used in analytical HPLC, they were not effective for the much lower flow rates in micro-HPLC. In this type of valve, a ruby ball seals on a sapphire seat using gravity and the pump pressure generated during the delivery stroke of the piston. When the piston withdraws from the pump the ball lifts from the seat to allow solvent to be pulled into the pump head. The Micro-Tech Scientific inlet check valves were unable to seal during the delivery stroke of the piston. This caused solvent which should have been delivered by the pump to simply be pushed back into

the inlet line. The leak rate, in both micro and analytical HPLC systems, is largely determined by the pressure in the pump head. In both cases these are about the same, typically in the 2000 to 5000 psi range. If a check valve leaks at a rate of about 5 μL/min, then at analytical HPLC flow rates of 1 ml/min this represents a 0.5% decrease in flow. This would not be detected as a problem. If however the flow rate is 10 μL/min, such as in a micro-HPLC system, then this leak rate represents 50% of the flow, which would be a significant problem. It was obvious that a more robust inlet check valve design was needed for the flow rates required.

The design of the other check valves in the system is very different from the design of the inlet check valves. They use elastomeric seal materials and a spring loaded system, referred to as a "poppet" check valve, to give very effective leak free seals. The actual poppet style inlet check valve did not exist however, and had to be custom ordered from Micro-Tech Scientific. The main disadvantage of the poppet check valves is a relatively high cracking pressure (i.e. pressure difference required for the valve to open) of about 40 to 50 psi in the case of the valves used by Micro-Tech Scientific. This is not a problem in the high pressure areas of the pump system which are generally at 2000 to 5000 psi. During the withdrawal stroke of the piston, the maximum pressure differential across the valve is only 15 psi, and so the valve will not open to let in solvent. The solution to this, was to maintain the solvent reservoirs at a pressure of about 60 psi under UHP grade helium. This had the added advantage of eliminating air from the solvent reservoir, so that the solvents became

somewhat degassed and also did not come into contact with lab air which could have contaminated the solvents. In this setup, the new custom poppet check valves were very effective and robust inlet check valves.

2.2.1.2.Flow Rate Calibration

Once the inlet check valve system was fixed, it was necessary to ensure linear and reproducible flow rates down to the ~1 μL/min range. Also, different solvents have slightly different compressabilities, so to ensure correct flow delivery, the flows should be calibrated for each solvent. This was done by measuring the time for the solvent to fill a known volume in a capillary, which allowed accurate flow rate measurements for the range needed. The ratio of actual flow rate to flow rate setting was used as a calibration factor, which was then used in the Micro-Tech Scientific software to automatically correct the flow rates. The results are shown in Figure 8. The reproducibility and linearity of the flow rates shows the effectiveness of the inlet check valve system, and the ability for the pump system to deliver reproducible flows.

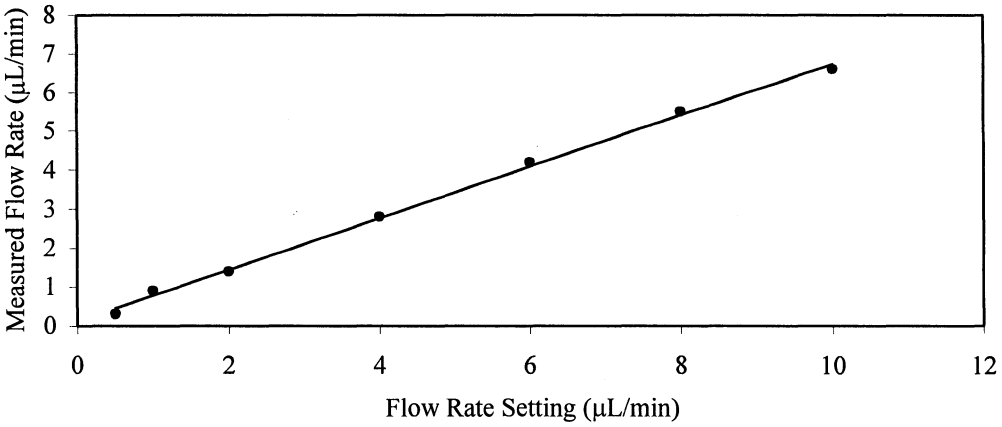

Figure 8. Pump flow rate calibration for acetonitrile. The slope of the least squares regression is used as the flow rate calibration in the pump control software.

2.2.1.3. Solvent Mixing

Two solvents are delivered by the pumps at different flow rates so that a gradient in the solvent composition over the course of a separation can be obtained. The solvents must be mixed well before entering the separation column, so that a uniform composition is obtained. A major problem resulting from inadequate mixing is excessive oscillations in the absorbance signal. This is mainly due to a significant refractive index difference between solvents, resulting in light level changes passing through the flow cell if the solvent composition is not consistent. This is obviously unacceptable, since it greatly reduces the signal to noise ratio for the detection system, which results in poor detection limits.

The mixing of the solvents is done with the Dyna-Mix Plus solvent mixing module. This consists of two chambers which are dynamically stirred with Teflon

coated magnetic stirring bars. The primary mixing chamber is a 20 μL chamber, with check valves for each solvent. The check valves prevent the flow from one pump from entering the other pump. This reduces the time needed to reestablish the solvent composition before the beginning of a run by preventing solvents from mixing before the mixer. The secondary mixing chamber has a larger volume of 100 μL. This volume is large enough for the solvents to be mixed adequately. Even with stirring, complete mixing can only be accomplished by diffusion. The volume of the secondary mixer is important since the residence time of the solvents must be long enough for the diffusion process to happen.

2.2.2. Direct Injection Sampling Methods

The following sections present the various methods of direct injection explored in this project. The experiments performed to test each method, and the results will be discussed.

2.2.2.1. Open Tubular Capillary Sampling

The principle of open tubular sampling was attractive because it addressed the issue of injection volume. A 75 μm I.D. capillary 4 cm long has a volume of about 0.18 μL. This is small enough in terms of injection volume, and could easily be adapted to fit into an injection valve as a sample loop. The main issue which had to be explored was the trapping efficiency of the capillary. The capillary used was a Supelco CElect H275 CE column sold as a separation column for capillary

electrophoresis. It has an I.D. of 75 μm, and the internal wall is silanized with C_{18} material. This column was chosen with the hope that acidified DNPH would be retained by the C_{18}. Sample air could then be pulled through the capillary allowing the carbonyls to come in contact with the DNPH coated on the walls, and hopefully be trapped as hydrazones.

Since the reaction rate between gas phase carbonyls and the DNPH coated on the walls of the tubing is not known, there was no way to predict a trapping efficiency for the capillary. The best possible case would be that each analyte molecule which collides with the wall is trapped. For this case, the Gormley-Kennedy equation can be used to estimate the effectiveness of the capillary (Fuchs, 1964). Taking only the first term, the ratio of the concentration exiting the capillary to the concentration entering is given by:

$$\frac{\bar{n}}{n_0} \cong 0.819e^{(-3.657\mu)} + \ldots \qquad \text{Equation 5}$$

where μ is the dimensionless quantity :

$$\mu = \frac{Dx}{R^2\bar{U}} \qquad \text{Equation 6}$$

D is the analyte diffusion coefficient, x is the length of the capillary, R is the radius of the capillary and $\bar{U}$ is the mean flow velocity in the tube. Using an estimated value of 0.2 cm^2/sec for D the ratio of $\bar{n} / n_o$ for this capillary at a flow rate of 5 mL/min is about 10^{-48}. One would expect essentially complete trapping for an

analyte which reacts with the DNPH coating on the tubing. The actual trapping efficiency could only be determined experimentally. This was done using various gas phase standards and various DNPH coating techniques. At air sampling flow rates in the 1 to 5 ml/min range, no experiments yielded results which could be considered promising. Trapping was generally less than 1%. To verify the results, two 4.0 cm long capillaries were connected in series, and gas phase standards were again delivered in the 1 to 5 ml/min range. Analysis showed that the amount of carbonyls trapped by the two capillaries was essentially the same (<1%), suggesting that little of the analytes were trapped by the first capillary. This experiment suggests that the reaction between gas phase carbonyls and DNPH coated on the walls of the capillary is very slow. To quantitatively trap all the carbonyls in sample air would require much lower flow rates. This would cause sampling time to be excessive, and render the method useless for atmospheric carbonyl analysis. Open tubular sampling was therefore abandoned, and sampling methods using packed cartridges were explored.

2.2.2.2. C_4 Packed Cartridge Sampling

The first packing material examined was a C_4 silanized silica material with a 30 μm diameter. This material was spherical, and non-porous. A C_4 material was chosen because of its lower retention for hydrazones, compared to C_{18}, which would allow peak compression at the head of the separation column. The much larger surface area than the open tubular capillaries would hopefully allow gas phase

carbonyls to be trapped more efficiently. This packing material showed some promise, but it was found that the trapping efficiencies were strongly flow rate dependent. The results of one of the experiments are shown in Figure 9.

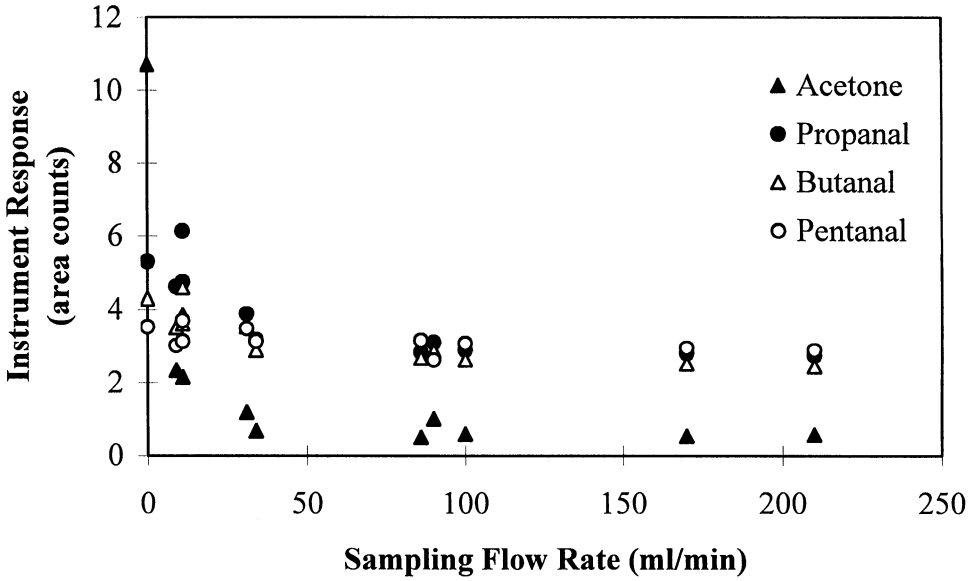

Figure 9. Dependence of instrument response on sampling flow rate using the non-porous C_4 packing material. Significant losses are seen at moderate flow rates of 10 mL/min most notably for acetone. The points at zero flow rate represents the expected peak area based on the amount of carbonyl sampled and the instrumental response.

The results suggested that a packed cartridge was more effective at trapping the carbonyls than an open capillary. The higher trapping was most likely due to the higher surface area of a packed cartridge, but incomplete trapping at the higher flow rates tested suggested that the surface area of this packing was too low. The non-porous nature of the C_4 packing means that the surface area is not as high as it would be for a porous material of a similar diameter. No commercially available porous C_4

silica packing could be found, and so a direct comparison based on surface area could not be made. Overall, this material showed promise, but was not as effective as one would like for atmospheric sampling, and so other materials were explored.

2.2.2.3.Silica Packed Cartridge Sampling

A silica packed cartridge was found to be effective for both sampling and peak compression. The material used was a 60/45 mesh irregular shaped porous silica. Silica is an ideal material for this application. The relatively polar carbonyls being sampled from the gas phase are well retained by this material. This is most likely due to both the large surface area of the porous material, and the hydrophilic nature of silica. The trapped carbonyls then react with DNPH to form hydrophobic hydrazones, which have little retention on the hydrophilic silica during injection. The hydrazone analytes can then be transferred to the head of the column using a polar solvent, where they are well retained by the C_{18} material, giving good peak compression. This silica material was used for all ambient sampling, and the conditions used will be discussed as they pertain to each field study. The experiments to evaluate the silica packed cartridge are discussed in Section 3.

2.2.3. Detector System

The absorbance detection system remained largely unchanged throughout the project. The three main components of the system are a light source, a detector and a flow cell. The light source and the detector were commercially available components,

while the flow cell was custom built specifically for this instrument, and is described in section 2.2.3.2. The light source was a model 63163 Oriel Instruments deuterium lamp housed in a Oriel Instruments model 77850 lamp housing powered by a model 68840 deuterium power supply. Light output from the lamp was delivered to the flow cell using a 1 mm single core fiber optic. Light exiting from the flow cell was delivered to the detector using a 200 μm fiber optic. The light collection fiber optic was positioned using a three dimensional translation stage. It was positioned so that the maximum light level was ~75% of the saturation level for the detector. The light delivery fiber optic was fixed in place relative to the flow cell. The flow cell and the translation stage were fixed to a 24" × 30" × ½" aluminum optical bench which also supported the HPLC system. The detector was an Ocean Optics Inc. model S2000 CCD spectrometer with an entrance slit opening of 100 μm. This 2000 element CCD detector was capable of collecting light in the 184 nm to 867 nm range using a diffraction grating with 600 lines/mm blazed at 400 nm. An optional cylindrical lens was purchased with the detector, placed in front of the CCD detector, to allow higher light collection efficiency. Signal from the detector was collected and processed by computer using a software program. The software was written using Visual Basic 4.0 and is discussed in section 2.2.3.1. The flow cell design and construction are discussed in section 2.2.3.2.

2.2.3.1. Spectrometer and Data Collection Software

The complete software program is given in Appendix A. Light intensity signal was collected by computer using an ISA board supplied with the CCD spectrometer. The light level signal was integrated for a time of 976 ms for each light intensity measurement. This integration time allowed complete spectra to be collected at an overall rate of 1 Hz. The spectrometer has a resolution of ~0.3 nm per CCD element. 10 CCD elements were grouped to give an operational resolution of 3 nm. Spectra were collected from 292 nm to 472 nm. A value for initial light intensity, I_o, was calculated for each group of 10 CCD elements by averaging the first 10 data points at the beginning of a separation. An absorbance signal was calculated for each group of 10 elements, by measuring the light intensity, I, and taking the $\log_{10}$ of the ratio I_o/I according to equation 7:

$$A_i = \log(\frac{I_o}{I_i}) \qquad \text{Equation 7}$$

where I_i is the light intensity for the i^{th} group of 10 diodes, and A_i is the calculated absorbance for the i^{th} group of diodes. Fifty absorbance signals covering the spectral range quoted above were calculated at each time interval, and stored separately for later spectral analysis. Chromatograms were plotted and stored by averaging all 50 absorbance signals at each time. The averaged signal is referred to as a 'total absorbance' signal, A_{tot}, as shown in Equation 8:

$$A_{tot,t} = \frac{\sum_{i=1}^{50} A_{i,t}}{50} \qquad \text{Equation 8}$$

Storage of all 50 absorbance signals allowed comparisons between spectra from standard injections, and spectra from ambient samples. This allows a qualitative check for both correct peak identification, and for possible peak overlaps with unknown peaks. Also, it allows the possibility of quantifying two peaks which may be overlapped if the spectra of the individual compounds are known, and are significantly different from each other.

2.2.3.2.Flow Cell

The flow cell built for this project is shown in Figure 10. The material used to build the flow cell was stainless steel. A two piece design allowed the machining of a long path length with minimal cross section, so that the volume was kept to a minimum. The light path in the flow cell was 12mm long, and had an estimated volume of 30 nl. It was machined by first grinding a cutter from high speed steel. The cutter was a 90° conical cutter, so that the final shape of the light path would be triangular. The top face of the bottom half of the flow cell was accurately ground to give a flat surface. The cutter was then pushed along the surface, so that small amounts of material would be removed from the stainless steel. Several progressively deeper passes created a groove slightly deeper than required. The surface of the piece was then accurately ground to the correct height. The volume of the light path was

estimated by measuring the width of the groove, and using the geometry for a 90° triangle. The depth of the groove is estimated to be 0.002". The upper half of the flow cell was constructed to create the top of the light path, and also to hold the connecting tubing. 1/16" O.D. Peek™ tubing with 0.005" I.D. was epoxied in place for the inlet and outlet. Holes for the tubing were accurately drilled as close to the edge of the light path as possible, to avoid excess dead volumes. The bottom surface of the top piece was accurately ground to allow the pieces to fit together, and two steel screws held the two pieces together tightly. The surfaces were found to leak slightly, so Teflon™ tape was used to create a seal between them. Quartz windows covered the ends of the light path, and were sealed with Teflon™ tape. The windows were held in place with pressure applied by an external holder. The outlet of the flow cell was fitted with a 10" long fused silica capillary with an I.D. of 75 μm. This capillary created a slightly increased pressure in the flow cell to prevent the formation of bubbles in the light path due to out-gassing of the solvent. Bubble formation was found to be a problem before the use of the capillary.

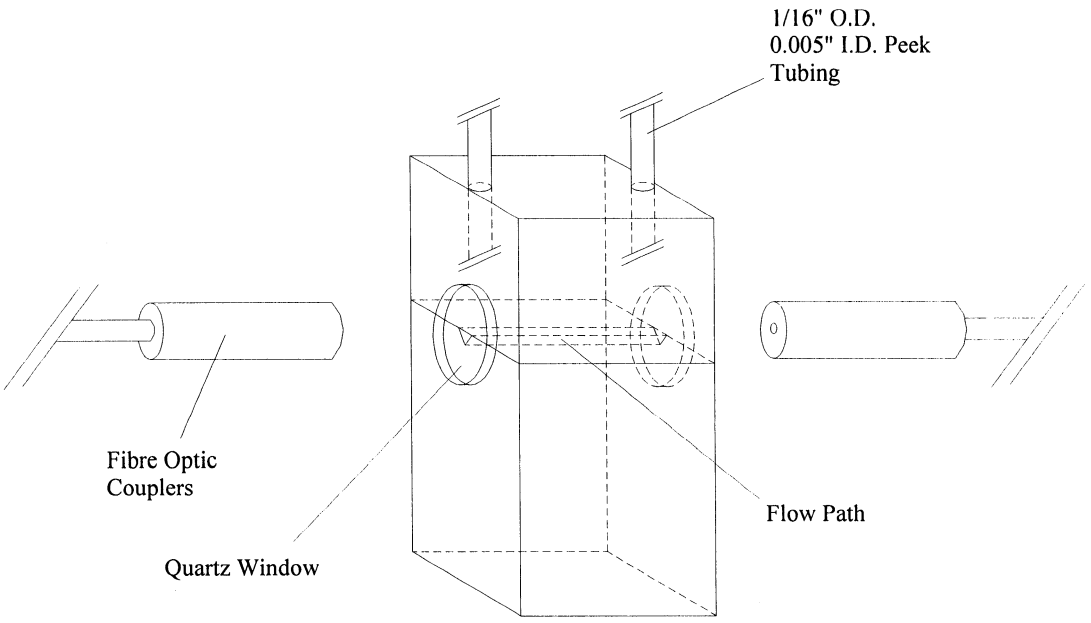

Figure 10. Micro Flow Cell.

2.3. Hamilton 1999 Study

The Center for Atmospheric Chemistry, York University, conducted a field study from July 7th to July 26th, 1999 at two separate sites located in Hamilton Ontario. The sites consisted of an urban site located in downtown Hamilton, and an upwind site, called Lynden station, located ~5 km to the southwest of the downtown site. Both the downtown station and the Lynden station are operated by the Ontario Ministry of the Environment on a continuous basis, and provided supporting data including O_3, NO, NOx, and PM2.5 data. Hydrocarbon canister samples were also collected at the same location, and were analysed by Dr. J. Rudolph's group, York University, Toronto, Canada. Carbonyl samples for this project were collected at the Lynden station. This field study provided an opportunity to conduct carbonyl measurements using a manually operated version of the direct injection method. The main purpose of this was to determine the viability of the method, using real samples with supporting data, before development of an automated direct injection system.

2.3.1. Hamilton 1999 Experimental Details

The analysis of carbonyls was performed *in situ* using the direct injection method, operated manually. One cartridge was used throughout the study. The packed cartridge was 27 mm long with a 1mm I.D. packed with 60/45 mesh porous silica. The cartridge was manually cleaned, before each loading, by passing 200 μL of acetonitrile through it with a syringe. The cartridge was then loaded with DNPH

by passing 50 μL of an acidified DNPH solution through the cartridge, and blowing out the excess with ultra high purity (UHP) helium. The coating solution was made by dissolving 0.2 g recrystalized DNPH in a solution of 90% acetonitrile/10 % water,

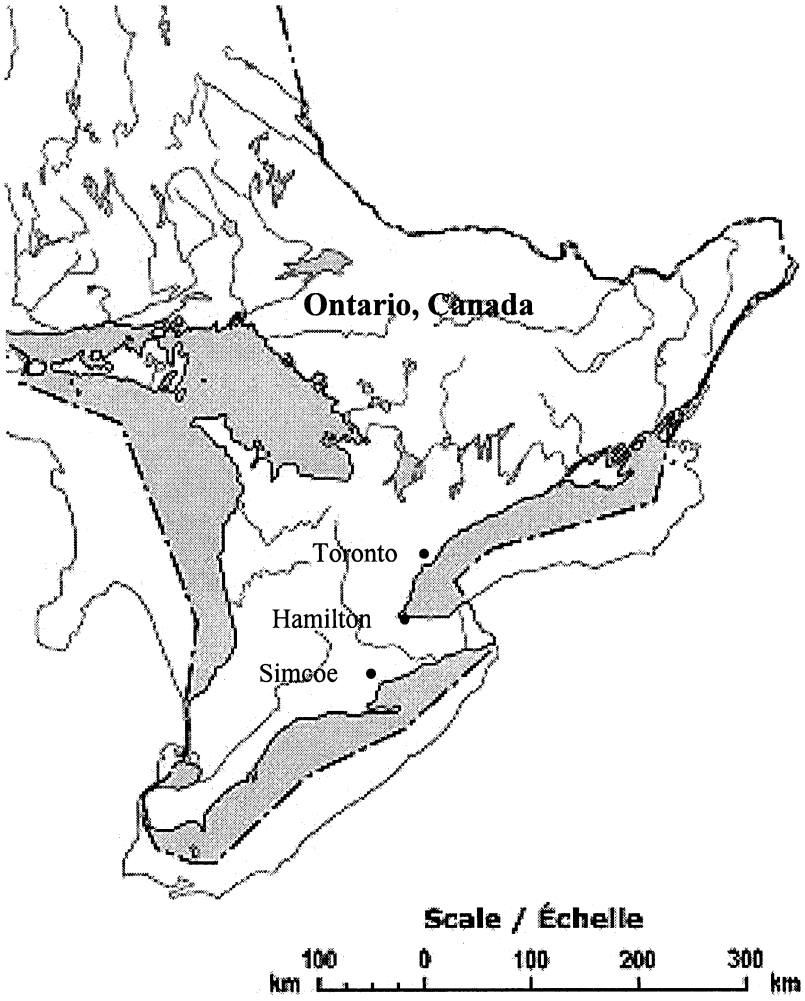

Figure 11. Map showing the location of the two sampling sites used in this project, Hamilton and Simcoe, Ontario. Map obtained from Natural Resources Canada.

boiling the solution for 10 min., and then adding 10 μL of concentrated H_2SO_4; the final solution volume was 25 mL. To prevent the formation of the precipitate of DNPH with sulfuric acid, 1 ml of water was added to the solution. Once made, the solution was maintained in a Teflon tube under UHP-helium at a pressure of 50 psig continuously. The tube was fitted with a septa to allow the withdrawal of solution without opening the DNPH solution to air.

To eliminate ozone from the sampling system, the inlet line was fitted with a ¼" O.D. Teflon tube filled with KI. The tube was filled so that a 6 mm section contained KI (~0.15 g). A 2 μm screen was used at the inlet to prevent the KI from entering the sampling cartridge. Before sampling began, the KI filled ozone trap and all the lines used were flushed with ambient air for ~5 min at a flow rate of 50ml/min. The cartridge was then inserted into the system to begin sampling. The samples were collected at an air flow rate of 50ml/min generally for 1 hour. The flow rate was controlled using a calibrated Tylan mass flow controller. The samples were collected from the roof of the Lynden station, at an estimated height of ~1.5 m. Once the sample was collected, the cartridge was removed from the sampling system, and sealed. The cartridge was capped and allowed to sit for 1 hour after sampling was complete. The air in the cartridge was then expelled by injecting water from a Millipore system to exactly fill the cartridge. The cartridge was then installed as the sample loop in a Rheodyne model 8125 micro-HPLC injection valve. The connecting

lines used in the sample loop were filled with water before installing the cartridge. The contents of the cartridge were analyzed by turning the injection valve to inject position, allowing the hydrazones to be transferred to the separation column by the solvents delivered by the pumping system. The HPLC and data collection systems were started simultaneously with the injection of the sample. The solvents used for separation were pure water in pump A and 25% tetrahydrofuran/75% acetonitrile in pump B. Two solvent programs were used. One was targeted at separations for C_1 to C_3 (Program 1), while the other was targeted at the separation of later eluting compounds (Program 2). These two programs are shown in Table 3.

Program 1			**Program 2**		
Time (min)	Pump A Flow (μL/min)	Pump B Flow (μL/min)	Time (min)	Pump A Flow (μL/min)	Pump B Flow (μL/min)
0	40	10	0	30	20
100	0	50	40	30	20
			80	0	50

Table 3. Solvent programs used during Hamilton 1999. Solvent gradients are linear for both programs.

Due to a co-eluting compound, much of the acetaldehyde data was discarded for this study. Spectra were examined for all other peaks for all samples collected, and agreed well with the spectra obtained using standard injections. The nature of the

compound with which acetaldehyde co-elutes is not known. The spectra show absorbance beginning in the UV at lower wavelengths than what is collected with this detector. Significant absorbance can be seen well into the wavelength range collected for peak quantification, and so the peak area for acetaldehyde was significantly affected by this compound. Spectra for the acetaldehyde peak for a quantified peak, and one in which no quantification was made are shown later on in Figure 16, section 3.2. Although the possibility exists for correction of the data, one must have a pure spectra for the unknown compound to be able to correct the absorbance signal. Until this information can be obtained, the data must be discarded.

2.4. Automated Instrument

A schematic of the automated instrument is shown in Figure 12. Three valves and a syringe pump are required for the automated process. These valves and the syringe pump were all controlled through four 24 volt power supplies on the Microtech system which are controlled through the HPLC software. The power supplies control 4 single pull double throw (SPDT) relays which create a contact closure. Three of the SPDT relays control the electric valve actuators (Valco Instruments Co. Inc. Houston Texas) to select the valve position. The fourth instructs the syringe pump to turn on or off. The positions for the two selection valves (i.e. load or inject for valves B and C) are selected by turning the power to the relay on or off. The position of the multiposition valve (valve A) is advanced by turning the

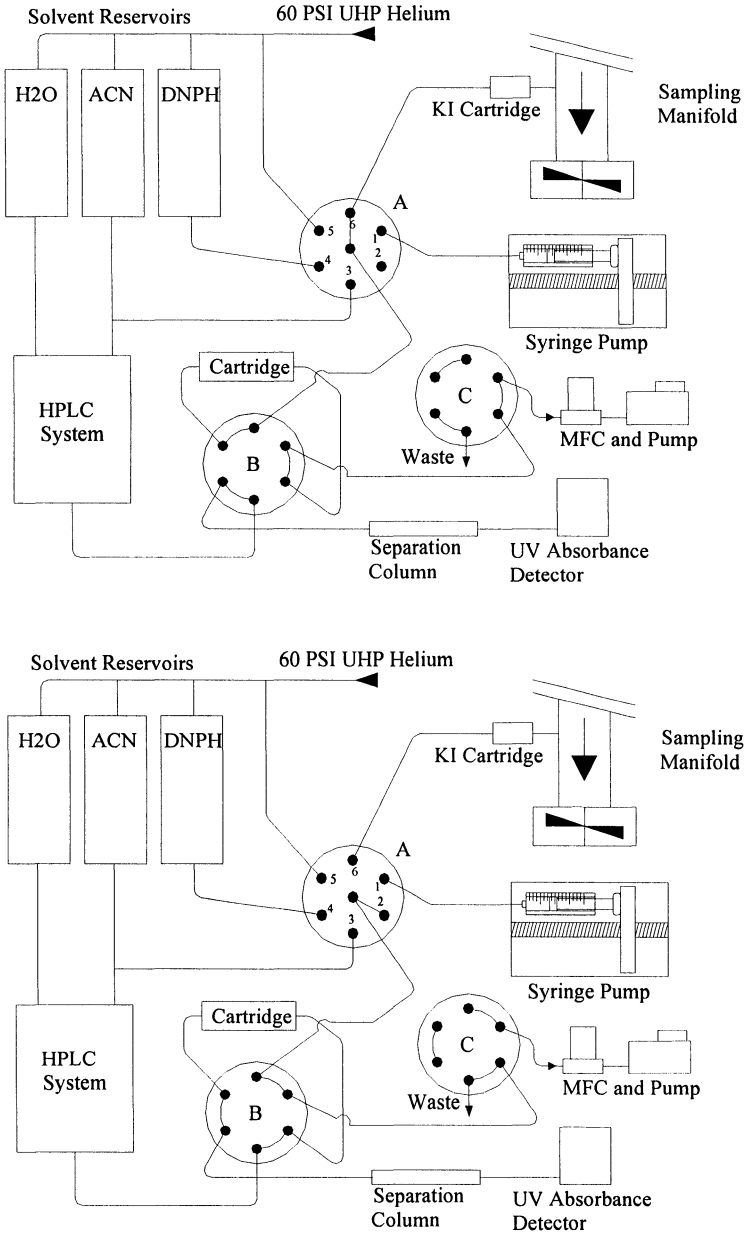

Figure 12. Automated Instrument Schematic. Upper figure shows valve positions during ambient sample collection with valve A in position 6, valve B in load position, and valve C in sample position. Lower figure shows valve positions during sample analysis, with valve C in waste position, and valve B in inject position.

power to the relay on and then off; each successive contact made by the relay advances the multiposition valve one position. The valves consist of one 1/16" 6 port multiposition Valco valve (valve A), one 1/16" 6 port Cheminert sampling valve with 0.010" I.D. flow channels and Tefzel rotor (valve B), and one 1/16" 6 port sampling valve (valve C). All valves were purchased from VICI Houston Texas. Valve B was custom ordered from the manufacturer to be leak proof to 7000 psi. All solvents used are maintained under ultra high purity helium at a pressure of 60 psig to maintain their purity. The pressure also serves to push solvents through the valve system, so that individual pumps are not required for non-HPLC solvents. The silica packed cartridge was installed as the sample loop in valve B to allow on-line sampling, derivatization and extraction. The cartridge was built in house and is a 1.0 mm I.D x 30 mm long stainless steel micro cartridge (Figure 13) packed with 60/45 mesh porous irregular silica. The sampling cycle begins with the cartridge being cleaned by passing acetonitrile through it. This is done by placing valve A in position 3 while valve B is in load position and valve C is in waste position. Valve A is then switched to position 4 to allow DNPH solution to coat the cartridge. The cartridge is then dried by switching valve A to position 5 to allow ultra high purity helium to pass through the cartridge. Sample collection begins by moving valve A to position 6 and valve C to sample position, so that the pump can pull sample air through the system. To quantify the volume of air sampled, and also control the flow rate, sample air is drawn through a calibrated Tylan mass flow controller. Ambient ozone is removed from the

sample air, by a small volume trap packed with crystalline potassium iodide in 1/4" Teflon tubing installed at the front of the inlet line. A 1/4" stainless steel screen with 10 μm openings is used at the inlet to prevent potassium iodide from entering the sampling line. No screen of any kind is used at the inlet to the KI filled ozone trap. After sampling, the air remaining in the cartridge and loop must be eliminated to avoid air bubbles entering the HPLC system. This is done with an exact volume of water delivered by a Harvard Apparatus model 22 syringe pump at a flow rate of 0.27 ml/min for 0.54 min using a 5 ml Hamilton Gastight glass syringe filled with pure water from a millipore system. Injection of the sample in a water matrix has the added advantage of compressing the hydrazone peaks on the head of the column (Nondek *et al*, 1991), giving significantly improved chromatographic resolution for a relatively large injection volume of 35 μL. The separation of the hydrazones is done using reversed phase micro-HPLC. The columns used for separation were different for each study, and so are discussed as they pertain to each study. The columns were generally 1 mm I.D. columns 25 cm long with either 5 μm or 3 μm C_{18} packing.

The software program written to collect absorbance data was modified to also control the automation of the system. The software was designed to allow samples to be collected and analyzed continuously, and also to allow the running of a "blank" method for the first run. A copy of the Visual Basic 4.0 code is given in Appendix section 7.1. Typically the automated sequence was stopped once per day, and restarted, so that blanks could be collected roughly once per day.

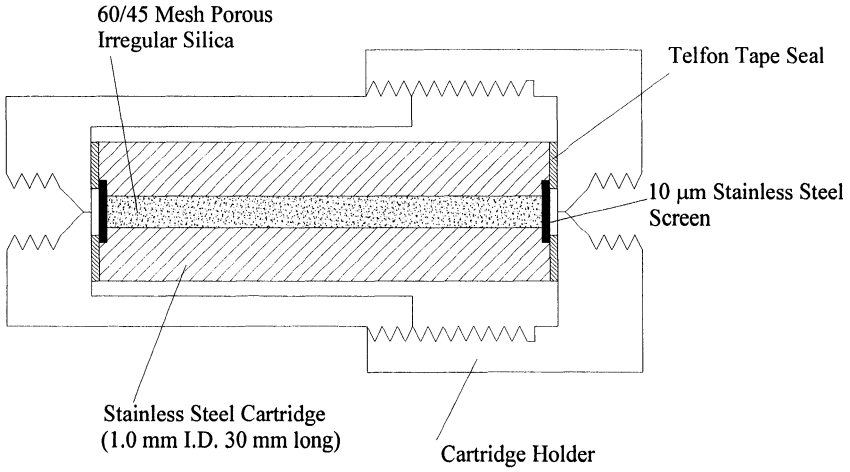

Figure 13. Silica packed micro cartridge.

2.5. Simcoe 2000 Study

The Center for Atmospheric Chemistry, York University, Toronto, Canada, conducted a second field study at two separate sites in the Hamilton area from June 19th to July 20th, 2000. The downtown Hamilton site was again used in 2000, however the second site was located ~70 km southwest of Hamilton in Simcoe Ontario. The automated instrument for this project was located at the Simcoe site. The Ontario Ministry of the Environment continuously operates a monitoring station at this site, with supporting data including O_3, NO, NOx, PM2.5, wind speed and wind direction. Temperature and relative humidity data were collected at the Simcoe site by Dr. R. McLaren's group, York University. Hydrocarbon samples were also collected at the same location, and were analysed by Dr. J. Rudolph's group, York University.

2.5.1. Simcoe 2000 Experimental Details

The instrument used in Hamilton 1999 was automated and used successfully in the field for SONTAS 2000. Close to 200 samples were collected over the study at a frequency of 1 sample every 2 hours during periods when the instrument was operational. The volume of acetonitrile used in the cleaning step was estimated as ~300 μL. To coat the cartridge with DNPH, ~50μL of coating solution was allowed to pass through the cartridge. The coating solution was made by dissolving 0.2 g

recrystalized DNPH in a solution of 90% acetonitrile/10 % water, boiling the solution for 10 min., and then adding 10 μL of concentrated H_2SO_4; the final solution volume was 25 mL. The cartridge was then dried by passing ultra high purity helium through the cartridge for 12 seconds. Sample volumes of 2 L were collected by sampling at a flow rate of 50 ml/min for 42 min through a calibrated Tylan mass flow controller. Ambient ozone was removed from the sample air, by a small volume trap packed with ~0.16g of crystalline potassium iodide in 1/4" Teflon tubing installed at the front of the inlet line. The trap was emptied and refilled roughly once per week during sampling. Outside air was pulled into the laboratory with a 4" glass manifold at a flow rate of 35 ft^3/min. from ~1m above the roof of the laboratory. The sampling height is ~ 4m above ground level. A 4' long 1/16" O.D. × 0.030" I.D. FEP Teflon line connects valve A to the glass manifold. After sampling, the air remaining in the cartridge and loop was eliminated at a flow rate of 0.27 ml/min for 0.54 min using a 5 ml Hamilton Gastight glass syringe filled with pure water from a Millipore system. The separation of the hydrazones was done with a 25 cm long 1mm I.D. column packed with 3 μm Supelcosil LC-18 packing purchased from Supelco. The column was purchased and installed just before the field study to ensure its performance would be as good as possible. No significant changes were made to the detector or data collection system, and are described in section 2.2.3. Thirteen blank determinations were performed during the field study. The procedure for blank collection was identical to ambient sample collection, with the sampling step being

reduced to 6 seconds. The average blank values were subtracted from the ambient sample peaks as a correction to the ambient data. The results of the blank determinations are discussed in section 3.5.

3. INSTRUMENTAL METHOD VALIDATION

The following chapter describes the experiments performed to validate the methodology used in this project. Great effort has been made to ensure that the ambient data collected are reliable, and within the estimated uncertainties. The possibility of interferences always exists, however remote, and so conclusion drawn from this work, or any other, must always keep this in perspective.

3.1. HPLC System Calibrations

The HPLC system response was determined using liquid phase hydrazone standard solutions, and verified using gas phase standards. The hydrazones were synthesized using a modified version of the standard methods (for example Grosjean and Grosjean, 1995). Briefly, twice recrytalized DNPH was added to acetonitrile, and heated to dissolve the DNPH. A small amount of water (~1 ml) was added to the solution, followed by the addition of the carbonyl to be derivatized. Two drops of concentrated HCl were added to the solution to catalyze the formation of the hydrazone. The solution was cooled to allow the formation of the hydrazone solid precipitate. The precipitate was then collected by filtration. The solid hydrazone was then thoroughly washed with water followed by acetonitrile, and gently dried with heat. The solid hydrazone was then dissolved in acetonitrile, and analyzed by HPLC to check the purity, and to ensure that no traces of DNPH reagent co-precipitated.

The carbonyl added to the solution was in stoichiometric excess relative to the DNPH. This ensured complete removal of the DNPH reagent, leaving behind an excess of carbonyl. The water soluble carbonyl was then easily removed by washing the precipitate with water. The proportions were different for the di-carbonyls glyoxal and methylglyoxal. For these, the DNPH was maintained in excess to ensure complete derivatization of both carbonyl groups. The solid formed was re-crystallized and thoroughly washed with acetonitrile to remove the excess DNPH. HPLC analysis shows no significant DNPH contamination in the crystals. Melting points were determined for many of the hydrazones made. In general the melting points were sharp (2-3°C range), and were found to be in excellent agreement with literature values (within 2 °C), (Rappaport, 1967).

Solutions of the hydrazones were made gravimetrically by weighing the dried hydrazones into calibrated volumetric flasks and filling with acetonitrile. The solution was then diluted by various amounts, with calibrated glassware, and injected to generate a calibration curve for the instrument. The injections were done using a model 8125 Rheodyne micro-HPLC injection valve, with a 5 μl sample loop. The actual injection volume is somewhat larger than the volume of the sample loop for this valve, since the internal valve components represent a significant volume relative to the injection. The total volume quoted by Rheodyne for the various components along with a 5 μL sample loop is 5.81 μL. A syringe was used to inject exactly 5 μL, so that the precise volume of the loop was not critical to the calibration. A typical

calibration curve is shown in Figure 14. The instrument response is determined by calculating the slope of the line. To ensure the reproducibility of the standard injections, the synthesis of the hydrazones, and the making of the solutions, the entire procedure was repeated for acetone. The results are also shown in Figure 14. Excellent agreement is seen for the two calibration curves (slopes of 0.99 ± 0.02 and 0.99 ± 0.05), which suggests that the calibrations are reliable. The instrumental responses for various carbonyls are listed in Table 4. The instrument response was checked before and after the field studies using many hydrazones, and was found to be stable to within <5%, as would be expected with an absorbance detector.

Carbonyl	**Response** (10^{10}AU·sec/mol)
Formaldehyde	0.984
Acetaldehyde	1.07
Acetone	0.987
Propanal	0.989
Benzaldehyde	1.52
Glyoxal	2.65
Methyl-glyoxal	2.31

Table 4. Instrument responses determined using liquid phase gravimetric hydrazone standards. The responses are in units of 10^{-10}×area counts per mole of carbonyl injected, where 1 area count is equivalent to 1 absorbance unit·second.

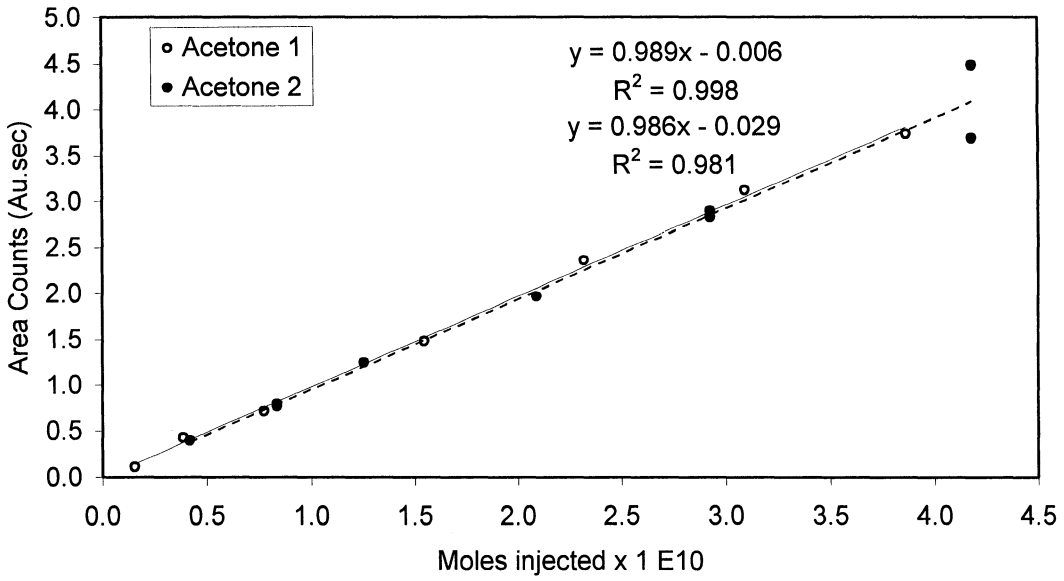

Figure 14. Liquid phase hydrazone calibrations for acetone. The two curves show the results obtained for two separately synthesized hydrazones of acetone. The two stock standards were prepared gravimetrically, and diluted to generate a range of concentrations.

3.2. Hydrazone Spectra

The use of a CCD detector allowed the collection of spectral information as well as absorbance intensity. To ensure correct peak identification for ambient samples, and to ensure that analytes were not co-eluted in the same peak, the spectra from standard injections were compared with spectra from atmospheric sample peaks. This added information over simply using retention time as a peak identification, adds significant certainty to the ambient data. The spectra are shown in Figure 15 and Figure 16.

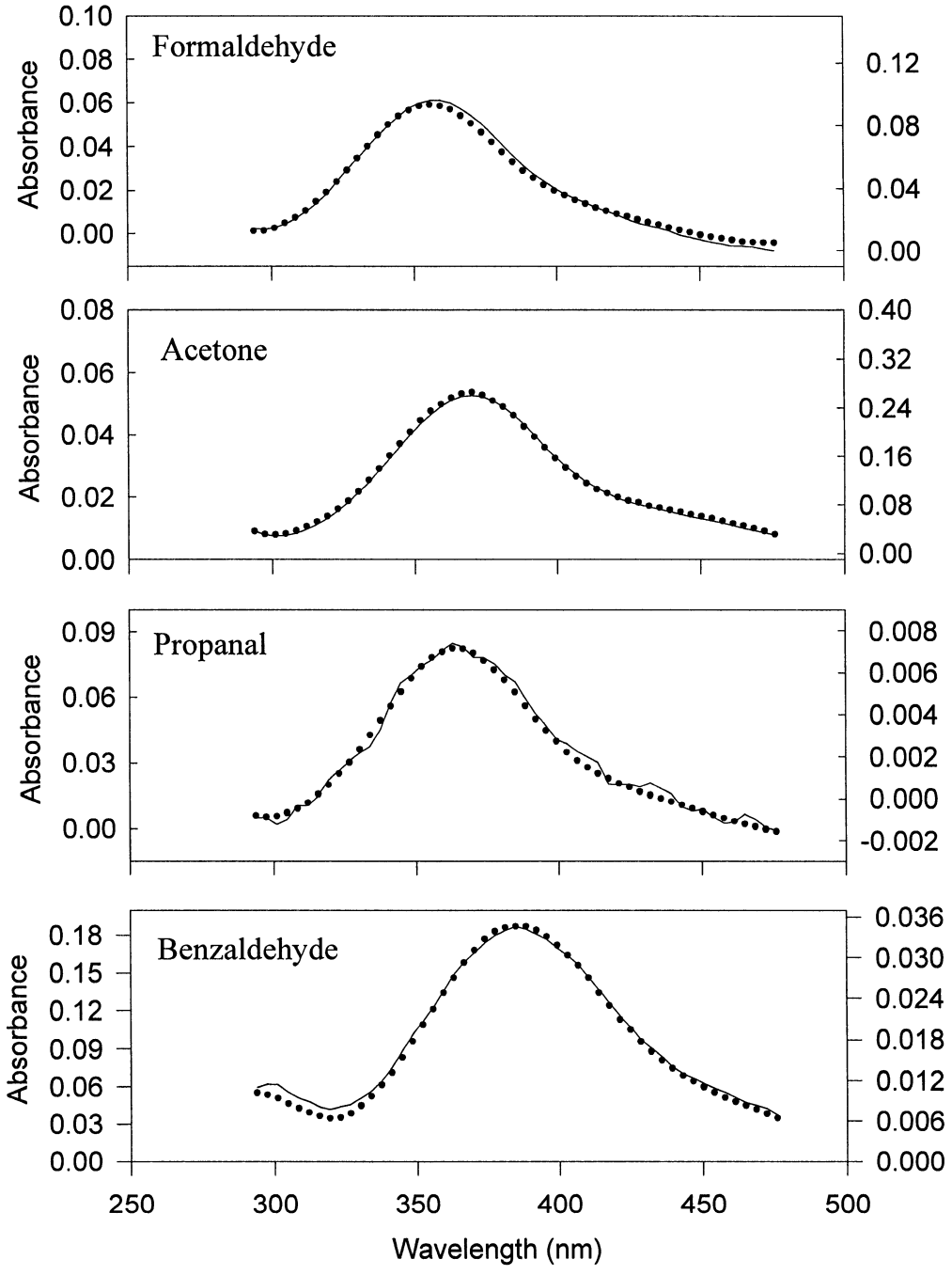

Figure 15. Spectra for carbonyl peaks compared to standard injection spectra. Solid lines show the spectra for ambient samples collected during the Hamilton 1999 study, and the circles show the spectra for standard injections. In all cases, the sample spectra are plotted on the right hand scale, and the standards are plotted on the left hand scale.

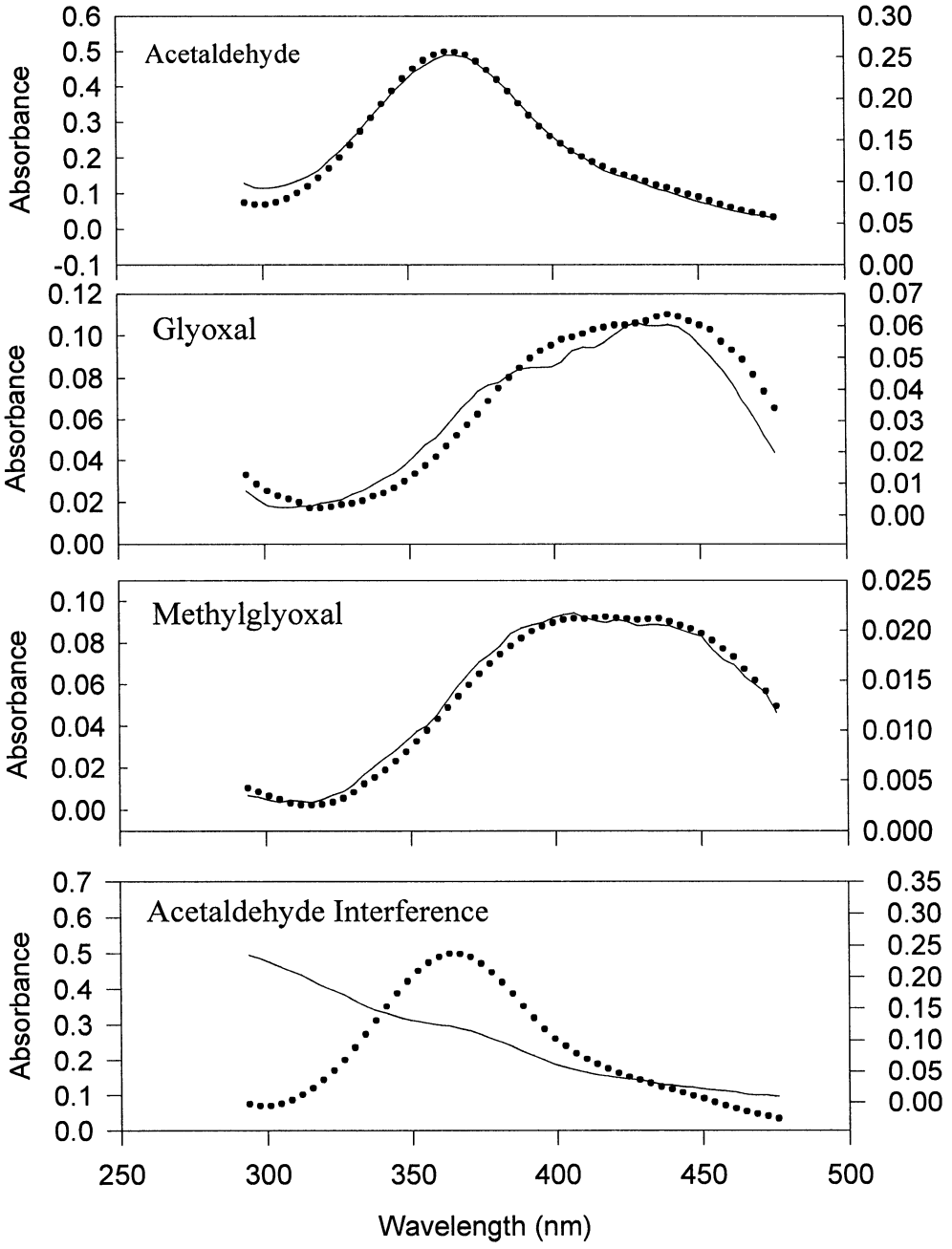

Figure 16. Spectra for carbonyl peaks compared to standard injection spectra. Solid lines show the spectra for ambient samples, and the circles show the spectra for standard injections. In all cases, the sample spectra are plotted on the right hand scale, and the standards are plotted on the left hand scale. An interference with acetaldehyde was found for several samples during Hamilton 1999. The compound is unknown, but its spectra has been included in the lower plot with the acetaldehyde standard for comparison.

To obtain a spectrum for a peak, it was necessary to perform a background correction on the raw data stored by the data collection software. The time at which the highest absorbance occurs for a given peak was used, to maximize the signal to noise ratio. In general, this was done by selecting times before and after the peak where a clean baseline signal exists. The absorbance spectra for those times were then linearly interpolated to the time of the peak of interest to provide a background spectrum. This spectrum was then used as a correction for the spectrum of interest. For peaks of low intensity, several spectra were averaged together both for the peak, and the background subtraction, to reduce the noise in the signal. The agreement between the atmospheric and standard spectra was excellent in general, and so the peaks were most likely correctly identified, and well resolved from other analytes. In the case of glyoxal, the background correction was difficult to perform due to other peaks eluting before and after the glyoxal peak. Some deviation is seen between the standard and the sample spectra because of this. The identification of glyoxal is nevertheless fairly certain. Agreement with literature spectra is also excellent (for example Druzik *et al*, 1990)

3.3. Standard Generation System and Carbonyl Recoveries

A dynamic gas standard generation system (Figure 17) was developed and used successfully for many of the carbonyls of interest. Development of a dynamic

calibration system was pursued due to the uncertainties associated with static gas phase carbonyl standards. Long term stability of carbonyl gas cylinder standards can be an issue, and the use of Teflon bags to make standards can also be problematic due to the permeability of carbonyls through the Teflon walls (Biesenthal, 1997b). The system developed here is based on a syringe pump delivering an accurate liquid flow into a known flow rate of clean air.

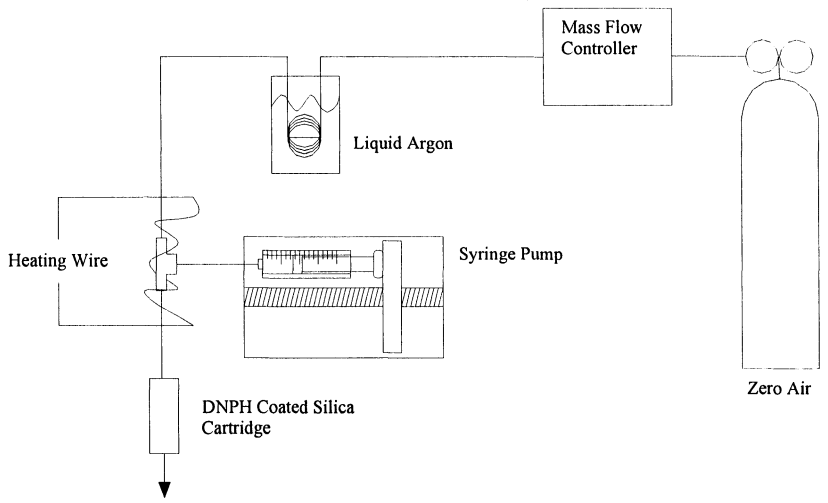

Figure 17. Dynamic Carbonyl Standard Generation System

The syringe pump system was seen as an inexpensive method to generate carbonyl standards of various concentrations quickly and without any long term stability issues. The system is quite simple, and allows the accurate dynamic generation of gas phase carbonyl standards. The liquid used in the syringe pump was

made by diluting a small volume of carbonyl in a solution of 50% water and 50% acetonitrile. The absolute amount of carbonyl added to the solution can be somewhat uncertain for compounds which are not available as a "pure" liquid. For example, formaldehyde is available as formalin solution which is ~40% formaldehyde in water. The carbonyl solution used is therefore calibrated by injecting a small accurate volume of standard solution into a DNPH solution to form the hydrazone. This solution was then diluted by various amounts and injected onto the HPLC to generate a hydrazone calibration curve. The linear slope of this calibration curve was used as the response factor for the instrument so that gas phase recoveries for the carbonyls passed through the cartridge can be determined.

The sampling flow rate used was 50 mL/min controlled by a flow controller. The sampling time used was ~1 hour. The relative humidity resulting from the water content of the carbonyl solution is estimated as ~25%. Air was supplied from a cylinder of zero air with a liquid argon trap installed after the flow controller to remove any impurities from the air. Experiments were done both with and without the liquid argon trap, and no difference was seen suggesting little or no carbonyl contamination from either the cylinder or the flow controller. A 1/16" stainless steel Swagelok tee piece was used to connect the syringe to the gas flow. The syringe was connected by a custom made syringe tip with a 1/16" stainless steel tube silver soldered onto it, so that no septa are needed in the system. This eliminates the potential for septum bleed when elevated temperatures are used. The tee piece and

tubing after it was heated to ~80°C to evaporate the liquid quickly and avoid losses to the walls. Gas phase concentrations were varied by changing the syringe pump flow rate and maintaining both the sampling time and the gas flow the same. The system was allowed to stabilize for about 1 hour prior to sampling. The recoveries were calculated by taking the ratio of the best fit slope for the gas phase runs to the best fit slope for the liquid injections. For both liquid and gas phase runs, for all compounds, the calculated zero intercept was not significantly different from zero, and so the slopes were determined by forcing a zero intercept. Reasonable results were obtained for these compounds, with ~100% recoveries seen. These results suggest that the use of a liquid hydrazone standard for calibration of instrument response is a valid calibration method. This is advantageous since gas phase calibrations in the field would significantly increase the complexity of the instrument, and also raise concerns about contamination from liquid carbonyls used to generate the standards. A plot of the results obtained for acetaldehyde is shown in Figure 18. Compounds for which recoveries have been determined are listed in Table 5.

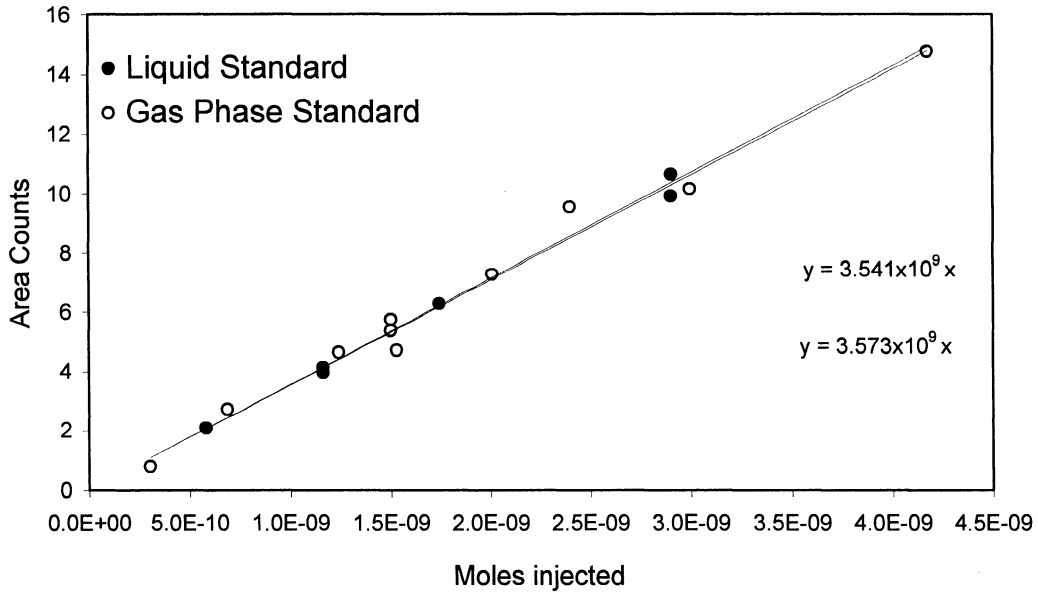

Figure 18. Acetaldehyde recoveries determined using the dynamic standard generation system.

Species	% Recovery (95%) CI)
Formaldehyde	99.3 ± 9.2
Acetaldehyde	100.9± 5.1
Propanal	107.8 ± 7.1
Acetone	108.7 ± 6.2
Benzaldehyde	105.1 ± 5.2

Table 5. Recoveries of gas phase carbonyls in the 1 to 10 ppbV range on the silica cartridge.

Compounds found to be problematic using this system were glyoxal and methyl glyoxal. Both of these compounds are only available as a pentamer made up of 3 molecules of carbonyl and 2 molecules of water. For the synthesis of hydrazone solids these compounds behave as the carbonyl would when reacting with DNPH. However, when generating a gas phase standard, it is difficult to know what form these carbonyls are in when they enter the gas phase. This makes it difficult to determine the true recoveries for gas phase glyoxal and methyl glyoxal. It was found that the gas phase concentrations were consistently low for glyoxal and methyl-glyoxal. To try to fix this problem, the lines were heated to higher temperatures, but it was found that elevated levels of formaldehyde and acetaldehyde resulted, most likely due to thermal decomposition of glyoxal and methyl-glyoxal (see section 3.11).

3.4. Sampling Flow Rate Experiments

The sampling flow rate of 50 ml/min was used because of the physical limits of pulling air through the silica cartridge. When a pump is used to pull air through the cartridge, the maximum pressure drop possible is 15 psi. The real pressure drop will be less than 15 psi since the flow controller adds a restriction to the flow. The maximum flow rate obtainable for the system and cartridge used was ~90 ml/min. To ensure reproducible flows during field operation a lower flow rate of 50 ml/min was used. The recovery experiments (section 3.3) showed that at 50 mL/min the carbonyls were quantitatively trapped. It is expected that at some higher flow rate

carbonyls may not be quantitatively trapped, due to either incomplete trapping on the packing material, or incomplete reaction, or a combination of both. This experiment did not give any information about the flow rate at which losses of analytes would be seen. Experiments were therefore done at higher flow rates using a cylinder of air to provide a higher pressure than what was possible by using a pump to pull air through the cartridge. The results of the experiment are shown in Figure 19. The results suggest that at flow rates up to 200 mL/min no losses were seen for this cartridge, adding confidence to the use of this cartridge at 50 mL/min.

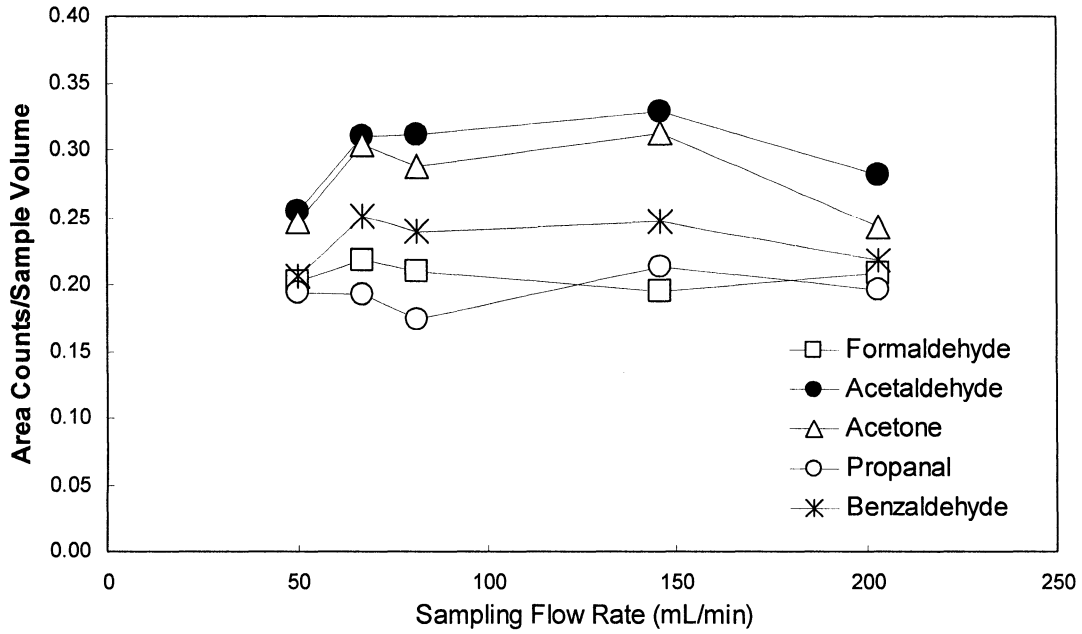

Figure 19. Sampling flow rate experiment showing complete trapping of analytes at flow rates up to 200 mL/min.

3.5. Detection Limits and Blank Determinations

To accurately quantify an analyte peak from an atmospheric sample, it is necessary to determine the blank value for the analyte. The blank value simply represents the instrumental response for a given analyte when no sample has been taken. This can be determined by performing the entire procedure, omitting only the sampling step. The concentration detection limit (C_{dl}) for an analyte is generally defined as $3\sigma_{bl}$ (Skoog and Leary, 1992), where σ_{bl} is the standard deviation of the equivalent atmospheric concentration represented by the blank determinations. If an analyte has a significant blank value, then the C_{dl} will be determined by the variability in the blank value. If an analyte has no significant blank value, then the C_{dl} is determined by the noise in the instrumental signal. If peak areas are used for quantification, then blank determinations for analytes with no significant blank value, can be determined by integrating an area of the chromatogram, obtained for the blank determinations, with the same retention time and baseline width as the analyte of interest. The atmospheric concentration C_{dl} for an analyte can then be determined using the standard deviation of the blank value, the atmospheric sample size, and the instrumental response for an analyte. Reduction of the C_{dl} in a method is usually desirable since it results in more reliable atmospheric data. Also a lower C_{dl} allows shorter sampling times, and therefore better time resolution for ambient sampling. Reducing the C_{dl} for compounds with significant blank values can be done by either

reducing the blank peak height to less than the noise levels of the signal, or by designing the method to give very consistent blank values.

The reduction of blank values can be accomplished by reducing the sources of contamination for analyte species. The most problematic carbonyl analytes are formaldehyde and acetone. Formaldehyde can be particularly problematic when using silica based packing materials, since formaldehyde is often a reagent in the manufacturing of silica. Also, formaldehyde polymerizes easily to para-formaldehyde and other similar compounds. If the silica packing material is exposed to ambient air before use, it is possible for it to absorb formaldehyde. Once on the packing, the formaldehyde can then polymerize making it difficult to remove. Researchers in the past have attempted to remove the formaldehyde by letting the packed cartridges soak in DNPH solution for 1 week before use (Sirju and Shepson, 1995). Another potential source of contamination is the cartridge itself. Typically used cartridges for the manual DNPH method, such as the Sep-Pak cartridges sold by Waters, are often made of polymeric materials, into which the packing materials are placed. These polymers could potentially allow carbonyls into the cartridge, since they are somewhat porous, and can allow the transfer of compounds through the walls of the cartridges. The polymers themselves may also emit carbonyls and so could be a source of carbonyl contamination. Acetone is a ubiquitous solvent, and its presence in a laboratory setting is unavoidable. Thus elimination of the acetone contamination requires a method where little or no contact between room air and the solutions is

possible. This would also eliminate the contamination for any other analytes which may be present in room air.

The issues of carbonyl contamination were addressed in this project, and resulted in a significant improvement in both blank levels and C_{dl} over the manual cartridge methods. The cartridge used in this project was made of stainless steel with minimal use of Teflon as a seal material. This was expected to be more reliable, in terms of contamination, than a polymeric cartridge casing. Also, since the same cartridge was used continuously, any impurities in the silica would eventually be removed through continuous use. All solvents used, including the DNPH coating solution, were maintained under ultra high purity helium continuously, to avoid any possibility of contamination from lab air. This also ensured that the blank levels from impurities in the DNPH solution would remain constant over time.

Reducing the C_{dl} was accomplished by automating the instrument using a single cartridge. This eliminates any potential cartridge to cartridge variability which may exist if multiple cartridges are used. It also allows blanks to be determined as part of the sampling cycle, so that blanks are determined using the same cartridge used for sampling. The use of an online sampling, derivatization and injection method allowed the elimination of the manual extraction procedure, which eliminates any possibility for contamination during manual handling. The result of the above steps was a significant improvement in the C_{dl} for the DNPH method. The blank value and C_{dl} for the carbonyls which were seen in significant concentrations during

the Simcoe 2000 study are listed in Table 6. Detection limits for other carbonyls can be estimated as being similar to acetaldehyde, since their responses will be similar to acetaldehyde, and the detection limit will be determined by the standard deviation in the blank value and the response.

A comparison of the detection limits obtained with this instrument and several of those obtained for other DNPH cartridge methods shows that an improvement has been realized. Typical detection limits for the generally problematic formaldehyde often reach levels which are quite high (Table 2, page 17-20). Grosjean E. *et al*, 1996f, for example, achieved detection limits of 480 pptV for a sampling time of 4 hours with a sample volume of 180 L. Benning and Wahner, 1998, realized 3σ formaldehyde detection limits of 600 pptV and 1200 pptV for two different periods of a study for 30 min, 32 L air samples. For acetaldehyde, Benning and Wahner, 1998, obtained 3σ detection limits of 600 pptV and 2700 pptV for the same two periods. Apel *et al*,1998, report 100 pptV detection limits for 3 hour, 180 L samples. The difference between the detection limits becomes more apparent when one realizes that the sample volume used in this project was 2 L, with a sampling time of 42 min. Also, as will be discussed in section 5, room for improvement still exists based on the experimental work performed here, with minor modification to the current system.

	Formaldehyde	Acetaldehyde	Acetone	Glyoxal
Blank Value	17	39	35	13
Detection Limit for Ambient Air Samples	89	54	54	39

Table 6. Detection limits and average blank values for 13 blank determinations during Simcoe 2000. Values are in pptV for both the detection limits and the blank values.

3.6. DNPH Reaction Kinetics Experiments

The kinetics of the reaction between carbonyls and DNPH on the silica cartridge were studied to determine whether or not the carbonyls would require some time for the reaction to go to completion before the sample could be injected on the HPLC system. This reaction was studied in two different ways. The first was to quickly sample a low volume, high concentration standard. This allows the sample to be collected in a short time, so that the reaction starting time can be determined with a precision of ~2 to 3 min. The other was to sample a more realistic typical ambient concentration in the low ppb level, for the normal sampling time. The two experiments were similar in all respects other than the sample concentration and sampling time, which were adjusted to maintain the total number of moles roughly equivalent in the two experiments. The estimated amount of DNPH loaded onto the silica packed cartridge for all work in this project is 1.8×10^{-7} moles. Under the

conditions of these experiments, and in the field, the total amount of DNPH consumed during sampling is always <2% of the loaded amount, and in most cases <1%, assuming a 3.0 L sample volume with 15 ppbV total carbonyl concentration.

The high concentration standards were generated using the syringe pump method with the experimental setup shown in Figure 20. A heated 19 mL stainless steel sample loop was connected to a 1/16" Valco sampling valve. A standard was generated using a syringe pump to inject a mixture of carbonyls at a flow rate of 4 μL/min into an air flow of 20L/min controlled by a calibrated MKS flow controller. The liquid carbonyl mixture was made by diluting 5 mL of each carbonyl into a 25 ml flask; 5 mL of this was then diluted into 100 mL total using 50% acetonitrile in water. The resulting gas phase concentration was about 500 ppbV. The sample loop was flushed out with this standard, after which the contents of the loop were transferred to the sampling cartridge by switching the valve from load to inject. The contents of the loop were transferred onto the cartridge for a short time of a few minutes at a flow rate of 69 mL/min using a calibrated flow controller. The reaction time is the total time from the switching of the sample valve to the time at which the cartridge was filled with water before injection.

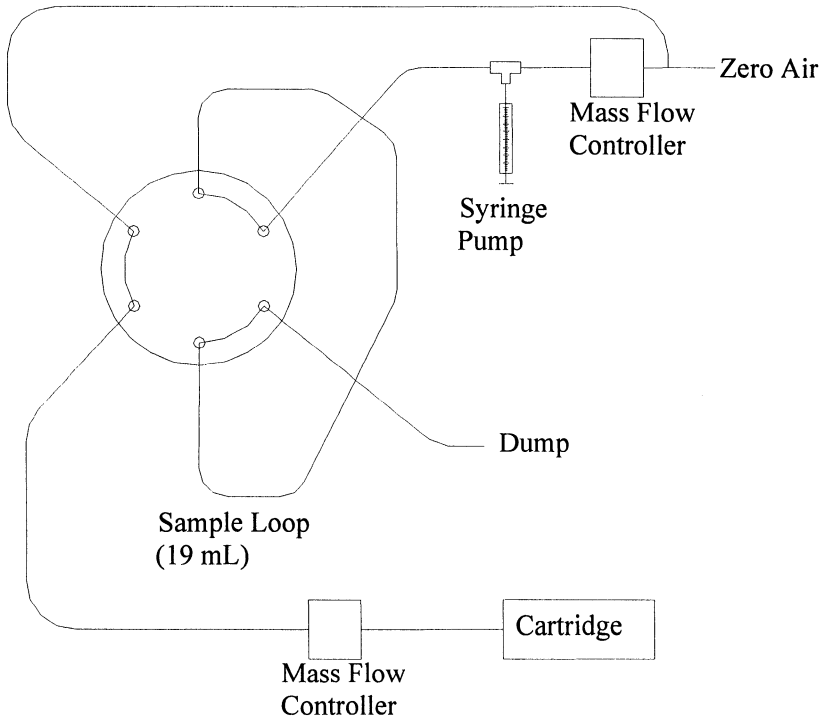

Figure 20. High concentration carbonyl standard system for testing reaction kinetics.

Low concentration standards were generated using the same system as in Figure 17 (section 3.3) with the dynamic syringe pump method. Carbonyl standards in the 2 to 4 ppbV range were used for the carbonyls of interest. A sampling time of about 50 min was used. The reaction time is the time the cartridge was allowed to sit after sampling was finished, and before being filled with water and injected onto the HPLC system for analysis.

Using high concentration standards, it was found that some carbonyls required a significant amount of time to be completely derivatized. The results of this experiment are shown in Figure 21. This was found to be true for all the ketones

tested up to C_5. The aldehydes however did not show the same results, and were all found to be completely derivatized in less than 3 minutes. The low concentration standards showed no significant difference between a 2 minute reaction time and a 3 hour reaction time as can be seen in Figure 22. This suggests that under the conditions used for ambient sampling, no significant reaction time is needed, and the cartridge can be filled with water and injected as soon as sampling is complete. This may only be true for sampling times of greater than 50 minutes however, and so these results do not necessarily suggest that complete derivatization will be seen for much shorter sampling times. As always, experiments must be done using conditions as similar to ambient sampling conditions as possible. The results here suggest that the data collected during the field studies in this project do not suffer from any incomplete derivatization problems.

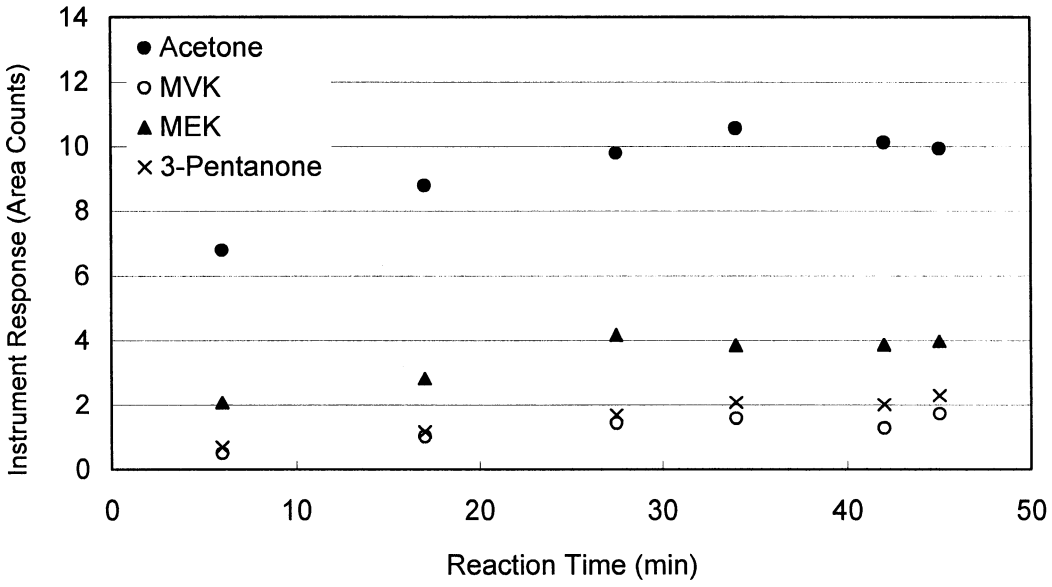

Figure 21. Reaction Kinetics for ketones on the silica cartridge using a high concentration standard.

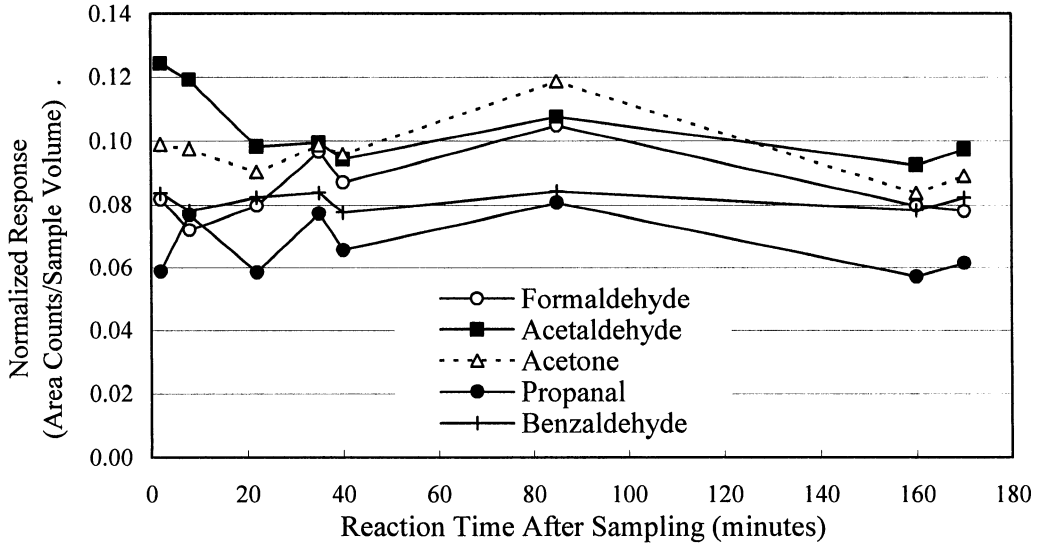

Figure 22. Reaction kinetics for carbonyls sampled for ~50 minutes at 50 mL/min in the 2 to 4 ppbV range.

3.7. Cartridge Filling Volume

After sampling is complete, the cartridge must be filled with a liquid before injection. The liquid used for this was water since the hydrazones are relatively insoluble in water, and water allows peak compression to happen during the injection. Filling the cartridge with the exact amount of water needed would be ideal, since no analytes could be lost. This however required a relatively expensive syringe pump to deliver the exact volume of water. It was hoped that the hydrazones would be insoluble enough in water, that the cartridge could be overfilled without losing any analytes. This would require an inexpensive solenoid valve to simply turn the water flow on and off. An experiment was performed to determine the amount of water where significant amounts of analytes would be lost. The dead volume within the cartridge is ~15 μL, thus for volumes larger than this, some amount of water, and possibly analytes, is lost from the cartridge. The analyte which showed the highest loss was formaldehyde, with the results shown in Figure 23. It is obvious, from these results, that the volume of water used to fill the cartridge must be controlled accurately, and so it was necessary to use a syringe pump in the instrument to fill the cartridge with water. The losses for formaldehyde were largest, most likely due to the higher solubility of the formaldehyde hydrazone relative to the other hydrazones. In fact the losses for individual hydrazones were in general related to their retention times on the instrument. Later eluting compounds experience smaller losses, as expected, since they are less water soluble.

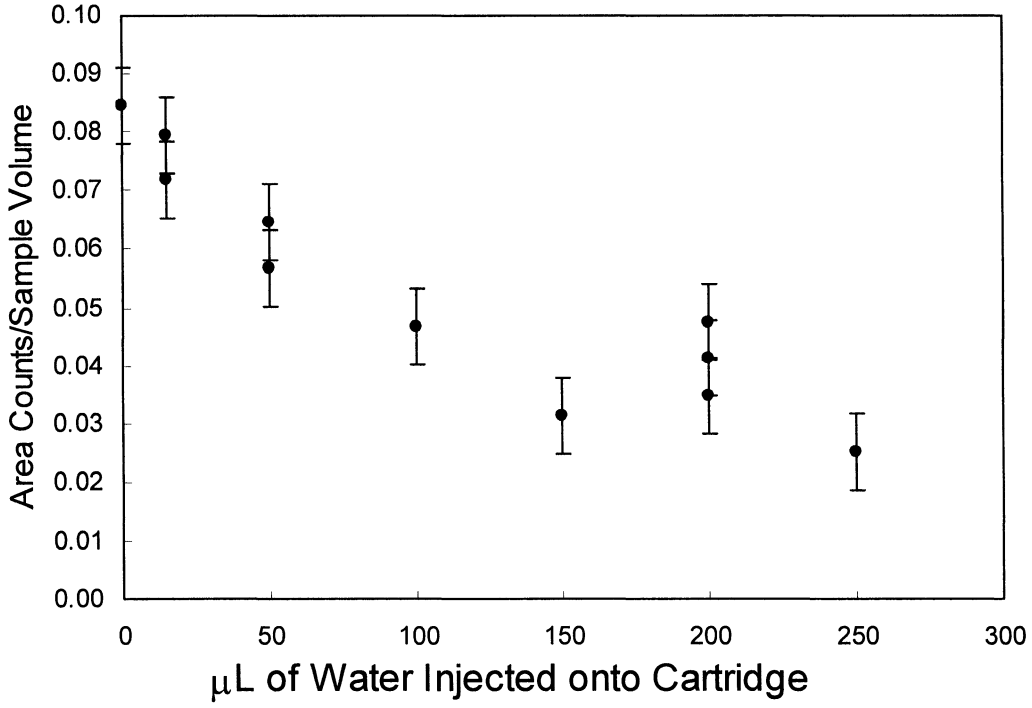

Figure 23. Effect of overfilling the cartridge with water after sampling on instrument response for formaldehyde.

3.8. Ozone Removal Experiments

The potential problem of ozone interfering with the analysis of trace atmospheric organic species, in methods using pre-concentration techniques, has been known for some time, along with the need for ozone removal from the sample matrix (Slemr, 1991; Rodier and Birks, 1994; Helmig, 1997; Kleindienst, 1998). A summary of the methods used for ozone removal, and the artifacts which have been

documented, is given by Helmig, 1997. For the various DNPH derivatization methods, both positive and negative interferences have been observed by researchers. Other observed effects include the formation of DNPH products which may interfere with the chromatographic separation, and also the depletion of the DNPH on the cartridges. The use of DNPH coated C_{18} cartridges, with no ozone removal, generally resulted in positive interferences. Pires and Carvalho, 1998, observed formation of artifact carbonyl hydrazones up to C_{18}. Arlander *et al*, 1995b, observed the formation of C_3 to C_7 artifact peaks. These artifacts are most likely due to the reaction of ozone with the C_{18} packing material, resulting in the formation of carbonyls that are subsequently derivatized by the DNPH present on the cartridge. The use of DNPH coated silica gel cartridges were found to generally suffer from losses of both the DNPH, and the carbonyl hydrazones. Arnts and Tejada, 1989, found significant losses of formaldehyde in the absence of ozone removal. Sirju and Shepson, 1995, observed both the loss of carbonyl hydrazones, and the loss of DNPH from the cartridge.

These observations guided the selection of the sampling system used in this project. The potential problem of positive artifacts was considered more significant than the problem of a small loss of analyte. The fact that artifact peaks were known to occur with carbon containing packing materials suggested that the use of these should be avoided. If silica gel were to be used as a packing material though, the issue of negative interferences would still have to be dealt with. This issue was

addressed by using an ozone removal trap filled with potassium iodide in the system inlet. The combination of a silica packed cartridge and an ozone removal system was seen as an effective combination to minimize both positive and negative artifacts due to ozone interferences.

3.8.1. Ozone Transmission Through the KI Ozone Scrubber

The reaction between O_3 and potassium iodide (KI) is (Vairavamurthy *et al*, 1992):

$$O_3 + 2KI + H_2O \rightarrow I_2 + 2KOH + O_2 \qquad \text{(R18)}$$

To ensure the KI filled O_3 scrubber was effective at removing O_3, two experiments were set up to test a KI trap of the same dimensions and from the same source of KI as the trap used in the field.

In the first experiment a ¼" Teflon tube was filled with 0.163 g of KI, and the outlet was fitted with a ¼" stainless steel screen with 10μm openings, to prevent the KI from leaving the trap. As in the field, the KI was obtained from a freshly opened Waters Sep-Pak ozone scrubber cartridge to ensure its purity. An Environmental Corp. Dasibi model 1003-RS instrument was used to both generate and measure the O_3. An air stream was provided from a cylinder of zero air. The air stream was humidified by passing the air flow coming out of the O_3 generator through a bubbler filled with pure water from a millipore water purification system. The resulting relative humidity was found to be 55% ±10% at 25°C. The flow rate of the

humidified ozone air mixture through the KI trap was 2 L/min since the O_3 monitor requires a flow rate of 2 L/min. The flow rate used in the field was only 50 ml/min, thus the experiment performed here are at a flow rate 40 times higher than in the field, and so is a rigorous test of the effectiveness of the trap. The highest level of O_3 seen in the field was ~90 ppbV, and so this was used as the test concentration. The O_3 level in air having passed through the cartridge was 1 ± 1 ppbV. Thus no significant O_3 concentration was seen downstream of the KI trap at the 2 L/min flow rate. It is therefore expected that at a flow rate of 50 ml/min flow rates used for sampling, the KI trap should be effective at removing O_3 to << 1 ppbV.

The second experiment was set up to determine how long the trap could be used for, since the effectiveness of the KI trap at removing O_3 is expected to decrease with use. The amount of O_3 which can be passed through a trap before a decrease in efficiency is seen, was checked by passing 25°C air at 55% ± 10% relative humidity with 250 ppbV of O_3 through the trap for several hours at a flow rate of 2 L/min. The amount of ozone which had passed through the trap can be expressed in terms of the product of the concentration of O_3 and the volume of air (i.e. 1 L of air with 1 ppbV O_3 = 1 ppb·L O_3). The results of the experiment are shown in Figure 24.

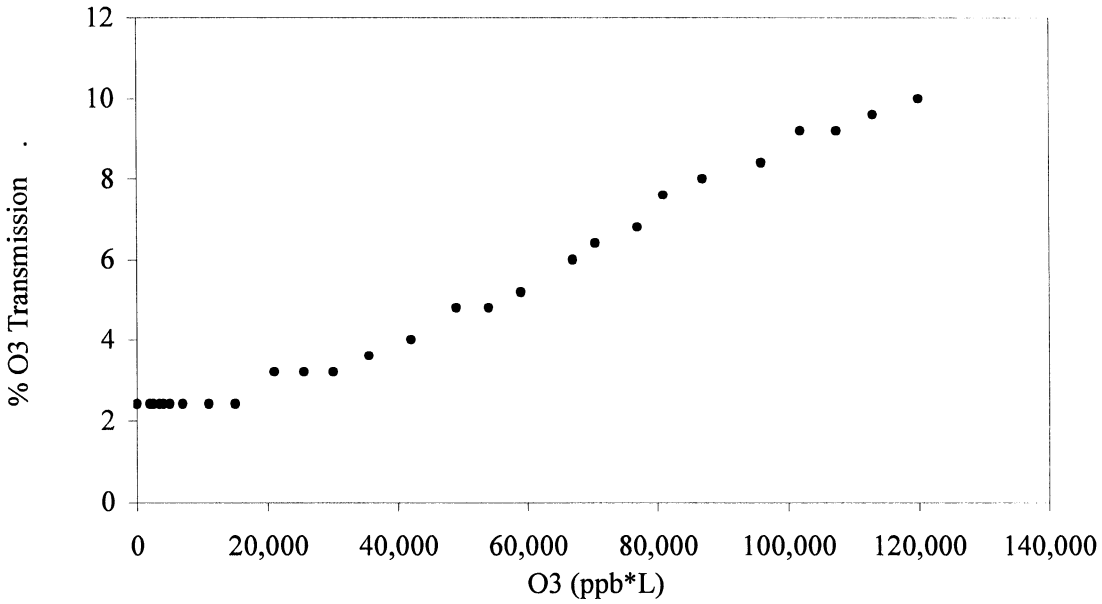

Figure 24. Increase in O_3 transmission through the KI filled O_3 scrubber. O_3 concentration of 250 ppbV at 2 L/min was used with a relative humidity of 55%.

The trap removes ozone at full efficiency until about 20000 ppb·L of O_3 have passed through the trap. In the field, the amount of O_3 passed through a trap can be estimated using the volume of a sample, the number of samples for which a trap was used, and the concentration of O_3. Each trap was used for <100 2L samples of air at <100 ppb of O_3. As an upper limit, the amount of O_3 scrubbed by a KI trap was 20000 ppb·L O_3. Generally the traps saw <10000 ppb·L of O_3, and so were changed well within their lifetime of highest efficiency.

3.8.2. Ozone Interference Experiment

To test the possibility of ozone creating a positive interference for any of the analytes of interest, in the analytical system, a gas phase concentration of 120 ppbV of ozone was sampled through the instrument. This test was performed to rule out the possibility of artifacts from any reaction between O_3 and any component of the sampling system, including the sampling lines, the valves and DNPH coated cartridge. The instrument was set up the same as it was in the field. A KI ozone trap was placed in the sampling line, and the same Teflon connecting line was used. Ozone was generated by photolysing O_2 in air using UV light from a mercury pen lamp and a ¼" quartz tube. A Thermo Instruments Corporation ozone monitor was used to monitor the concentration of ozone. Many large analyte peaks were seen when a cylinder of zero air was used as the air source, which caused a great deal of concern. In the absence of UV light no analyte peaks were seen, suggesting the source of the contamination was not the air cylinder. Attempts were made to remove any contaminants from the air cylinder by passing the air through a ¼" stainless steel open tube cooled in liquid argon. Many of the anaylte peaks decreased in size, but were still significant. However, the decrease in the contaminant peaks suggested a connection between the use of a cryogenic trap and the contamination. To improve the trapping efficiency of the tube, it was packed with ~100 μm glass beads, and again cooled with liquid argon. With this setup, no significant analyte peaks were seen, suggesting that ozone does not create positive artifact peaks using this instrument for

ozone levels up to 120 ppbV. The most likely explanation for these results, is that hydrocarbons in the zero air cylinder were oxidized in the quartz tube creating artifact peaks. Removal of the hydrocarbons using a packed tube cooled in liquid argon eliminated the hydrocarbons, and the artifact peaks disappeared.

Several samples were taken in lab air, using the UV pen lamp to generate ozone in the lab air. The purpose of this experiment was to determine whether realistic air samples would be affected by the presence of ozone. The ozone level was monitored at the same place as the inlet to the sample line. High ozone concentrations in the ~100 ppbV range were generated. Samples taken with a laboratory concentration of 30 ppbV ozone and 100 ppbV of ozone were not significantly different. Although this experiment can not be used to rule out any interferences at very low levels (<0.1ppb) due to the changing concentration of carbonyls in the lab, it suggests that there are no major artifacts created by ozone, at least for the air found in a laboratory setting, when a KI ozone trap is used on the inlet line. The possibility of ozone artifacts are still possible for different air samples, if highly ozone reactive hydrocarbons are present. The possibility of a significant interference is remote however due to the effective use of an ozone scrubber.

3.8.3. Carbonyl Transmission Through the KI Ozone Scrubber

The loss of carbonyls on the KI O_3 scrubber has been seen by other researchers (Biesenthal, 1997), where the losses were found to be due to an excessive amount of KI used in the ozone trap. Smaller amounts of KI allowed complete transmission of the carbonyls tested, although no information was available for several carbonyl species of interest in this project. To ensure that the carbonyl analytes of interest here were not lost on a KI filled trap of the same mass used in the field, low ppb level carbonyl standards were generated using the standard generation system described in section 3.3. The standard was sampled alternately with and without the KI trap. Three samples were collected without the KI trap, and four were collected with the KI trap in place. The average response with and without the trap is shown in Figure 25. No significant carbonyl losses were seen using a scrubber with the same mass of KI as what was used in the field, while providing adequate ozone removal. The error bars represent the 1σ uncertainty based on the number of measurements made in each case.

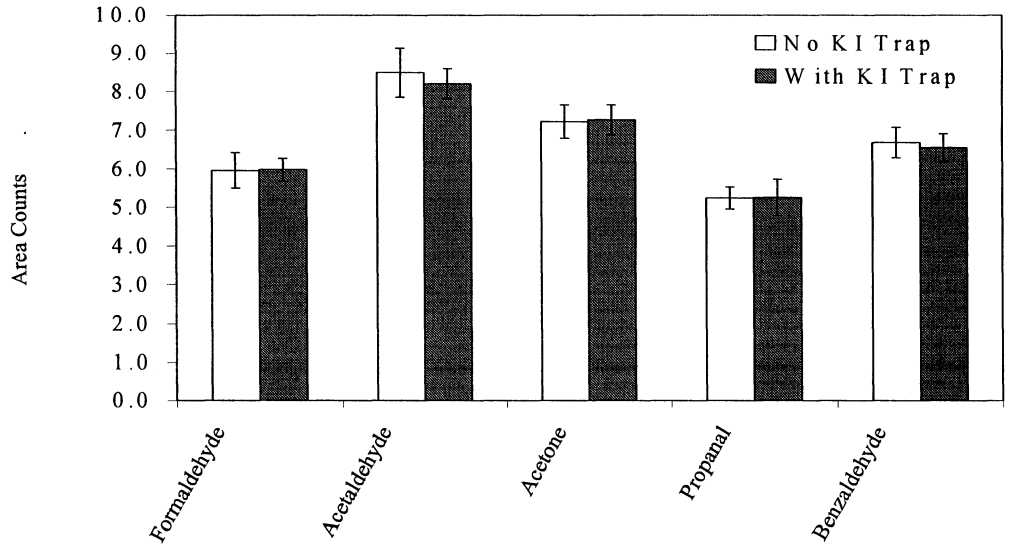

Figure 25. Carbonyl transmission through the KI filled cartridge.

3.9. Instrument Reproducibility

The reproducibility of the final automated instrument was tested using a high concentration (~200 ppb) gas phase acetone standard prepared in an air cylinder. The cylinder was allowed to sit for several months after being made so that the acetone concentration would be stable. This high concentration standard was then diluted down to more realistic concentrations for ambient samples using a cylinder of zero grade air as a dilution gas, and 2 calibrated Tylan mass flow controllers. The concentration of the final standard was close to 4 ppbV. The instrument was allowed to sample as it would for ambient air, by drawing in standard air using the air pump

and the instrument mass flow controller at 50 ml/min for about 45 min. The results are shown in Figure 26.

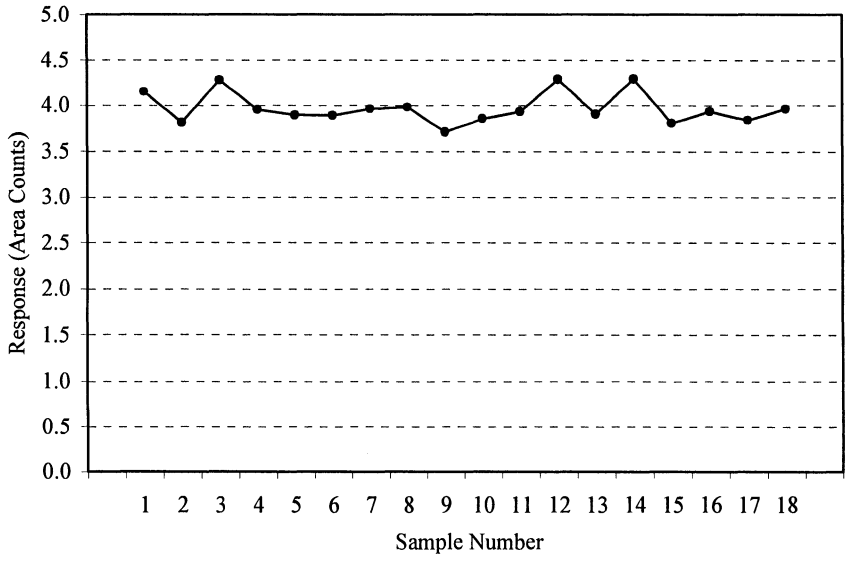

Figure 26. Instrument reproducibility for acetone using automated instrument in its final form, as used in the field.

The relative standard deviation was 4.3% for 18 samples. The true precision of the instrument must be lower than this value since the experiment relies of the precision of 2 mass flow controllers for the results. The flow controllers' precision is estimated at ~1% to 2%, and may be a significant contribution to the stated instrumental precision. The 4.3% precision determined with this experiment is nevertheless quite adequate for atmospheric sampling.

3.10. Carbonyl Gas Phase Calibrations

To test the entire system, using the automated method, gas phase calibrations were done using standards generated with the syringe pump system (section 3.3). The gas phase concentrations used were ~2 ppbV for the carbonyls of interest in zero air with ~ 40% relative humidity generated using a bubbler filled with water from a Millipore filtration system. Experiments were performed using instrumental conditions identical to those used for sampling in the field, including a KI filled ozone scrubber. Gas phase responses for the carbonyls tested were found to be within 10% of the liquid phase hydrazone standard calibrations for formaldehyde, acetaldehyde, acetone and propanal. Benzaldehyde was found to be somewhat lower than expected, with losses of 20%. Although the cause for the losses could not be determined, most likely there was a problem in the procedure used for generating the standard. The ambient data has not been corrected for this loss, since it is not certain that the loss is instrumental, rather than an experimental setup problem. The uncertainty in the benzaldehyde data has been increased to reflect this 20% loss.

3.11. Glyoxal and Methylglyoxal Gas Phase Calibrations

Significant time was spent to try to generate a glyoxal gas phase standard in the low ppb range with minimal results. Commercially available glyoxal is sold as a 40 % aqueous solution. In the presence of water however, glyoxal is present in a polymerized form, rather than simply being dissolved. Despite significant effort, gas

phase standards generated with the system described in section 3.3, with this glyoxal solution, were consistently found to yield low glyoxal recoveries. It was found that the newer the solution was, the higher the glyoxal gas phase concentration was when sampling through the instrument. Also, it was found that the higher the concentration in the liquid phase was, the closer the gas phase concentration was to the calculated value. These results suggest a problem in the generation or the stability of the liquid solution. For this reason, the possibility of synthesizing pure glyoxal for the purpose of generating gas phase standards was explored. The procedure and results are described below.

Pure glyoxal was synthesized from paraglyoxal dihydrate using the procedure of Steacie *et al* (1935). Briefly, the solid glyoxal dihydrate was heated with phosphorous pentoxide to yield gas phase glyoxal, in a small round bottom flask. The reaction vessel was kept under zero grade air for the entire process. The gas generated was cryogenically trapped in a glass tube, by connecting the tube to the reaction vessel, and allowing the air to flow through the tube. The tube was fitted with two Teflon valves so that it could be sealed and refrigerated. To trap the gas, the tube was placed in liquid argon. Once trapped, the valves were sealed, and the solid was refrigerated. To determine whether the gas produced in the synthesis was in fact glyoxal, gas phase FTIR spectra of the generated gas were obtained, and were found to be in excellent agreement with the literature values (Shimanouchi, 1972). Attempts to extract the glyoxal from the glass tube with a syringe, after being warmed

to room temperature, proved to be difficult due to the viscosity of the liquid. It is not known whether or not the glyoxal was pure, or had polymerized, since glyoxal polymerizes with traces of water. This method of generating a glyoxal standard proved to be difficult, with no results obtained for gas phase calibrations.

To generate a reliable gas phase glyoxal or methylglyoxal standard is a challenging task, which could not be completed. For this reason, the responses for both glyoxal and methylglyoxal are based entirely on the calibrations performed using liquid phase hydrazone standards. Since no information is available as far as gas phase concentrations are concerned, no comparison can be made. The parts of the system where problems may be expected are the KI filled ozone scrubber, and the sampling cartridge. The crystalline KI is hydroscopic, and so will absorb some amount of water during sampling. Glyoxal and methylglyoxal have high water solubilities, and so could possibly be lost on the KI trap, until the water becomes saturated. This of course represents a loss process in the system, and would cause a decrease in measured ambient concentrations if it were significant. The potential problems with the sampling cartridge are incomplete trapping and incomplete derivatization. Both of these problems, if they exist, represent losses of glyoxal and methylglyoxal. The ambient glyoxal and methylglyoxal data collected as part of this project should therefore be considered a lower limit since potential gas phase losses exist with this sampling method.

3.12. Estimate of Measurement Uncertainty

The total uncertainty in the atmospheric analysis of carbonyls using this instrument can be estimated as,

$$\frac{\sigma_i}{[carbonyl]_i} = \sqrt{\left(\frac{\sigma_{A_i}}{A_i}\right)^2 + \left(\frac{\sigma_{B_i}}{B_i}\right)^2 + \left(\frac{\sigma_{C_i}}{C_i}\right)^2} \qquad \text{Equation 9}$$

where σ_i is the absolute uncertainty in $[carbony]_i$, σ_{Ai} is the uncertainty in the response (A_i) determined with liquid phase standards, σ_{Bi}/B_i is the relative error in the instrumental reproducibility, and σ_{Ci}/C_i is the realtive error in the gas phase recovery for $carbonyl_i$. σ_{Ci}/C_i is estimated to be 10% for all carbonyls except for benzaldehyde, where gas phase calibrations agreed with the liquid phase values within ~20%. The value of σ_{Bi}/B_i is estimated to be 4.3% as given in section 3.9, and of course includes the uncertainty in the sample volume. The uncertainty in the liquid phase calibrations is estimated to be 5%. This gives an estimated uncertainty of ~12%, at the 1σ confidence level. In the case of benzaldehyde, the uncertainty is estimated to be ~21%.

3.13. Sample Chromatogram

A representative sample chromatogram collected during Simcoe 2000 is shown below. The sample was collected at approximately 10:00 PM on July 16th 2000. The signal plotted, is described in section 2.2.3, and is referred to as a 'Total Absorbance' signal.

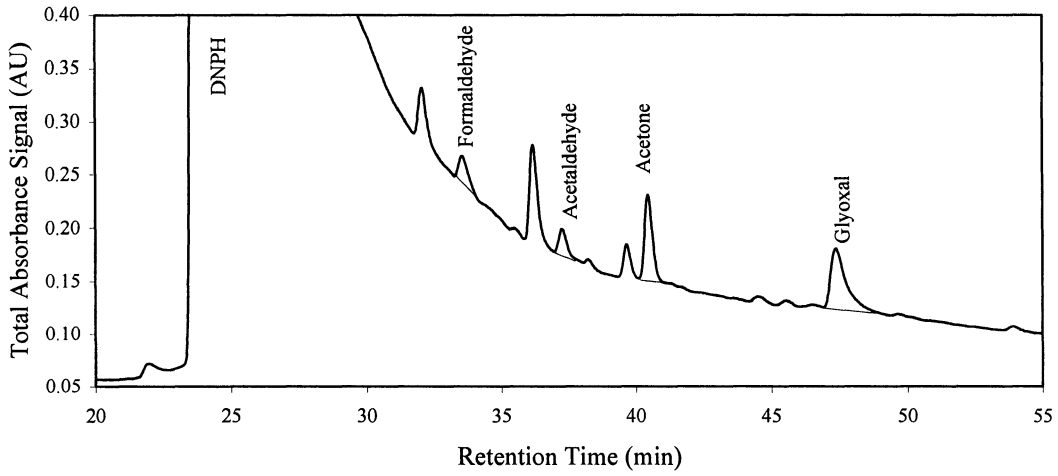

Figure 27. Sample chromatogram collected using the automated system during Simcoe 2000.

4. RESULTS AND DISCUSSION

4.1. Hamilton 1999 Study

The time series for compounds measured during the study conducted in Hamilton in the summer of 1999 are presented in Figure 28, Figure 29 and Figure 30. The compounds for which significant concentrations were seen during the Hamilton 1999 study were formaldehyde, acetaldehyde, acetone, propanal, benzaldehyde, glyoxal, and methyl glyoxal, with median concentrations of 4.8, 4.1, 2.3, 0.13, 0.27, 0.07, and 0.18 ppbV respectively. The time series for several other supporting measurements conducted at the same site are also included. A significant urban smog event occurred during the study on the days of July 14, 15, and 16. This time period was associated with high temperatures and south to southwest winds. The ozone level exceeded 80 ppbV at its peak each of the three days during the event at this site. Also, significant airborne particulate levels were seen during the same period and are also plotted in Figure 30. The elevated ozone and particulate levels indicate significant photochemical activity occurring during this period. Carbonyl measurements will be discussed with respect to this polluted period and also the somewhat cleaner air conditions that occurred later in the study. One of the most interesting carbonyls measured at this site was glyoxal. Its peak concentrations coincided with the smog event and the high ozone levels seen. A significant difference between the episode period and the cleaner period following the episode can be seen in the glyoxal data

presented in Figure 29. Possible reasons for these observations, and the significance of the other carbonyls measured will be discussed.

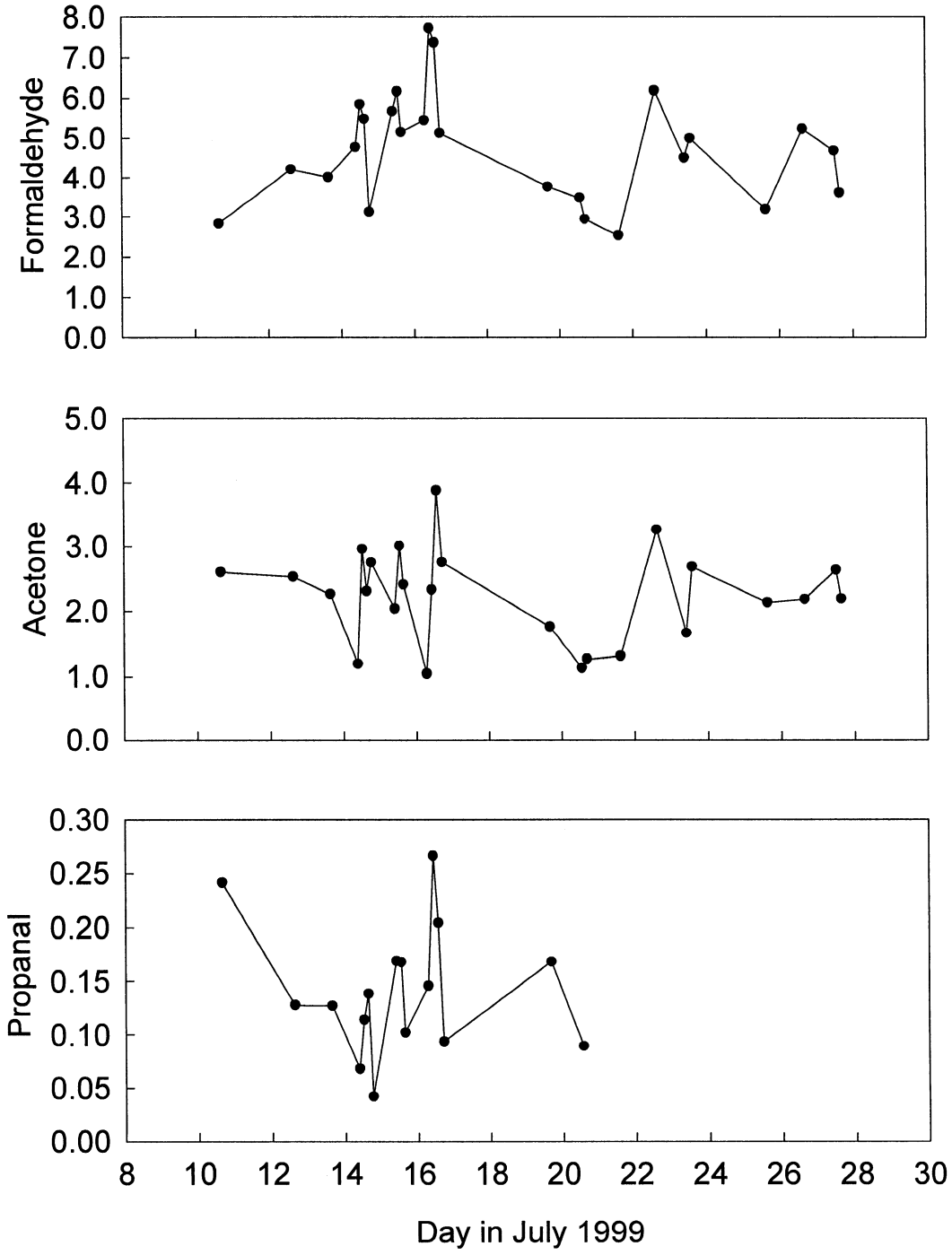

Figure 28. Formaldehyde, acetone and propanal concentrations at the Lynden site in Hamilton for July 1999. Concentrations are in ppbV.

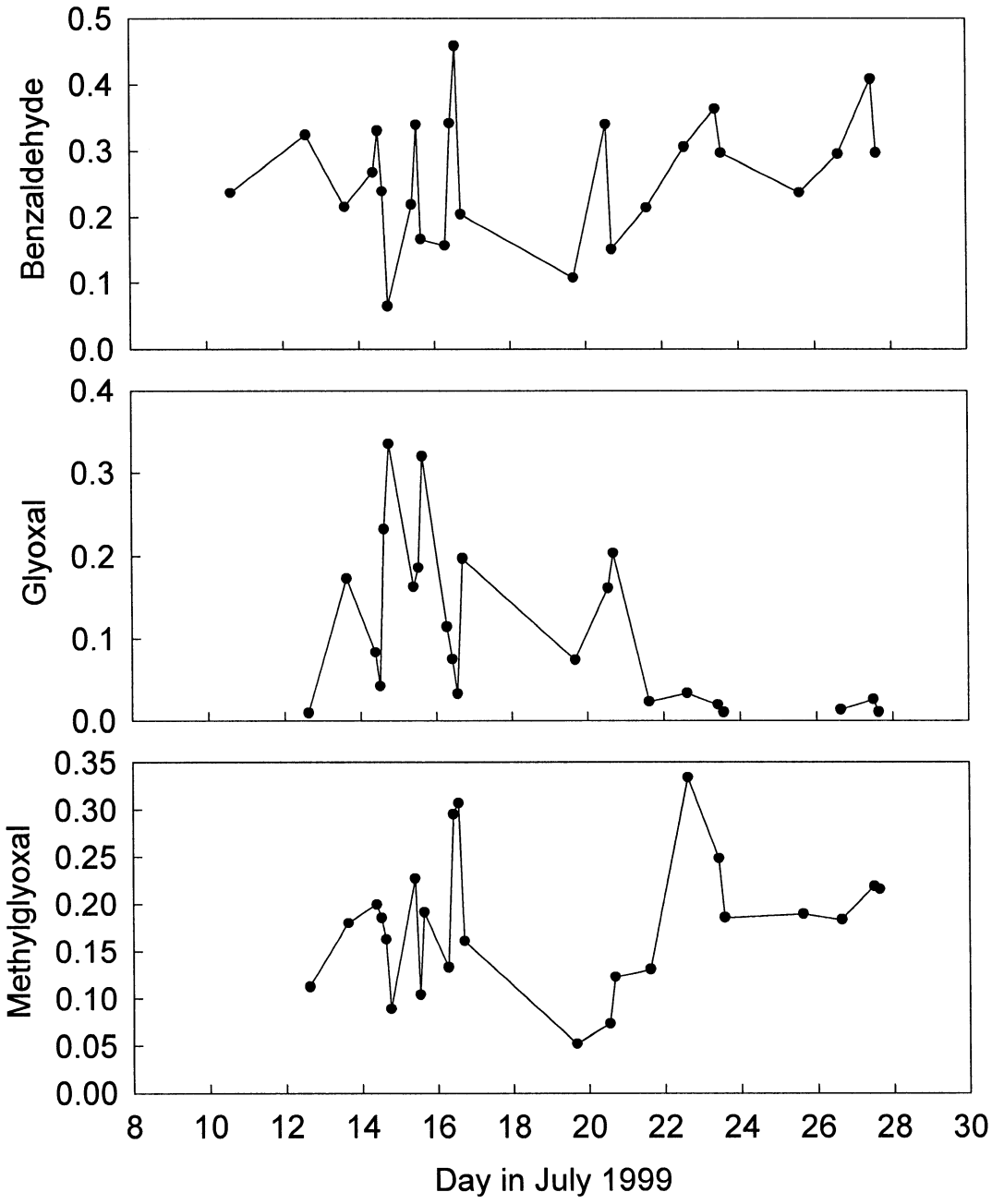

Figure 29. Benzaldehyde, glyoxal and methylglyoxal concentrations at the Lynden site in Hamilton for July 1999. Concentrations are in ppbV.

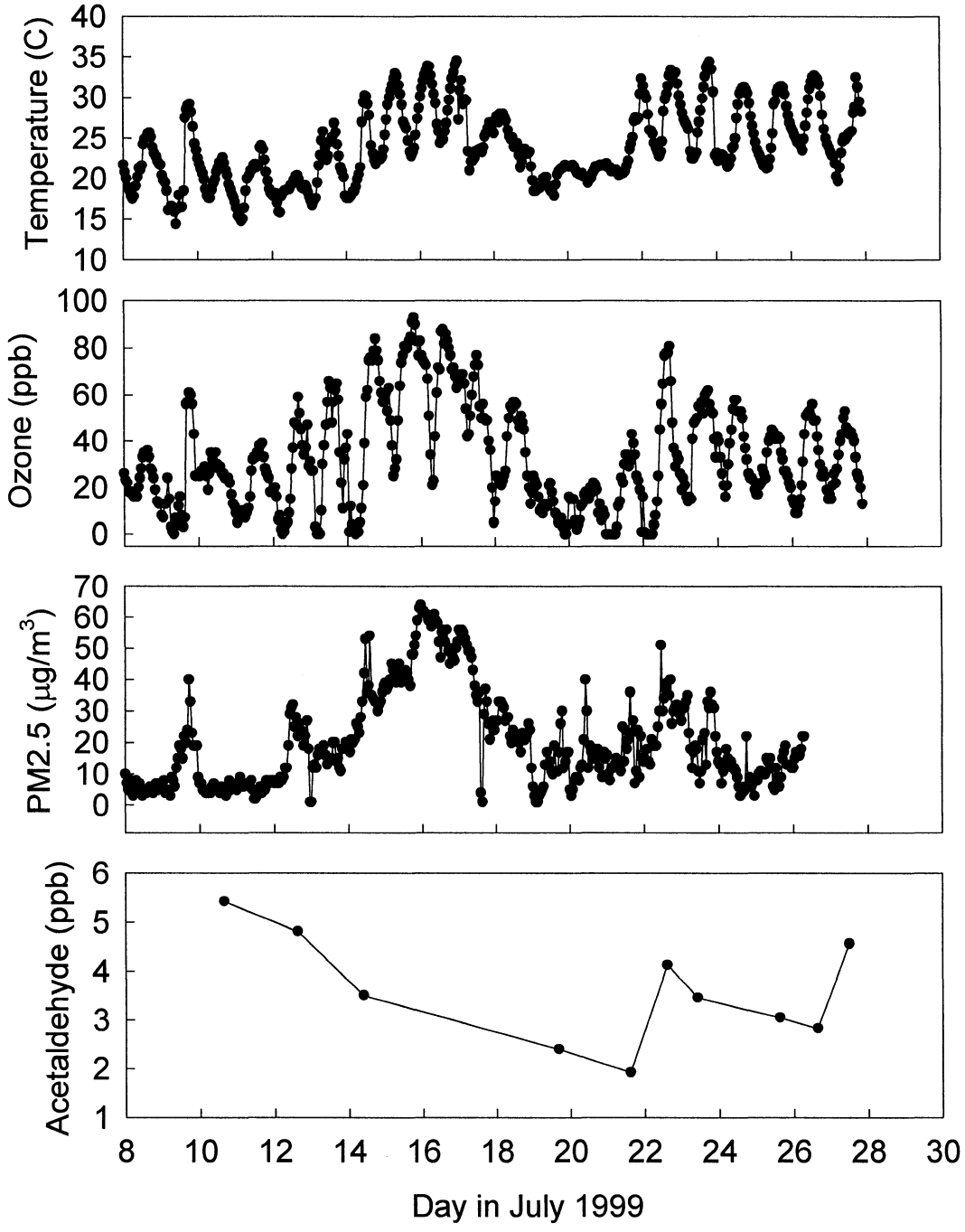

Figure 30. Acetaldehyde, ozone and PM2.5 concentrations at the Lynden site in Hamilton for July 1999. Temperature data was obtained from the Woodward site in Hamilton.

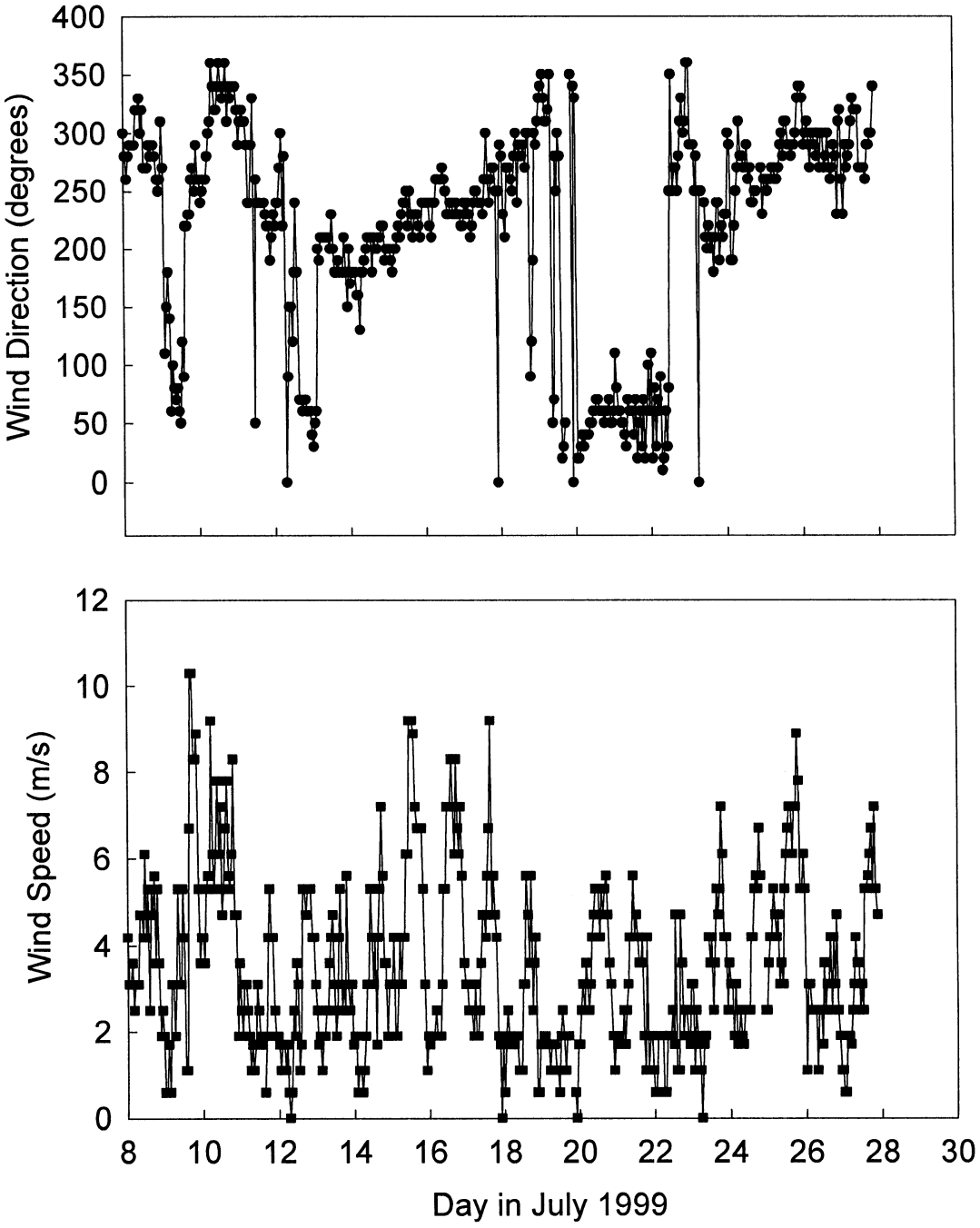

Figure 31. Wind speed and wind direction at the Hamilton Airport for July 1999.

4.1.1. Discussion of Glyoxal Measurements

The oxidation of aromatic hydrocarbons is known to lead to the formation of airborne particulate matter (Forstner *et al*, 1997). In urban areas, aromatic hydrocarbons are emitted in significant amounts from vehicular emissions (Fraser *et al*, 1998). Measurement of the oxidation products of aromatic hydrocarbons can be used to give some insight into the aromatic chemistry occurring in the atmosphere. The carbonyl species resulting from the oxidation of aromatic hydrocarbons that have been measured in this study include benzaldehyde, glyoxal and methylglyoxal (Dumdei and O'Brien, 1984) . Glyoxal and methylglyoxal are formed in various yields from many aromatic hydrocarbons, as can be seen in Table 7. Glyoxal is also formed from the oxidation of acetylene, and this source must also be considered when interpreting the glyoxal concentrations.

Compound	Yield			10^{12}×k(HO) ($cm^3molecule^{-1}s^{-1}$)
	Glyoxal	Methylglyoxal	Aromatic Carbonyl	
Acetylene	0.7±0.3	-	-	0.815
Benzene	0.207±0.019	-	-	1.23
Toluene	0.08-0.15	0.075-0.146	0.07-0.12	5.96
Ethylbenzene	-	-	-	7.1
O-xylene	0.034-0.087	0.116-0.246	0.05-0.10	13.7
M-xylene	0.086-0.13	0.319-0.42	0.04	23.6
P-xylene	0.225-0.24	0.105-0.12	0.08	14.3
1,2,3,-Trimethylbenzene	0.072-0.058	0.152-0.18	0.06	32.7
1,2,4,-Trimethylbenzene	0.048-0.078	0.357-0.37	0.06	32.5
1,3,5,-Trimethylbenzene	-	0.602-0.64	0.03	57.5
O-Ethyltoluene	-	-	-	12.3
M-Ethyltoluene	-	-	-	19.2
P-Ethyltoluene	-	-	-	12.1

Table 7. Rate constants and product yields for the formation of α-dicarbonyls and aromatic aledehydes from the oxidation of acetylene and aromatic hydrocarbons. The range shown represents the highest and lowest values reported in the literature. Values obtained from Atkinson, 1990 and references therein.

To estimate the production rate of a carbonyl compound in the atmosphere, several pieces of information are required. These include the atmospheric concentrations of the parent hydrocarbons that produce the carbonyl, the production yield of that carbonyl from each hydrocarbon, the reaction rates of the parent hydrocarbons with the various atmospheric oxidants, and the concentration of the oxidants themselves. The aromatic hydrocarbons do not react with O_3 or NO_3 to any significant extent under atmospheric conditions, and so only reactions with $HO^{\cdot}$ need to be considered (Atkinson, 1990). For short lived species such as glyoxal (atmospheric lifetime of ~2 hours, Table 1, section 1.4.2), it is reasonable to assume a

local steady state, during midday periods, when conditions are expected to be reasonably stable. Assuming a local steady state exists for glyoxal, the production rate of glyoxal (P_{gly}) then is equal to the removal rate of glyoxal (R_{gly}):

$$P_{gly} \approx R_{gly} \qquad \text{Equation 10}$$

The removal rate of glyoxal is given by

$$R_{gly} = k_R[\text{glyoxal}] \qquad \text{Equation 11}$$

where k_R is the rate constant for the removal of glyoxal. Combining Equation 10 and Equation 11 gives:

$$[\text{glyoxal}] \approx P_{gly}/k_R \qquad \text{Equation 12}$$

Since $1/k_R$ is simply the lifetime (τ), the expression becomes,

$$[\text{glyoxal}] \approx P_{gly} \cdot \tau \qquad \text{Equation 13}$$

The production rate of glyoxal from toluene ($P_{gly,tol}$), can be given by,

$$P_{gly,tol} = k_{tol,HO}[HO][toluene]\gamma_{tol,HO} \qquad \text{Equation 14}$$

where $\gamma_{tol,HO}$ is the yield of glyoxal from toluene oxidation by HO$^{\cdot}$, and $k_{tol,HO}$ is the reaction rate of toluene with HO$^{\cdot}$. The total production of glyoxal from all the aromatic hydrocarbons and acetylene (P_{gly}), can be estimated by adding the production terms together giving:

$$P_{gly} = k_{tol,HO}[HO][toluene]\gamma_{tol,HO} + k_{benz,HO}[HO][benzene]\gamma_{benz,HO} + \ldots \qquad \text{Equation 15}$$

The $HO^{\cdot}$ radical concentration is assumed to be 5×10^6 molecules/cm^3 for typical midday conditions. The atmospheric lifetime of glyoxal can be estimated as follows. The major loss mechanisms during the day will be via reaction with $HO^{\cdot}$ and photolysis, since ozone reaction is known to be negligible (Plum *et al*, 1983). It is also assumed that deposition to the surface is a minor loss mechanism during the day. A rate constant with $HO^{\cdot}$ of 1.15×10^{-11} molecules$^{-1}\cdot cm^3 s^{-1}$ (Plum *et al*, 1983), gives a pseudo first order rate of 5.75×10^{-5} s^{-1} for glyoxal with $HO^{\cdot}$. The glyoxal photolysis rate for a solar zenith angle of 50° is estimated as 7.4×10^{-5} s^{-1} using the methods and values given by Jenkin *et al*, 1997. The overall removal rate for glyoxal can then be estimated as the sum of the two removal rates giving 1.3×10^{-4} s^{-1}. The lifetime of glyoxal can then be estimated as ~2 hours.

Hydrocarbon concentrations were determined during this study by Dr. J. Rudolph's research group, York University. Using the hydrocarbon data, the contribution of acetylene and aromatic oxidation to the production of glyoxal can be estimated. Unfortunately separate concentration values are not available for meta-xylene and para-xylene, and only a sum is available for these two species due to incomplete chromatographic separation. The sum was assumed to be entirely para-xylene, since para-xylene has a greater glyoxal yield. Where more than one literature value for glyoxal yield from a hydrocarbon is given in Atkinson 1990, the value is given as a range in Table 7, and an intermediate value has been used for the calculations. For hydrocarbons where no glyoxal yield has been measured, a value

similar to the yield from toluene of 0.12 has been assumed. 1,3,5-trimethylbenzene is assumed to have a glyoxal yield of zero.

The estimated steady state concentrations of glyoxal from some selected hydrocarbons are shown in Figure 32. The total estimated steady state glyoxal is also shown in Figure 32. Only data having been collected between 12:00PM and 6:00PM local time have been included. The total steady state concentration from these oxidation sources is shown with glyoxal concentrations in Figure 34 for comparison. The high value seen on the day of July 19th has been omitted from the calculations, but has been included in Figure 32 and Figure 34. Rain occurred at the site on the day of the 19th and conditions were generally cloudy throughout the day. The site was also influenced by wind directly from the city of Hamilton on the days of the 19th and 21st. The hydrocarbon concentrations for the samples taken on these two days are then strongly influenced by local emissions, and therefore may not be useful for examining secondary chemistry. Also, the assumption of local steady state may not be reasonable under these conditions, with strong influence from nearby primary emissions. Also, since the glyoxal values on these two days, when winds were directly from the city, are fairly low (107 pptV and 66 pptV respectively), it is likely that any direct urban source of glyoxal is minor.

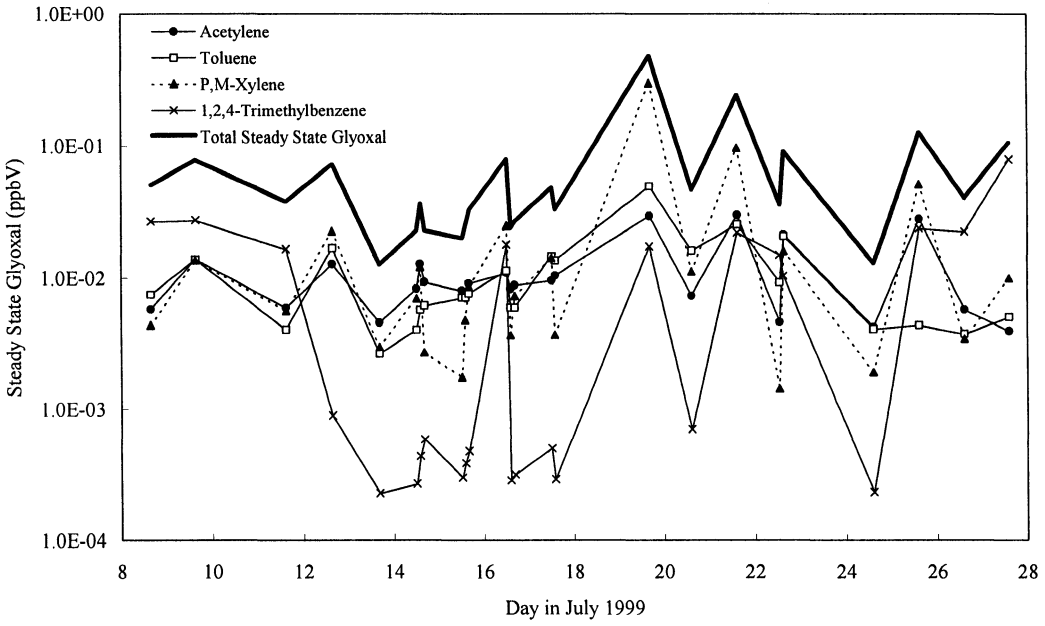

Figure 32. Estimated glyoxal concentration (molecules cm^{-3}) from the oxidation of acetylene and selected aromatic hydrocarbons at Lynden station. Note the logarithmic concentration scale. Only samples collected during the period between 12:00PM and 6:00PM local time have been included. Note that not all individual hydrocarbon contributions have been plotted, although all have been included in the total glyoxal production curve.

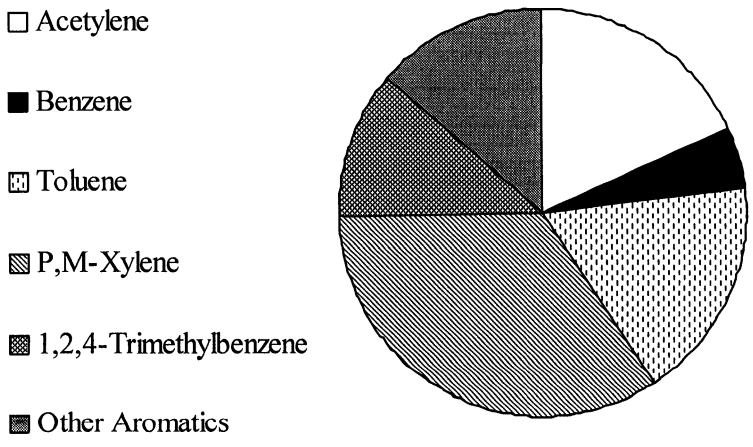

Figure 33. Distribution of estimated hydrocarbon contribution to glyoxal production during Hamilton 1999.

The distribution of estimated glyoxal production from the hydrocarbons has been plotted in Figure 33. Para-xylene and meta-xylene together represent about 34% of the glyoxal from these hydrocarbon sources. This is an uncertain estimate however, since the individual hydrocarbon values are unknown. Acetylene, toluene and 1,2,4-trimethylbenzene represent 18%, 18%, and 12% respectively. The measured and estimated concentrations of glyoxal are shown in Figure 34. The observed concentration of glyoxal is ~4 times higher than the steady state concentration that can be attributed to the oxidation of these hydrocarbons during the episode period of July 14th to 16th, and ~6 times lower during the cleaner period of July 22nd to 27th. The high glyoxal during the episode period suggests that some other source of gas phase glyoxal exists, other than the oxidation of the hydrocarbons examined here, or that the lifetime of glyoxal has been underestimated.

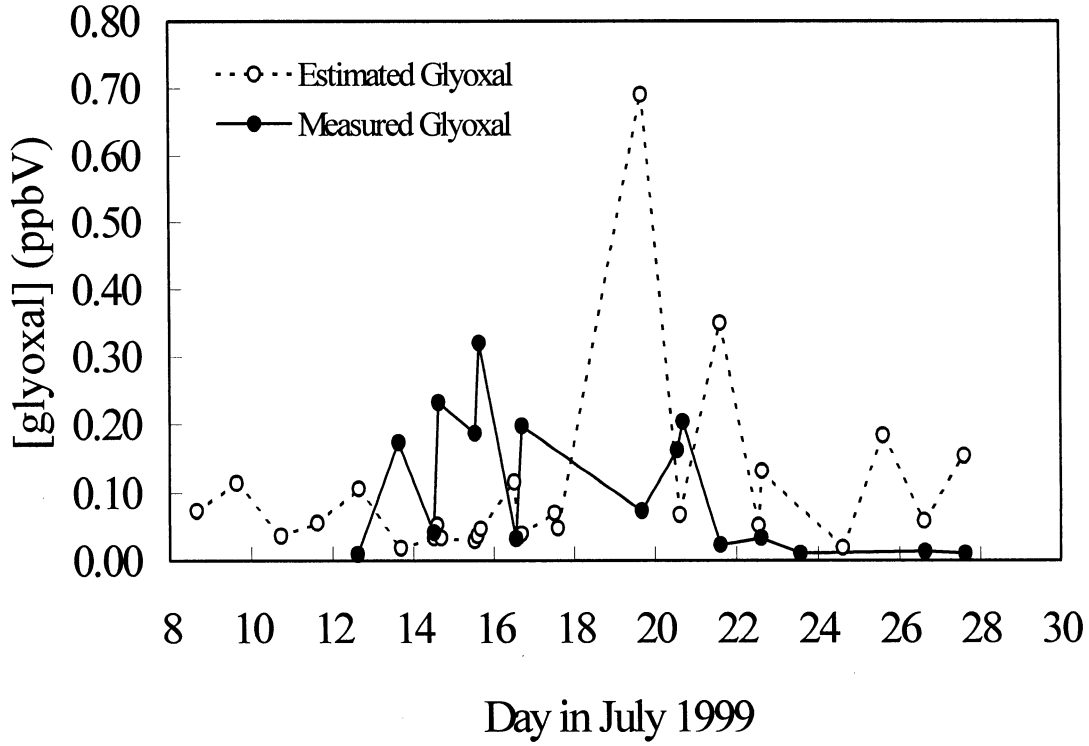

Figure 34. Glyoxal estimated and measured concentrations from the oxidation of acetylene and aromatic hydrocarbons. Only data collected between 12:00PM and 6:00PM local time has been included.

This analysis is somewhat uncertain however, since the estimate of the glyoxal production from hydrocarbon oxidation can be affected by many factors, including the estimated $HO^{\cdot}$ concentration. There overall uncertainty in the estimated glyoxal can be estimated to detrmine the significance of the differences between the measured and estimated glyoxal values. An error in the hydroxyl concentration will affect both the production rate and the removal rate of glyoxal. Since the production is dominated by hydroxyl reactions and the removal by photolysis is slightly higher than for hydroxyl

reaction, an underestimate in the hydroxyl will result in an underestimated glyoxal concentration. The assumed hydroxyl is perhaps within a factor of 2, leading to an uncertainty in the glyoxal at steady state of approximately a factor of 2. This uncertainty alone is significant relative to the fairly small difference seen between the estimated and measured glyoxal. Other potential sources of uncertainty include the uncertainties in the yields. Although difficult to estimate, the error this introduces again would diminish the significance of the difference seen between measured and estimated steady state glyoxal. The uncertainty in the identity of meta and para-xylene will cause the estimated glyoxal to be somewhat high. The most significant uncertainty though is likely to be the estimated hydroxyl concentration, leading to an overall uncertainty of perhaps a factor of 2 in the estimated glyoxal concentrations.

If in fact another source of glyoxal exists, then the source could be secondary (*i.e.* from the gas phase oxidation of other hydrocarbons not examined here), primary anthropogenic emissions, or from some other unknown source. The glyoxal concentrations seen after the episode, appear to be lower than the calculated values. The reasons for this difference are unclear. Wind directions and temperatures during the two periods are reasonably similar, with winds coming from the south west, and peak temperatures of ~30°C. A minor difference is seen in the peak ozone values during the two periods, where on the 15th, 16th and 17th the ozone was over 80 ppbV, after the 22nd, the ozone was below 60 ppbV. Although small, this difference in peak

ozone levels possibly suggests a link between ozone and the observed glyoxal. The nature of this link is unclear however.

Examination of the glyoxal data during the episode period along with the ozone data shows an interesting relationship as seen Figure 35. Although a slight temporal shift exists, there is a definite similarity between the glyoxal and ozone concentrations on July 14th and July 15th. For comparison with the ozone data, a 3.6 hour shift has been applied to the glyoxal data, which is also shown Figure 35. The time of 3.6 hours used here has been arbitrarily chosen, since there appears to be a 3 to 4 hour temporal lag between the glyoxal and the ozone data. Although the significance of the fact that there is a shift in time between the glyoxal and ozone is not clear, it is clear that there is a similarity between the two compounds on these days as shown in Figure 36. The calculations based on aromatic chemistry suggest that a source of gas phase glyoxal may exist which has not been accounted for. The relationship between glyoxal and ozone may suggest a secondary source of glyoxal since ozone is a product of oxidation chemistry. If this were the case, then one would expect a reasonably good relationship between glyoxal and other secondary species of similar lifetime for this period. Figure 37 shows the relationship between glyoxal and benzaldehyde. It is obvious that no significant correlation exists for either the episode days of July 14th and 15th or for the rest of the period. Benzaldehyde was chosen as a species for comparison since it is a product of toluene oxidation, with a yield of ~10% (Atkinson, 1990; Yu, 1997). The poor correlation between glyoxal and benzaldehyde again suggests that toluene

oxidation is most likely not a major source of the observed glyoxal, and further that aromatic oxidation is also not a major source of glyoxal.

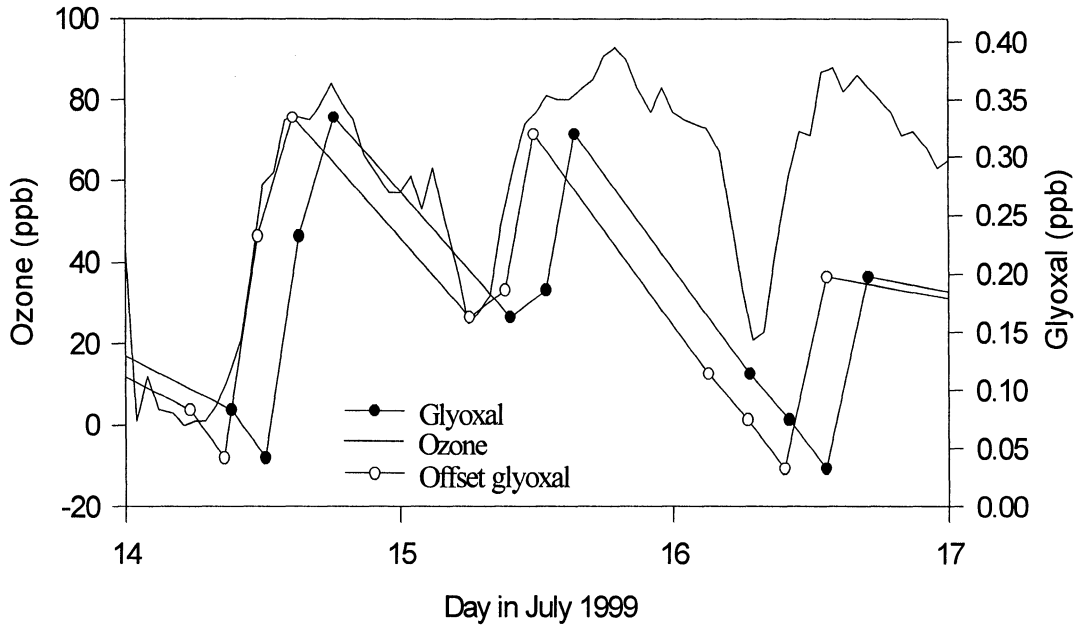

Figure 35. Glyoxal and ozone during the episode period of July 14 to July 16. The open circles are the glyoxal data after a temporal shift of 3.6 hours.

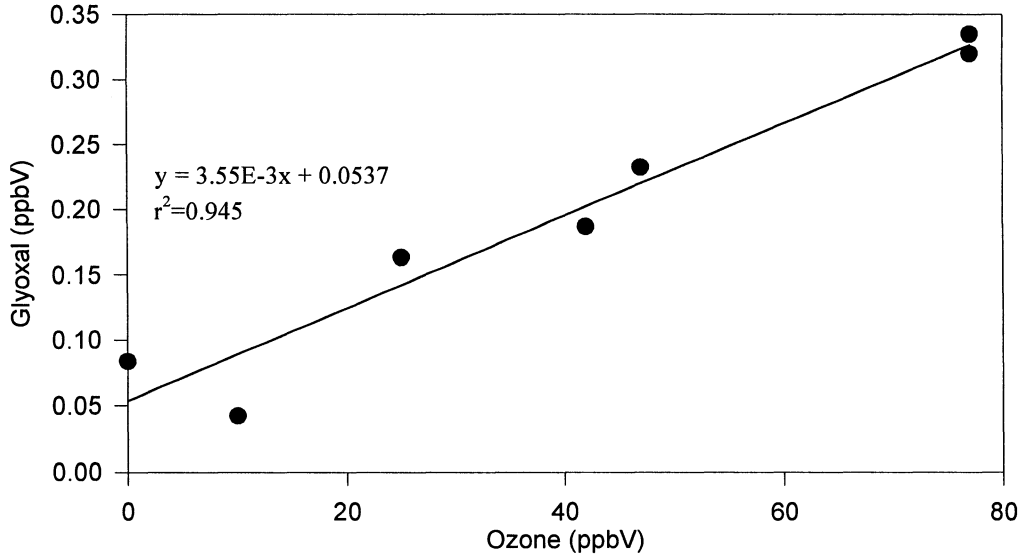

Figure 36. Relationship between glyoxal and ozone on July 14th and July 15th after application of a 3.6 hour shift to the glyoxal data.

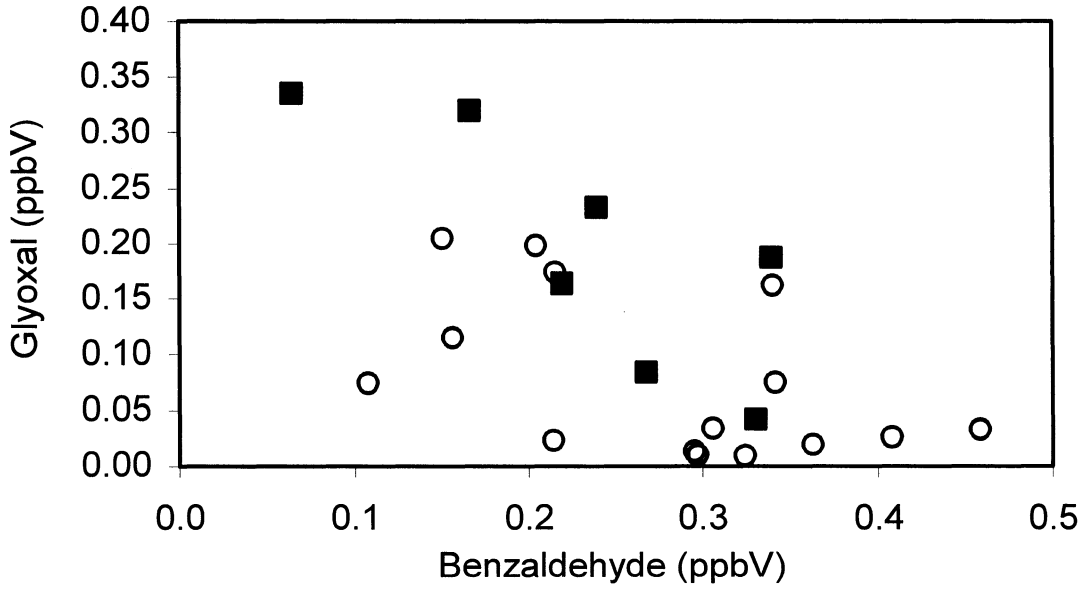

Figure 37. Glyoxal vs benzaldehyde. Filled squares are data from July 14th and 15th. Open circles are from the rest of the study.

Glyoxal and methylglyoxal are two compounds which are closely related in both their sources and sinks. Both are formed in the troposphere through the reaction of aromatic hydrocarbons, and both have very similar properties in that they are α-dicarbonyls and as such have reasonably short lifetimes due to their relatively fast photolysis rates. It is interesting to compare the concentrations of these two compounds measured at the same site to try to gain some insight into their oxidation sources. The yield of methylglyoxal from certain aromatic hydrocarbons can be quite high, as in the case of 1,3,5-trimethylbenzene which has a yield of ~60%, and so the levels produced from these hydrocarbons would also be expected to be higher than in the case of glyoxal. However glyoxal has a significant source in acetylene (~70% yield) which must be accounted for in any analysis.

Using the hydrocarbon data collected at the site, it is possible to calculate the theoretical production ratio for these two carbonyls. Given the production yields and $HO^{\cdot}$ reaction rates from Table 7, the production rate for glyoxal can be estimated using Equation 15, and similarly the production rate for methylglyoxal (P_{megly}),

$$P_{megly} = k_{tol,HO}[HO][toluene]\gamma_{tol,HO} + k_{benz,HO}[HO][benzene]\gamma_{benz,HO} + \ldots \qquad \text{Equation 16}$$

The ratio of P_{gly}/P_{megly} can then be calculated. The result of this calculation for this period at this site gives an average ratio of 0.24 ± 0.15. The range represents the 1σ standard deviation for all hydrocarbon samples collected, and is due to variations in the

hydrocarbon distribution. This production ratio is plotted along with glyoxal vs. methylglyoxal in Figure 38.

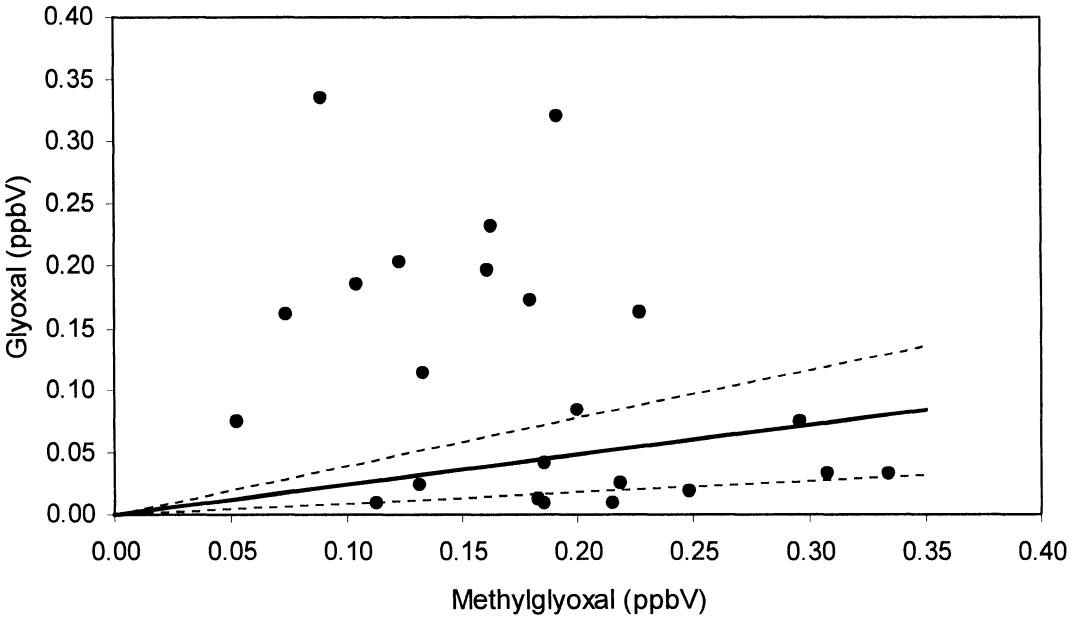

Figure 38. Production ratio of glyoxal to methylglyoxal during the Hamilton 1999 study. The solid line represents the average production ratio of 0.24, while the dotted lines represent the 1σ standard deviation in the calculated ratio.

From Figure 38 it can be seen that significant deviation from the theoretical production slope is seen at this site. While many observations lie well within the range predicted for these species, higher than predicted glyoxal values are seen for a significant number of samples. This again suggests a possible source of glyoxal other than gas phase aromatic or acetylene oxidation chemistry. Similar results could be seen if there exists a sink for methylglyoxal that does not exist for glyoxal, or if the

magnitude of a sink is larger for methylglyoxal than it is for glyoxal. The two important loss processes for glyoxal and methyl glyoxal during the day are photolysis and reaction with HO·. The reaction rate for methylglyoxal with HO· is somewhat higher than that for glyoxal (1.73×10^{-11} vs 1.15×10^{-11} molecules^{-1}·cm^{3}s^{-1}), however this difference is not large enough to explain the difference seen between the observations and the predicted ratio. The photolysis rates are quite similar with values of 8.6×10^{-5} s^{-1} and 10×10^{-5} s^{-1} for glyoxal and methyl glyoxal (Jenkin *et al*,1997) respectively, assuming a solar zenith angle of 35°. Thus the difference between the observed and predicted ratio for these two species cannot be explained on the basis of known sinks for the two. Thus these results are consistent with the possibility of an additional source of glyoxal, other than aromatic or acetylene chemistry.

The glyoxal observations at this site, and comparison of the glyoxal to other observations at this site, suggest that a source of glyoxal may exist during part of the episode period in addition to aromatic hydrocarbon oxidation. Since the calculations rely entirely on known gas phase chemistry, and mostly on the aromatic oxidation products, it is possible that other unknown chemistry is occurring in the gas phase, or possibly that some unknown source of glyoxal exists.

The interesting relationship between ozone and glyoxal could possibly be explained if it is assumed that both are being transported to the site, rather than being produced locally. The period of July 14th to 16th was associated with winds from the south to southwest. The time of the ozone peak during the day was ~ 6:00PM to

8:00PM during the episode. This time is somewhat later than what would be expected from local scale oxidation chemistry, and so it is likely that the ozone reaching the site was produced some distance away and transported to the area. The relationship between glyoxal and ozone may then suggest a similar situation for glyoxal, where the glyoxal has been transported in from some location to the southwest. The relationship between the two then may be fortuitous in that both are coming from the same area and appear to be related because of other factors such as temperature or meteorological effects. The data collected during this study is insufficient to make any conclusions beyond this.

4.1.2. Discussion of Other Carbonyl Measurements

4.1.2.1. Formaldehyde and Acetaldehyde

Unfortunately, no useable acetaldehyde data was collected during the July 14th to 16th episode, due to the presence of a large concentration of an interference on those days (see section 3.2). The analysis is therefore limited to periods before and after the episode. Figure 39 shows the relationship of formaldehyde with acetaldehyde for samples taken at about 2:00 PM local time. The ratio of formaldehyde to acetaldehyde for this period was ~1.3±0.3, calculated simply as the ratio of the concentrations. The overall concentrations of formaldehyde and acetaldehyde compare well with measurements made by other researchers in other urban areas (Grosjean and Fung, 1982), (Anderson *et al*, 1996). The ratio of formaldehyde to

acetaldehyde also compares well with various measurements, for example Slemr *et al*, 1996, measured a ratio of 1.42 at a site in Germany. The Hamilton 1999 field study site then, is similar to other continental areas studied for these compounds.

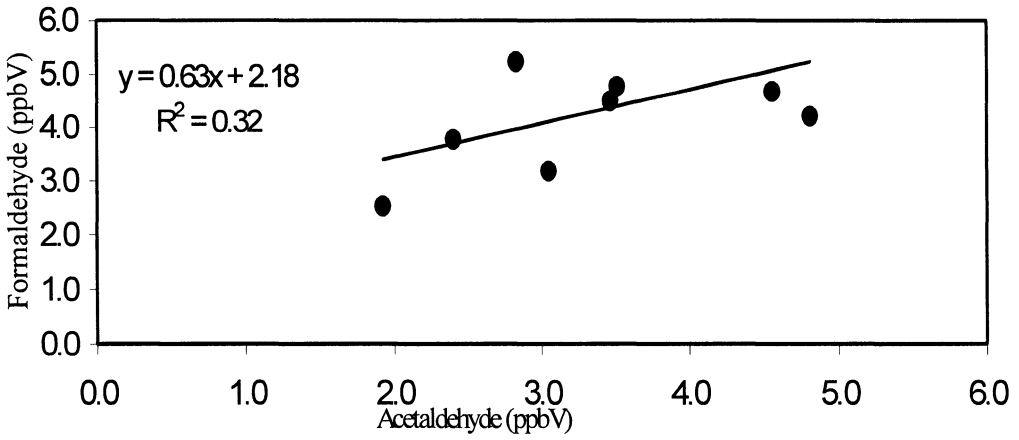

Figure 39. Formaldehyde vs. Acetaldehyde during the Hamilton 1999 study. The solid line represents the least squares best fit to the data.

A large intercept of 2.2 ± 1.2 ppbV is seen for formaldehyde, where the error is the 1σ error in the intercept. Since the intercept is significant, a somewhat more meaningful method of determining the relationship between formaldehyde and acetaldehyde is through a least squares regression analysis. The relatively large intercept value implies the presence of a source of formaldehyde, which is not a source for acetaldehyde, or possibly the existence of a sink for acetaldehyde, which is not a sink for formaldehyde. Some amount of the formaldehyde intercept is due to the background level of formaldehyde in the air arriving at the site, although the background formaldehyde can

only account for a fraction of the observed intercept since formaldehyde has a background level of between ~0.15 ppbV (Heikes *et al*, 1996) and ~0.6 ppbV (Lowe and Schmidt, 1983). The largest contribution to the intercept is most likely higher primary emissions of formaldehyde than acetaldehyde. Although the nature of these emissions is difficult to determine from this data, several possibilities exist, including biogenic emissions (Martin *et al*, 1999), vehicle exhaust (Fraser *et al*, 1998), or industrial emissions. Vehicle exhaust emissions are estimated as ~6.5 times higher for formaldehyde than acetaldehyde on a molar basis (Fraser *et al*, 1998). Also, for urban areas, the primary and secondary sources are estimated to be equivalent for formaldehyde, whereas secondary sources of acetaldehyde are generally much larger (Altshuller, 1993). Secondary hydrocarbon oxidation then favours a lower slope for a plot of formaldehyde vs. acetaldehyde (Fried *et al*, 1997). The large intercept then is an indication of larger primary sources of formaldehyde than acetaldehyde, while the slope of 0.63 is due to a larger net production of acetaldehyde from secondary sources. These results are reasonable for the suburban sampling site for Hamilton 1999, where large primary emissions of formaldehyde from vehicle exhaust are expected, along with significant secondary production of carbonyls from hydrocarbon oxidation.

4.1.2.2.Acetone and Propanal

Acetone and propanal are related to each other through their common source in propane oxidation. Some comparison between these species can be made on this basis,

with knowledge of the relative yields of acetone and propanal from propane oxidation. The estimated yield for propane oxidation is ~66.1% acetone production and ~30.3% propanal production based on the estimation methods described by Atkinson, 1997. The production ratio of acetone to propanal can then be estimated as ~2.2. The plot in Figure 40 shows the relationship between acetone and propanal during the study. Only data from samples collected between 12:00PM and 6:00 PM local time have been included. The slope of the best-fit line in Figure 40 of ~6.25 is somewhat larger than the production ratio expected for propane oxidation, although a relatively large error exists in the slope of ±4.4 at the 1σ confidence level.

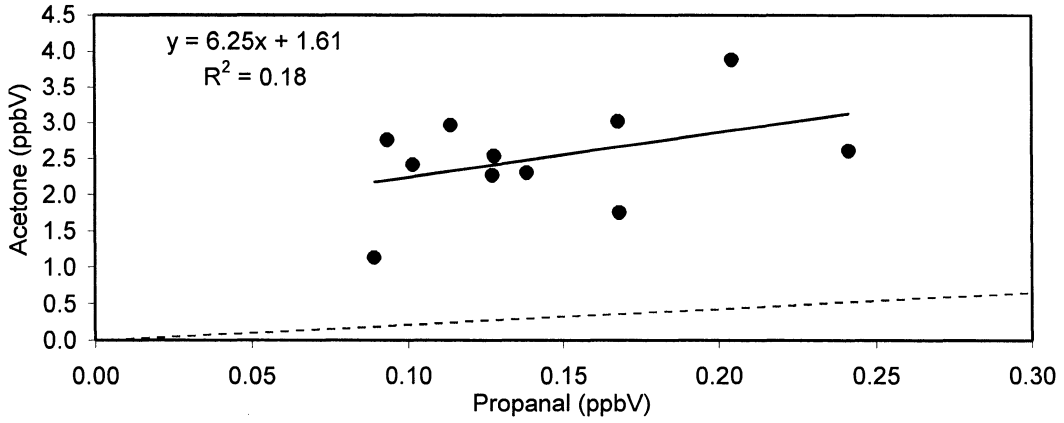

Figure 40. Acetone vs. Propanal. The dotted line represents the production ratio for acetone to propanal of ~4. The solid line is the least squares linear best fit to the data.

The large intercept of 1.61 ± 0.67 ppb for acetone is most likely due to both significant primary emissions of acetone and the background level of acetone combined. The significant scatter in the data suggests that these two compounds, although linked to

propane chemistry, are quite different in their overall sources, giving significantly different ratios on different days. Also, because acetone has a much longer lifetime in the atmosphere, the acetone to propanal ratio will be affected by the age of the air mass (refer to Table 1, Section 1.4). Aged air masses will tend to be rich in acetone relative to propanal, whereas fresh air parcels will be closer to the calculated ratio from propane oxidation, assuming the primary emissions of acetone do not mask the effect of the atmospheric chemistry. Primary emissions of acetone are known to come from various sources such as vehicular emissions (Harley *et al*,1992), biogenic emissions (Kotzias *et al*, 1997), or solvent use (Harley *et al*,1992). It is expected that the slope of the line will tend to be larger than the production ratio. The relationship seen between acetone and propanal seen here is fairly reasonable considering the various sources and sinks for these species.

4.1.2.3.Formaldehyde and Propanal

The relationship between formaldehyde and propanal is shown in Figure 41.

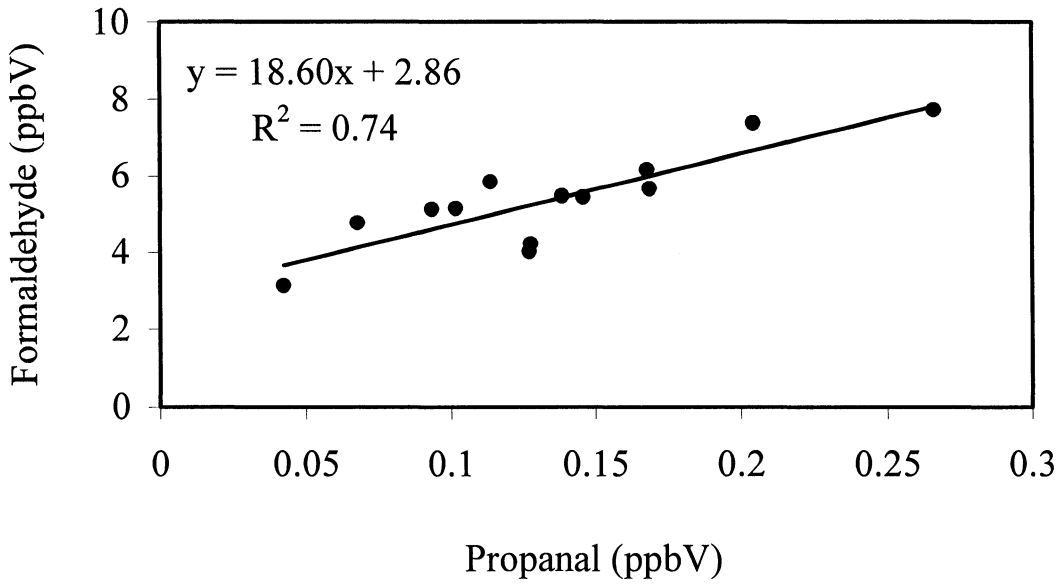

Figure 41. Formaldehyde and propanal during the Hamilton 1999 study. The line represents the least squares best fit.

A reasonably good correlation is seen between these two species (r^2=0.74), with a slope of ~18.6 ± 3.4 and formaldehyde intercept of ~2.9 ± 0.5. These values are somewhat difficult to interpret due to the large number of atmospheric oxidation sources for formaldehyde. The slope suggests that the net formaldehyde production is ~19 times larger than the net propanal production. The high degree of correlation suggests that propanal and formaldehyde are related in their sources. Since propanal is likely to be, for the most part, from secondary atmospheric oxidation of hydrocarbons,

this suggests that secondary oxidation of hydrocarbons represents a significant fraction of the observed formaldehyde. The formaldehyde intercept of 2.9 ± 0.5 ppbV is in reasonable agreement with the intercept of 2.2 ± 1.2 ppbV seen for formaldehyde vs. acetaldehyde in Figure 39. The midday background formaldehyde during this study can then be estimated from these two values to be ~2.4 ppb. This background value represents the formaldehyde levels expected in the absence of secondary chemistry, and so suggest a significant primary source of formaldehyde. The formaldehyde to acetaldehyde relationship, and the formaldehyde to propanal relationship then are consistent, in that both suggest significant contributions of both primary and secondary sources of formaldehyde during the Hamilton 1999 study. From an analytical point of view, the close relationship between formaldehyde and propanal is important in that it gives increased confidence in the quality of the data. Both species are most likely determined with reasonably good precision with this method.

4.2. Simcoe 2000 Study

The compounds for which significant concentrations were seen during the Simcoe 2000 study were formaldehyde, acetaldehyde, acetone and glyoxal, with median concentrations of 0.68, 0.33, 1.10, 0.48 ppbV respectively. The time series for this data and the ozone and temperature data from the Simcoe site are plotted in Figure 42, and Figure 43. The glyoxal data collected are quite interesting, and much of the discussion of the Simcoe 2000 results will be related to the interpretation of the glyoxal concentrations. Relatively high concentrations of glyoxal reaching ~1 ppbV or more were seen during the study. The short lifetime of glyoxal, and its photolysis to yield free radicals in the atmosphere, makes these high concentrations significant in terms of free radical production. Although the source of the glyoxal remains uncertain, some clues as to possible sources will be explored and discussed. Also, the carbonyl contribution to the production of free radicals will be calculated and discussed.

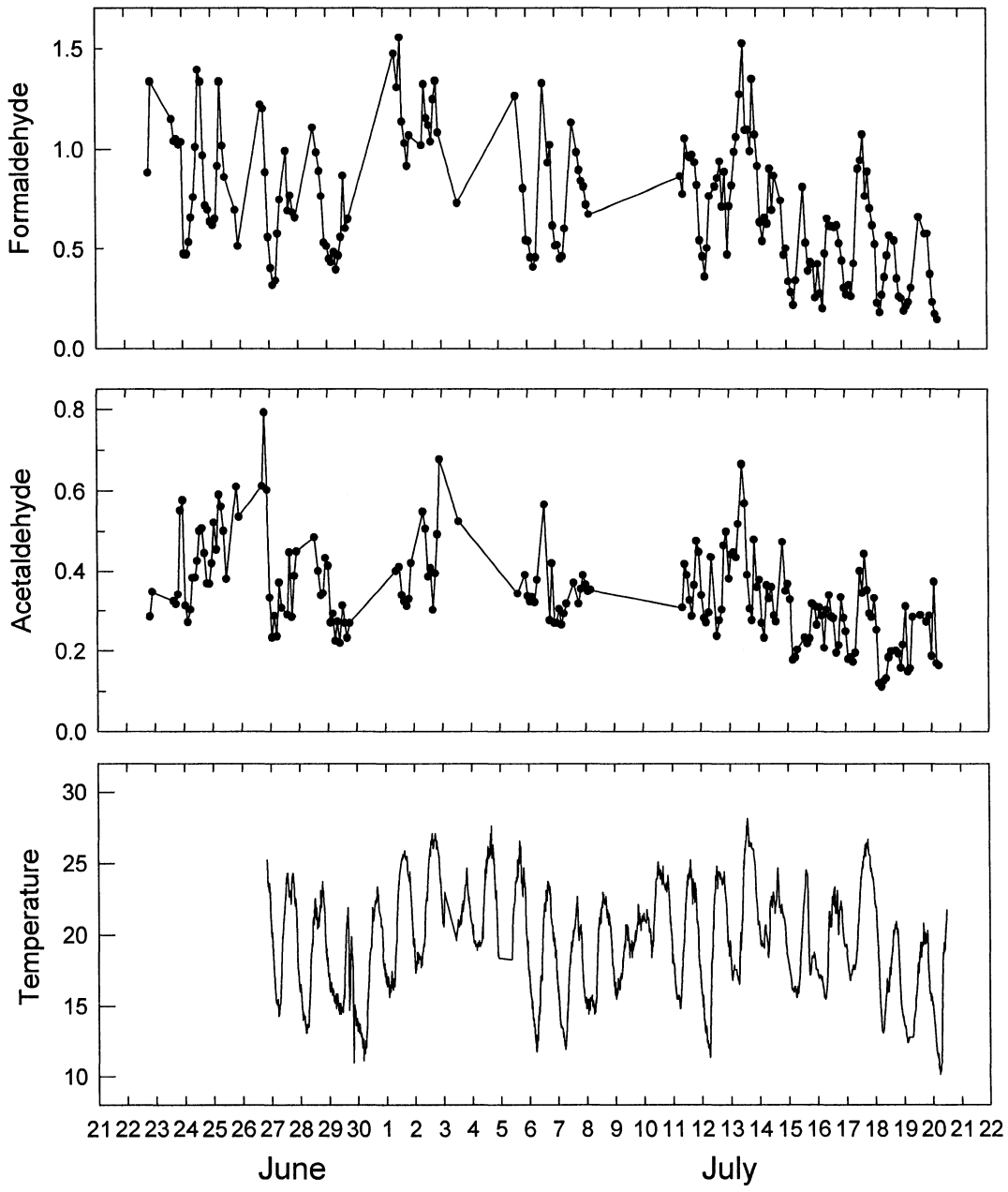

Figure 42. Time series of formaldehyde and acetaldehyde data collected during the Simcoe 2000 study. Carbonyl concentrations are in units of ppbV, and temperature is in °C.

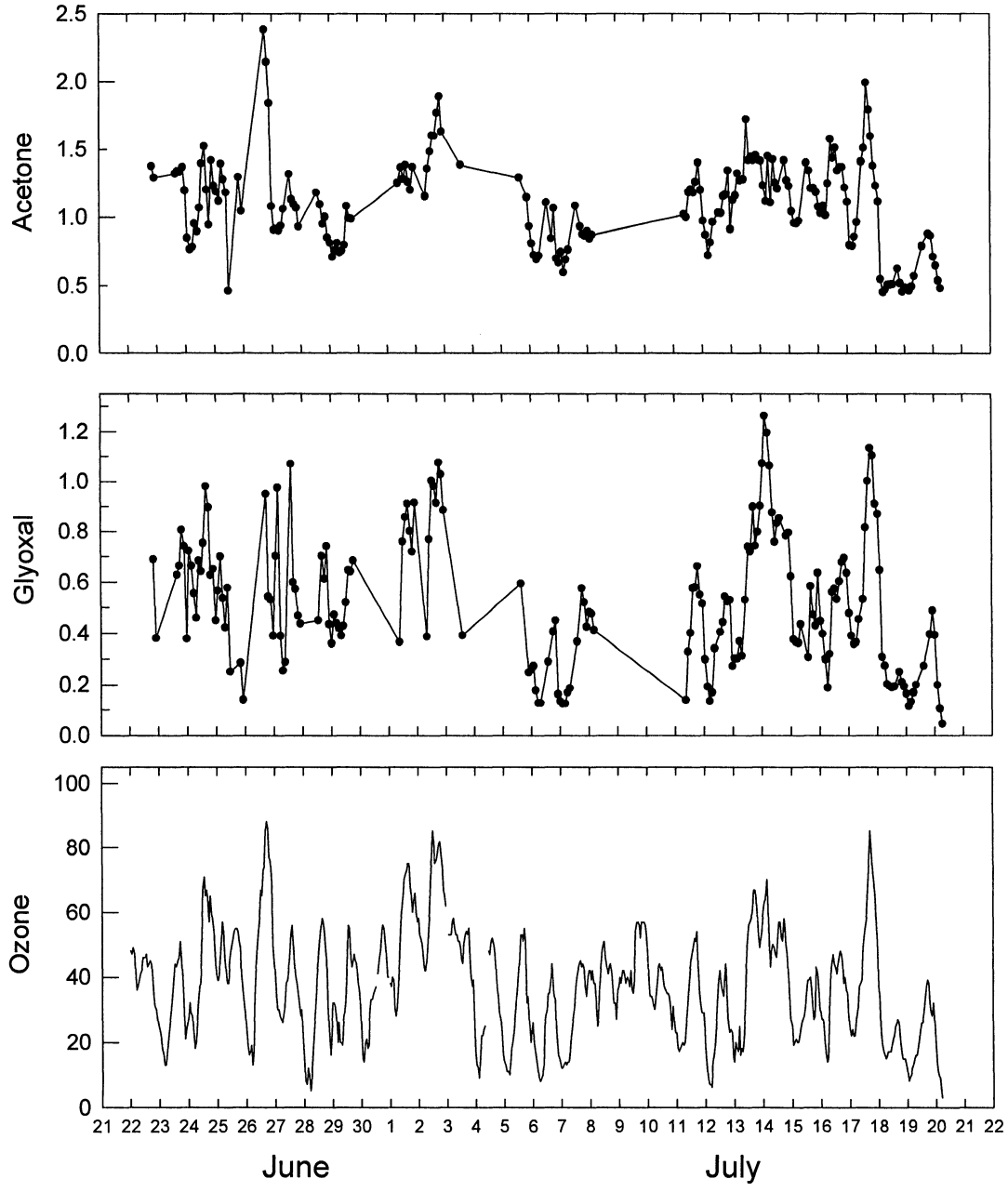

Figure 43. Time series of acetone, glyoxal and ozone data collected during the Simcoe 2000 study. Concentrations are in units of ppbV.

4.2.1. Hydrocarbon Chemistry and Glyoxal Production

Significant glyoxal concentrations were seen during the Simcoe 2000 study, which were somewhat unexpected. Glyoxal is a product of aromatic hydrocarbon oxidation, and has a fairly short lifetime of a few hours during the daytime. High concentrations were not expected at the rural agricultural site at Simcoe. The daytime steady state concentration of glyoxal from acetylene and aromatic oxidation have been estimated using the same method as described in section 4.1.1, using the hydrocarbon data collected during the study by Dr. J. Rudolph's group (York University). For hydrocarbon samples which were collected during the day (12:00 PM to 5:00 PM local time), and coincided with a carbonyl sample, the concentrations of glyoxal from acetylene and aromatic chemistry were estimated, and are plotted in Figure 44. The

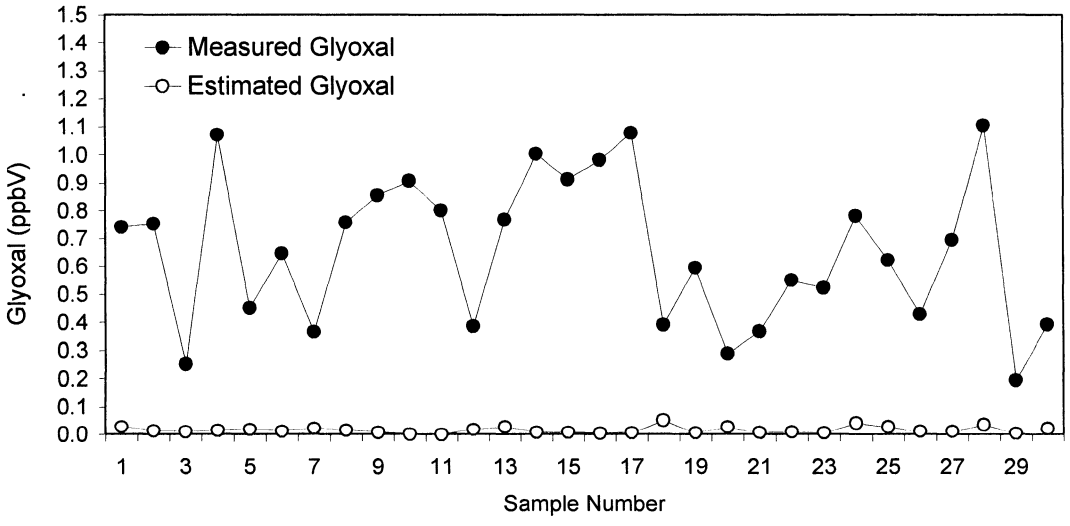

Figure 44. Glyoxal estimated from acetylene and aromatic oxidation and measured glyoxal concentrations during Simcoe 2000.

[HO·] is estimated as 5×10^6 molecules·cm^3, and the lifetime of glyoxal is estimated as 2 hours, assuming midday photolysis rates estimated for the Simcoe study and reaction with HO radical as the sinks. The measured glyoxal concentrations for these samples have been included in the plot for comparison. It is obvious, from Figure 44 that the estimated glyoxal concentration falls far short of predicting the measured level of glyoxal. The measured values are on average ~40 times higher than the predicted values. This difference suggests a large source of glyoxal which has not been accounted for, and that acetylene and aromatic chemistry cannot account for more than a few percent of the observed glyoxal.

At a rural site such as Simcoe, the contribution of isoprene chemistry should be considered for a mid-summer study. Isoprene has a glyoxal yield of ≤ 2 % (Paulson and Sienfeld, 1992) and an average concentration of < 0.3 ppbV during Simcoe 2000. Assuming [HO·] is 5×10^6 molecules·cm^3, and given an isoprene reaction rate with HO· of 101×10^{-12} cm^3·molecules·$^{-3}$·s^{-1} (Finlayson-Pitts and Pitts, 2000), the production rate of glyoxal from isoprene is estimated as ~0.01 ppb/hour. For a glyoxal lifetime of 2 hours, the glyoxal level expected from isoprene chemistry is then ~0.02 ppbV at midday. This contribution, while comparable to the production of glyoxal from aromatics and acetylene, represents an insignificant source of glyoxal during Simcoe 2000.

Glyoxal is also known to be a product of ozone reactions with alkenes, through the decomposition of the energy rich Criegee bi-radical (Grosjean E. *et. al.* 1996a).

This source is expected to be minor, since the yields of glyoxal from ethene, propene, 2-butene and 2-methyl-2-butene are 0.4 %, 8 %, 16 % and 6 % respectively. As will be shown in section 4.2.4, the ozone reaction with alkenes is of minor importance in the production of formaldehyde. Glyoxal in general has a smaller yield than formaldehyde from the reaction of ozone with alkenes (e.g.~1 from ethene for formaldehyde). It is therefore expected that the glyoxal source from ozone-alkene reactions will be minor. A potential loss process that has not been included in the alnalysis is the possibility of losses to atmospheric particles. Little information exists on this process, and so it is difficult to estimate as a potential loss process. This is an uncertainty in this analysis, and the results here must be viewed with this in mind.

4.2.2. Discussion of Possible Glyoxal Sources

Although a definite answer to the question of the source of glyoxal at this site is difficult to determine from these data, some possibilities can be explored, and certain sources can be ruled out. The oxidation of hydrocarbons including acetylene and the aromatics has essentially been ruled out as the major glyoxal source during Simcoe 2000. The relationship between glyoxal and ozone seen during Hamilton 1999 on the days of July 14th and 15th was seen again during Simcoe 2000, although no temporal shift between the glyoxal and ozone is present in the Simcoe data. The time series for glyoxal, ozone and air temperature are plotted in Figure 45 for the period of July 11th to 21st. During this period, the instrument was operational on a fairly regular

basis making diurnal patterns clearly visible. The correlation between glyoxal and ozone has been plotted in Figure 46, with all data collected during the Simcoe 2000 study included.

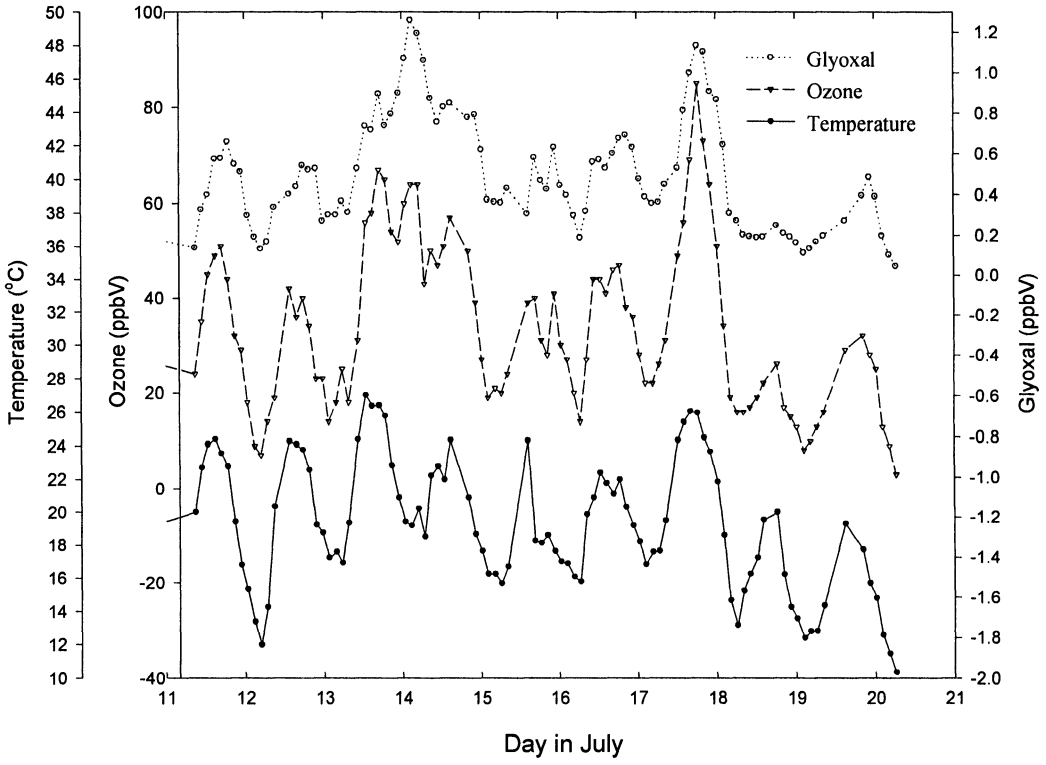

Figure 45. Time series of glyoxal, ozone and temperature, July 11th to 21st. Note the offsets in the Y axes for clarity.

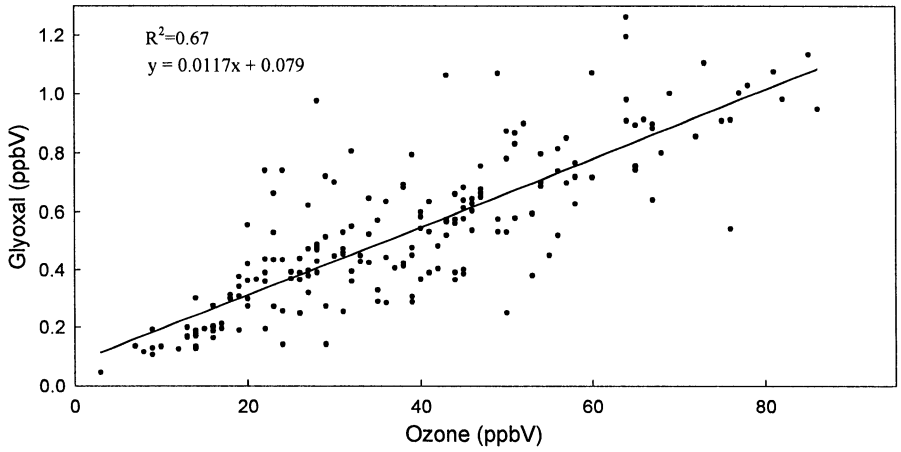

Figure 46. Simcoe 2000 glyoxal data plotted vs. ozone. All data collected during Simcoe 2000 have been included in the plot.

While ozone and glyoxal show a significant correlation with a regression coefficient (r^2) of 0.67, from the time series in Figure 45 it is obvious that there is also a relationship between ozone, glyoxal and temperature. Ozone will always be fairly well correlated with temperature, since high temperatures are generally associated with periods of high photochemical activity and ozone production. So the question must be addressed as to whether the glyoxal concentrations are in fact related to ozone, or only coincidentally related to ozone due to the relationship between ozone and temperature or possibly some other coincident factor. Plotting glyoxal vs. ozone (Figure 46) and glyoxal vs. temperature (Figure 47) and examining the regression coefficients can give some indication as to which of these two cases is most likely occurring.

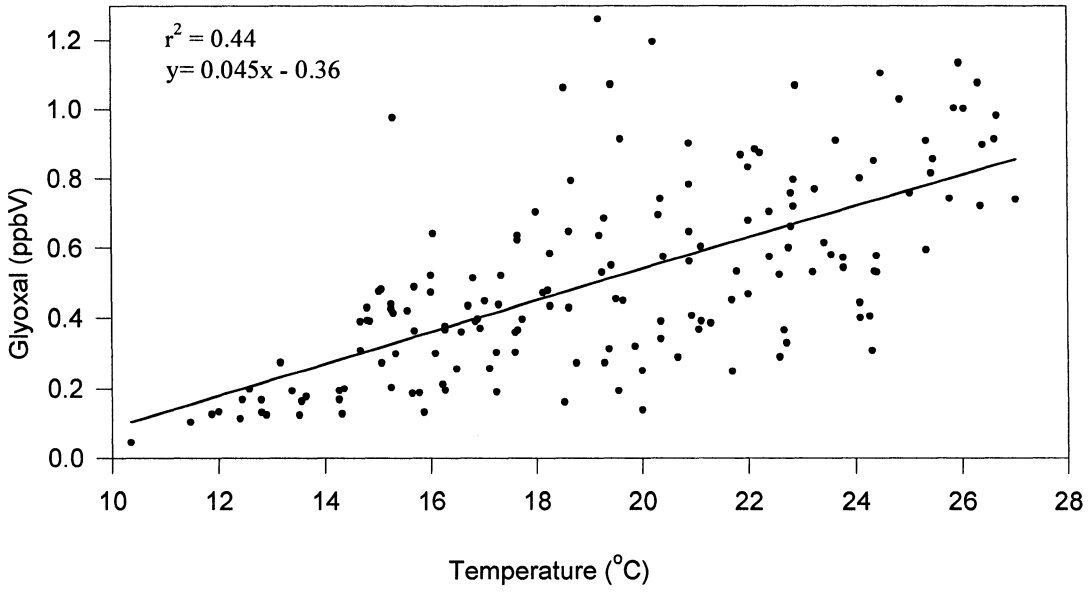

Figure 47. Glyoxal vs. Temperature during Simcoe 2000.

The calculated regression coefficient (r^2) of 0.44 in the case of glyoxal vs. temperature, compared to 0.67 for glyoxal vs. ozone suggests that the relationship of glyoxal is more likely to be with ozone rather than with temperature. The reasonable correlation seen between glyoxal and temperature then is most likely due to the general correlation between ozone and temperature ($r^2 = 0.67$, not plotted), rather than a mechanistically linked correlation between temperature and the major source of glyoxal at the Simcoe site. This data is insufficient however to say with certainty that the relationship between ozone and glyoxal is mechanistically linked, rather than coincidental with some other unexamined parameter or species.

Assuming glyoxal is in fact related to ozone in some way, then there should exist a difference between the nighttime and daytime correlation between glyoxal and

ozone. Glyoxal has a fairly short lifetime of a few hours with respect to photolysis during the daytime, and if the production rate of glyoxal is simply related to ozone, then the equation of the best fit line should be shifted to lower glyoxal values during the daytime due to photolysis. The glyoxal vs. ozone data have been separated into 'night' and 'day' values, and plotted in Figure 48. Nighttime values include data collected between 11:00PM and 5:00AM local time. Daytime values include data collected between 12:00PM and 7:00PM. Intermediate times in the early morning and late evening have been removed so that the difference between day and night can be seen clearly.

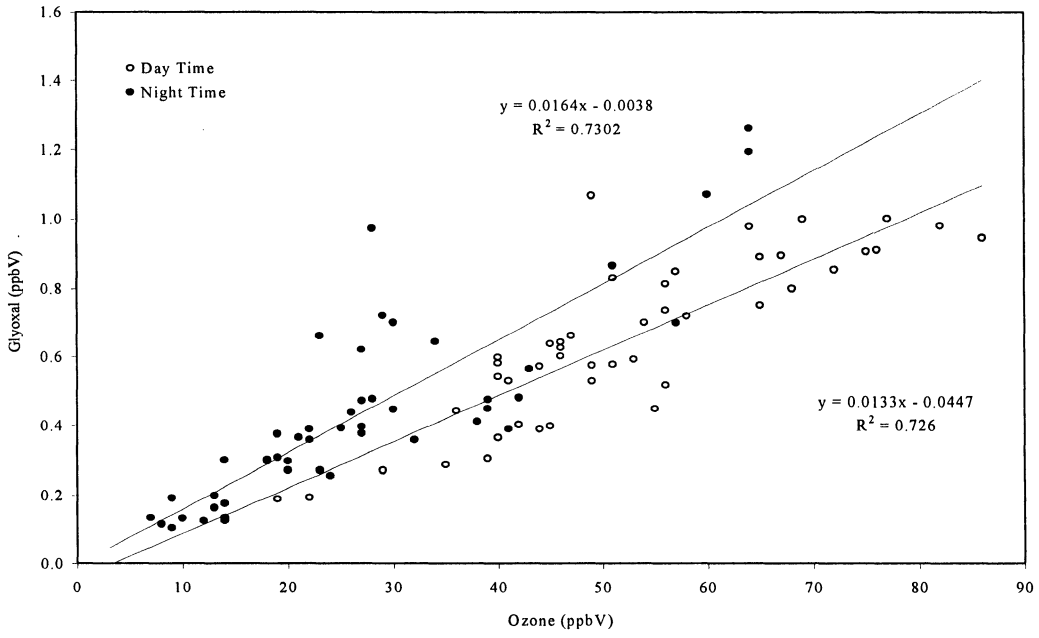

Figure 48. Daytime and nighttime glyoxal vs. ozone. The daytime values include samples collected between 12:00 PM and 5:00 PM local time, and the nighttime values include samples collected between 11:00 PM and 5:00 AM local time. The solid lines are the least squares regression best fit lines.

It is clear from Figure 48 that a difference exists between the daytime samples and the nighttime samples. Also, the direction of the difference is reasonable if glyoxal has a longer lifetime at night than during the day, with a slight shift in the equation of the line to higher glyoxal values at night.

Some spatial sense of how far away from the sampling site the formation of glyoxal is occurring can be inferred from the magnitude of the difference between the daytime and nighttime values. Since the intercept values for both the daytime and nighttime best fit lines are not significantly different from zero, the slope of each line can be determined by forcing the intercept to zero in the calculation of the best fit line. This results in slopes of 0.0125 ± 0.0003 and 0.0162 ± 0.0007 for daytime and nighttime respectively, with the errors given for a 1σ confidence interval. The slopes then represent the ratio of glyoxal (ppbV) to ozone (ppbV) during the day and at night respectively. The daytime depletion of glyoxal relative to ozone can then be estimated as the percentage difference between the two slopes. This results in a daytime depletion for glyoxal of ~23% ± 3% relative to ozone. Assuming a first order decay rate with $\tau \sim 2$ hours, the temporal difference between the formation and sampling of glyoxal, t, can be estimated as

$$\frac{[glyoxal]_t}{[glyoxal]_o} = e^{-t/\tau} \qquad \text{Equation 17}$$

The ratio of $[glyoxal]_t/[glyoxal]_o$ can be calculated from the estimated daytime depletion of 23%, giving a value of 0.77. Rearranging and solving for t, gives a time

of 0.52 hours. The spatial difference between the source of glyoxal and the sampling site can be estimated using typical daytime wind speeds during the study. The average wind speed at the Simcoe site was ~5.8 km/hr ± 2.5 km/hr. The error in the wind speed is simply the 1σ standard deviation of all measurements. This gives an average distance for the source of glyoxal from the sampling site of ~ 3.0 km. Thus one would expect that the source of glyoxal is fairly close to the sampling site, or perhaps covers a wide area close to the site, so that a small difference between daytime and nighttime glyoxal is seen. Mixing must also be considered in this analysis, since the height of the mixed layer above the ground will certainly be larger during the day than at night, and this will cause a similar shift in the glyoxal concentrations. The effects of wind speed differences between night and day can also be significant, and effect dilution as well. Wind speeds at night tend to be lower, and could enhance the nighttime levels relative to daytime levels. This effect would cause larger differences between night and day, than what would be predicted using removal by photolysis and $HO^{\cdot}$ reactions. Differences between daytime and nighttime deposition velocities will also have an effect on the analysis here. Nighttime dry deposition is expected to be lower than daytime deposition for most species (Wesely and Hicks, 2000), suggesting that a loss process for glyoxal which is higher in the day has been omitted from the analysis. However the height of the mixed layer will be larger in the daytime, and so the effect of deposition velocities on the overall glyoxal levels is difficult to predict. For highly water soluble species like glyoxal, the possibility of enhanced absorption onto wet

surfaces exists, the magnitude of which may be higher at night, further complicating the analysis.

The above analysis of the difference between daytime and night time glyoxal suggests only that the source of glyoxal is relatively close to the sampling site, perhaps within a few tens of kilometers. No information beyond this can be inferred from this data, unless reliable daytime deposition velocities for the area can be determined for both glyoxal and ozone, and the height of the mixed layer determined for night and day with reasonable certainty.

The above analysis suggests that glyoxal is possibly related to ozone, and that the source is fairly close to the sampling site. This analysis suggests nothing however about the nature of the source. The question which results is: can a plausible mechanism be found for the production of glyoxal from ozone chemistry? A possible mechanism to addresses this question is presented in the following sections, and the likelihood of its role in the formation of glyoxal is discussed.

4.2.2.1. Reaction of Ozone with Plant Surfaces

One possibility for the formation of glyoxal through ozone chemistry, is through the reaction of ozone with plant surfaces. Ozone is known to deposit onto surfaces via dry deposition. Once deposited, the ozone can react with the surfaces to which it has deposited. If these surfaces contain unsaturated hydrocarbons, then they will most likely be converted to carbonyls. Although this possibility is somewhat

speculative as a source for glyoxal, evidence exists for the formation of certain carbonyls found in the atmosphere which had previously been difficult to explain.

The possibility of heterogeneous reactions between gas phase ozone and plant surfaces has recently been explored by Fruekilde *et al*, 1998. In their study, epicuticular waxes were extracted from leaf surfaces and dispersed on glass wool. At zero ozone, no carbonyl products were formed, however at 100 ppbV of ozone significant amounts of acetone, 4-oxopentanal, 6-methyl-5-hepten-2-one, and geranyl acetone were formed. The formation of these carbonyls is presumed to proceed by ozonolysis of carbon-carbon double bonds found in the hydrocarbons in the plant's epicuticular lipid layer. These results have shed new light on the ubiquitous occurrence of 6-methyl-5-hepten-2-one which has been measured in ambient samples in the range of 0.1-5 ppbV (Ciccioli *et al*, 1993), and was found to be highest close to vegetation and with midday maxima in the diurnal variations. No information is available however on the formation of glyoxal from epicuticular layers from this study.

Evidence for the formation of carbon atoms bonded to oxygen atoms in the outer layer of pollen when exposed to 100 ppbV of ozone has been reported by Goschnick and Schuricht, 1996, although the exact nature of the moieties formed in this process was not reported. The formation of these bonds, was presumed to be due to the reaction of ozone with polycarotinoids in the outer pollen wall, leading to the formation of carbonyls. Although no direct evidence exists for the formation of glyoxal through these types of heterogeneous ozone alkene reactions, the formation of

glyoxal must occur by the same ozonolysis mechanism if an alkene contains the correct structure. The alkene must have two carbon-carbon double bonds, separated by a carbon-carbon single bond. Ozonolysis of each double bond would then form glyoxal via the mechanism shown in Figure 4, section 1.3.1. A polycarotinoid which contains such a structure is β-carotene shown in Figure 49, although other similar compounds may exists. Whether or not an alkene with such a structure is present in sufficient amounts in the epicuticular layer of plants is not known, and is beyond the scope of this work. The possibility certainly exists, and only speculation can be made as far as glyoxal production via this mechanism is concerned.

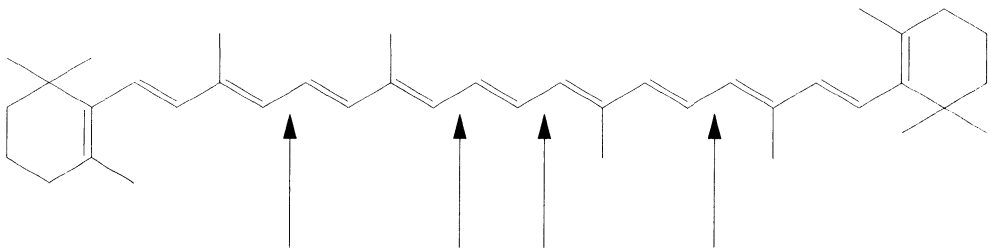

Figure 49. β-carotene. Arrows indicate sites on molecule able to produce glyoxal via ozonolysis.

4.2.2.2. Ozone Deposition Rates and Glyoxal Formation

The deposition of ozone to surfaces is a well-known process, and several measurements of deposition velocities for ozone have been made over various surfaces (Wesely and Hicks, 2000). While the variability in ozone deposition velocities is fairly

large, an estimate of the amount of ozone deposited onto surfaces can be made, and used to estimate the relative amount required to produce the levels of glyoxal which were measured during the Simcoe 2000 study. Obviously if the amount of glyoxal produced is greater than the stoichiometric amount of ozone deposited, then the possibility of a heterogeneous ozone reaction with plant surfaces would be unrealistic. If however a small percentage of the total deposited ozone is required for the formation of glyoxal, then this possibility is certainly not proven, but remains plausible.

The amount of ozone depositing to the surface can be estimated by knowing the ozone deposition velocity (v_{dep}), and the approximate height of the inversion layer. While the literature values for ozone deposition velocity are quite variable, depending on vegetation, time of year, wetness of the surface, type of vegetation, and even light level (Wesely and Hicks, 2000), some rough estimate can still be made for the location of interest. The value used here was chosen for agricultural land, in midsummer with lush vegetation, for a solar irradiance of 500 Wm^{-2}. The deposition velocity for ozone under these conditions is ~0.9 cm/s (Wesely and Hicks, 2000). Similar values are given for the deposition of ozone over deciduous forest in midsummer, with values of ~0.7 cm/s for similar conditions. The area surrounding the Simcoe site was dominated by agricultural land, and so the value of 0.9 cm/s was used in the calculations here. The surrounding area also had some deciduous forest cover, but since the deposition velocities for both are reasonably similar, taking into account the forest cover would

have little effect on the calculation results. The rate of deposition of ozone to the surface (D_{O_3}) can be estimated in the following way:

$$D_{O_3} = \frac{[O_3] \cdot v_{dep}}{H} \qquad \text{Equation 18}$$

For a boundary height (H) of 1000 m, and an ozone concentration of 50 ppbV, an ozone deposition rate of ~1.6 ppbV/hr is obtained. The lifetime of glyoxal is ~2 hours, and so the amount of ozone depositing in 2 hours is ~ 3.2 ppbV. For 50 ppbV of ozone, ~ 0.7 ppb of glyoxal were seen during the Simcoe study. The required yield can then be expressed as:

$$Yield = \frac{0.7\,ppbV}{3.2\,ppbV} = 0.22 \qquad \text{Equation 19}$$

This gives a required glyoxal yield from ozone deposition of ~22%. This estimate assumes that each molecule of ozone depositing to the surface yields a molecule of glyoxal. This is a possibility, if the compound with which the ozone is reacting is a 2-alkeneal. However if the reacting hydrocarbon is a di-ene before the first ozone oxidation, then the number of moles of ozone required to create glyoxal is twice as large as this estimate. In this case, ~44% of the deposited ozone must be directly converted into glyoxal. These values are somewhat overestimated however, since the analysis assumes that the glyoxal produced at the surface, will be immediately mixed

into the entire boundary layer. In reality a gradient of glyoxal will exist with the highest values close to the surface.

The deposition of ozone to plant surfaces may be responsible for some amount of the glyoxal production, although this glyoxal source would have to be specifically targeted in well designed experiments to be able to quantify the amount of glyoxal which could be reasonably expected from this mechanism. The result of ~44% ozone deposition required is somewhat high, considering that many loss mechanisms must exist for the deposition of ozone onto leaf surfaces, or within the interior of leaves. This suggests that either the deposition velocity of ozone is underestimated for the vegetation at this site, or that this mechanism is not the major one responsible for the production of glyoxal from ozone reactions. In the case where only 22% of the ozone deposited is required for glyoxal production, the conclusion is similar, and there most likely exists another mechanism for the production of glyoxal, or possibly the deposition velocities have been underestimated for the vegetation in the surrounding area. This conclusion is further supported by the results of Moise and Rudich, 2000 where the reaction rate of ozone with alkenes in monolayers is relatively slow.

4.2.2.3.Plant Stresses

A possible connection between ozone and glyoxal, may be through the stress induced on plants by ozone. Plants are known to emit various VOCs in response to various stresses, including high ozone levels (Heiden *et al*,1999), (Kesselmeier and Staudt, 1999). If a compound is emitted from a plant, and can react quickly in the gas phase to yield glyoxal, then a correlation between glyoxal and ozone would be expected. The presence of a carbon-carbon double bond, next to a single bond connected to the aldehyde carbon is required to yield glyoxal from an ozone reaction, as shown in Figure 50.

Figure 50. 2-Alkenal reaction with ozone to produce glyoxal. Other reaction pathways have been omitted for clarity.

Experimental evidence exists for this process to be efficient in the production of glyoxal. Grosjean E. and Grosjean D., 1997, measure glyoxal yield of 47% from crotonaldehyde (2-butenal) reacting with ozone. Glyoxal will also be formed from $HO^{\cdot}$ reaction with an alkenal via addition to the double bond, followed by O_2 addition and oxidation of NO to NO_2, followed by decomposition of the carbonyl-alkoxy

radical to yield the dicarbonyl (Atkinson, 1994). Emissions of various oxygenated VOCs from biogenic sources are well-established (Puxbaum, 1997; Ciccioli *et al*, 1997), including trans-2-hexenal, referred to as 'leaf aldehyde', (Kesselmeier and Staudt, 1999), and new information on emissions caused by stresses on plants has become available recently.

Alkenals have been identified from certain plant species in response to injury. Although little information is available on this subject for many plant species, the emission of C_{12} to C_{14} 2-alkenals has been documented as a major component of the odour of a common weed found in North America, *Bifora radians* (Latrasse *et. al.*, 1991). The weed was found to be relatively odourless until injured, when the major odour components were identified as (E)-2-dodecenal, (E)-2-tridecenal, and (E)-2-tetradecenal. The biogenic emission of several 2-alkenals by wounding, pathogen attack and ozone stress has also been documented by Heiden *et al*,1999. Plants, which were found to emit compounds of this nature, included corn, tomato and tobacco, with significant emissions of (E)-2-hexenal, and various other alkenals. The emission rates from the various plants, and the distribution of emitted compounds were found to vary with plant species, as would be expected. Variations were also seen for different species of the same type of plant. Two different tobacco species were investigated, with one species emitting VOCs under ozone stress, while the other species emitted no observable amounts of the investigated compounds. Significant uncertainty therefore exists if one would like to extrapolate the emission rates induced

by various stresses to more realistic atmospheric situations. The combination of various stress factors on the emissions may also play a role in the emission rates, and so estimating their importance in the atmosphere becomes a challenging task. The emission rates estimated by Heiden *et al*, 1999, are useful qualitatively however in that the emissions of significant quantities of alkenals induced by ozone stresses has essentially been established for several plant species. The emitted alkenals will have a short lifetime with respect to oxidation, and will certainly react with $HO^{\cdot}$ and with ozone to form glyoxal. Whether or not the emission rates of the alkenals for the plant species found surrounding the Simcoe site are sufficient to account for the glyoxal levels measured, is uncertain.

What is simply not known, is whether or not glyoxal is directly emitted as a response to plant stresses. Since alkenals are emitted as a response to various stress, along with various other aldehydes and alcohols, it is possible that glyoxal is emitted directly from plants under stress. This would have to be examined in experiments specifically targeting these types of emissions from stressed plants. Also, information about other types of surface emissions of glyoxal, natural or otherwise, has not been found. Potential sources would have to be directly targeted in further experiments to either quantify or rule out possible glyoxal sources in the Simcoe area.

4.2.3. Contribution of Carbonyls to Radical Production

An important property of atmospheric carbonyls is their ability to photolyse under normal daytime conditions to yield radicals. Perhaps the most important oxidant in the atmosphere is the HO radical, although its concentrations are generally very low, on the order of ~1×10^7 molecules/cm^3 or less, which is the equivalent of ~0.3 pptV (Finlayson-Pitts and Pitts, 2000 and references therein). These low concentrations generally make the measurement of HO difficult, and HO levels must often be determined through model calculations. The ability to perform these calculations requires measurement of the concentrations of the major source species, which are generally ozone and carbonyls (Lee *et al*, 1998). The contribution of the carbonyls measured during Simcoe 2000 to the production of radicals has been estimated and will be discussed.

Calculation of the source strength for radical production requires knowledge of the photolysis rates, and the carbonyl concentrations. Calculation of the photolysis rate (J_a) for a given species requires knowledge of the actinic flux (F), the quantum yield for the process (ϕ), and the absorption cross section (σ), all of which are wavelength dependant (λ) as shown in Equation 20:

$$J_a = \int_{\lambda} \phi(\lambda)\sigma(\lambda)F(\lambda)d\lambda \qquad \text{Equation 20}$$

The radical production rate from a given species (P_a) can be calculated using:

$$P_a = 2J_a[Carbonyl_a] \qquad \text{Equation 21}$$

The production rate is double the photolysis rate since each carbonyl molecule which photolyses results in the formation of two radicals as shown for formaldehyde in (R12), section 1.4.1. Photolysis rates (J_a) have been evaluated for the radical producing channels for formaldehyde, acetaldehyde and glyoxal. In general, the J_a values are wavelength dependant, and so must be evaluated as a function of time of day, since the intensity and wavelength distribution of light at ground level change as a function of solar zenith angle. Photolysis rates of several carbonyls as a function of solar zenith angle have been compiled and are given by Jenkin *et al*, 1997. The J_a values are calculated using the following parameterized equation:

$$J_a = l(\cos\chi)^m e^{(-n\sec\chi)} \qquad \text{Equation 22}$$

where χ is the solar zenith angle, and l, m, and n, and are given in Table 8.

Reaction	l	m	n
$HCHO \rightarrow HCO^{\bullet} + H^{\bullet}$	4.866×10^{-5}	0.781	0.349
$CH_3CHO \rightarrow HCO^{\bullet} + CH_3^{\bullet}$	8.443×10^{-6}	1.177	0.437
$(CHO)_2 \rightarrow HCO^{\bullet} + HCO^{\bullet}$	3.887×10^{-5}	0.695	0.289

Table 8. Parameters for the calculation of J values in units of s^{-1} as a function of solar zenith angle (Jenkin *et al*, 1997 and references therein).

Solar zenith angles have been calculated for all carbonyl samples, taken during Simcoe 2000, based on Eastern Standard Time, and the global position of Simcoe Ontario.

The photolysis of ozone to produce radicals in the atmosphere proceeds by the following reactions (Atkinson, 2000):

$$O_3 + h\nu \rightarrow O_2 + O(^1D) \quad \text{(R19)}$$

$$O(^1D) + H_2O_{(g)} \rightarrow 2HO^{\cdot} \quad \text{(R20)}$$

$$O(^1D) + M \rightarrow O(^3P) + M \quad \text{(R21)}$$

The reaction of $O(^1D)$ with gas phase water to produce radicals is in competition with the deactivation by air (M). For an atmospheric pressure of 1 atm and 50% relative humidity at 298 K, ~0.2 HO radicals are produced per $O(^1D)$ atom formed (Atkinson, 2000). The rate of loss of O_3 by photolysis is then given by:

$$\frac{d[O_3]}{dt} = -J_{O_3}[O_3] \quad \text{Equation 23}$$

Solar light intensity was not measured during the Simcoe 2000 study, so actinic fluxes as a function of solar zenith angle for clear sky conditions have been used. All the values required were obtained from Finlayson-Pitts and Pitts (2000), and references therein. The actinic flux for ground level calculated for a best estimate surface albedo have been used. In practice, the values required are averaged over similar wavelength intervals so that the integral becomes a sum over the wavelengths of interest, rather than an integral:

$$J_{O_3} = \sum_{\Delta\lambda_i}^{\Delta\lambda_f} \phi_{avg}(\lambda)\sigma_{avg}(\lambda)F_{avg}(\lambda) \qquad \text{Equation 24}$$

The resulting J_{O3} is plotted in Figure 51 as a function of solar zenith angle, along with the J_a values calculated for the aldehydes.

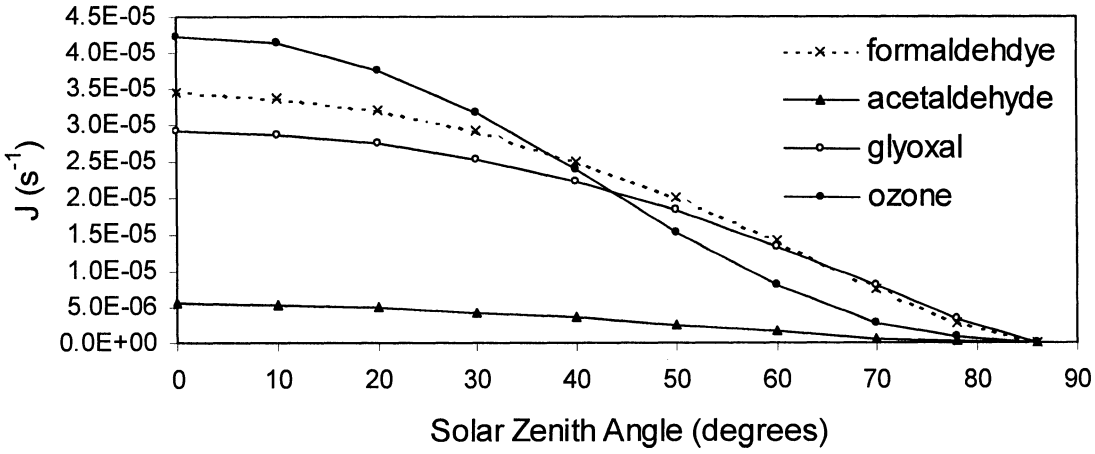

Figure 51. Photolysis values as a function of solar zenith angle for ozone and the carbonyls measured during Simcoe 2000.

The relative importance of carbonyl photolysis is somewhat enhanced, during the early morning and late evening hours, due to the somewhat red shifted carbonyl photolysis relative to ozone (Lee *et al*, 1998). Note that high values of zenith angle are for early morning, and evening, while low values are for the middle of the day, since

zenith angle is measured relative to the local upward vertical. The radical production rates from carbonyl photolysis are shown in Figure 52.

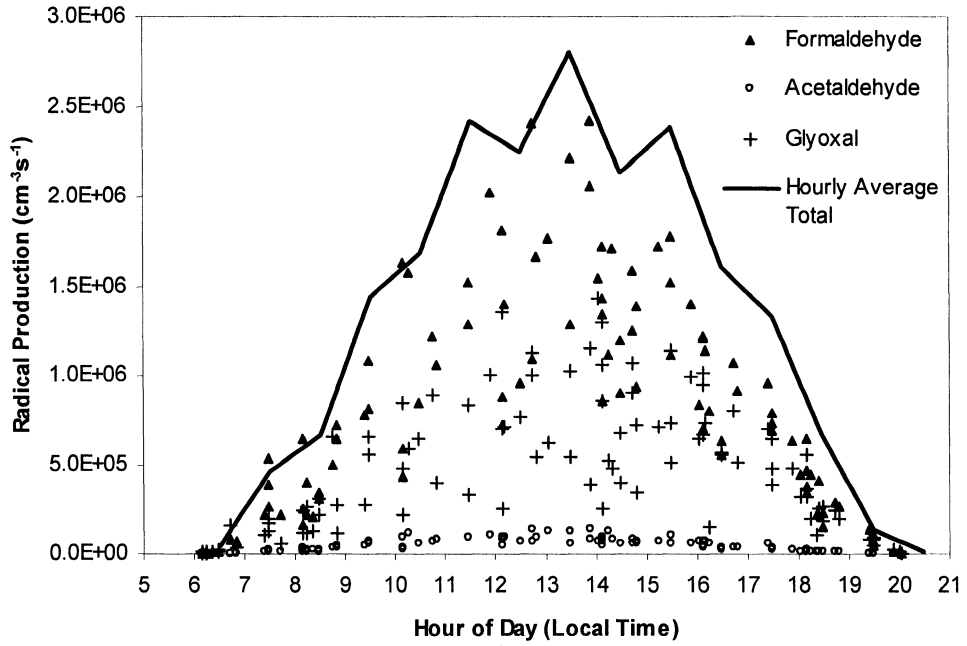

Figure 52. Radical production from formaldehyde, acetaldehyde and glyoxal photolysis during Simcoe 2000. The solid line represents the average of the sum of radical production for all three species, on an hourly basis for the study period.

Formaldehyde was found to be the largest radical source of the three carbonyls, giving ~$1.4\times10^{6} \pm 5\times10^{5}$ radicals·cm^{-3}·s^{-1} during the midday hours of 12:00 PM to 3:00PM local time. Compared to formaldehyde, the glyoxal radical production was found to be quite significant. For all daytime data collected during the Simcoe 2000 study, the average ratio of radical production from glyoxal to radical production from formaldehyde was 0.75 ± 0.47. The error in this value represents the 1σ standard

deviation for all data used in the calculation. Acetaldehyde was found to be a relatively minor radical source, contributing ~5% as many radicals as formaldehyde.

The contribution of the carbonyls to the radical production relative to the total radical production has been evaluated for the Simcoe 2000 data, and is shown in Figure 53.

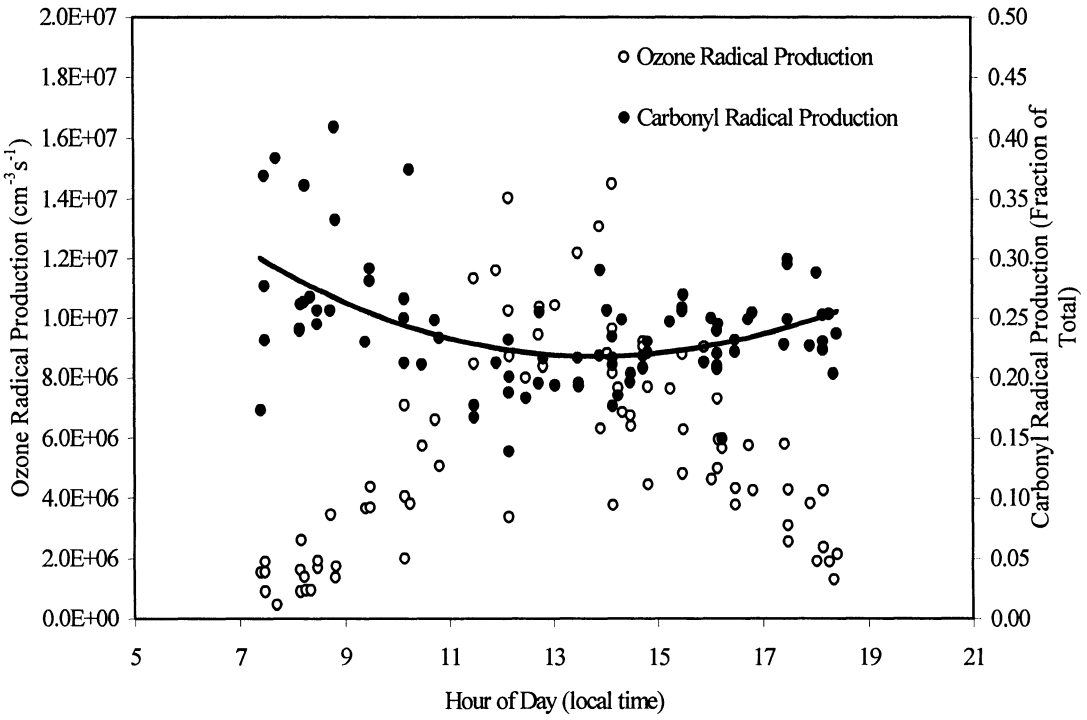

Figure 53. Diurnal plot of radical production from ozone, and % carbonyl contribution to the total radical production. Data from between 7:00 AM and 7:00 PM have been included. The solid line is a third order polynomial fit for the % carbonyl contribution data. Clear sky conditions have been assumed.

From Figure 53, it can be seen that the carbonyl radical source is significant throughout the day. The % carbonyl radical production is given by:

$$\%\ carbonyl\ radical\ production = \frac{P_{formaldehyde} + P_{acetaldehyde} + P_{glyoxal}}{P_{formaldehyde} + P_{acetaldehyde} + P_{glyoxal} + P_{ozone}} \times 100\%$$

Equation 25

where P is the radical production for each species calculated for each sample. The midday carbonyl contribution to radical production is estimated as ~21% of the total. The percentage contribution to radical production from carbonyls is somewhat enhanced during the early morning hours. A slight evening enhancement in the carbonyl contribution to the radical production is also seen, but not as significant as in the morning. This enhancement is obviously due to the slightly red shifted photolysis of the carbonyls relative to ozone. The contributions from each individual carbonyl, to the total radical production are shown in Figure 54. For formaldehyde, the percent radical contribution is given by:

$$\%\ formaldehyde\ radical\ production = \frac{P_{formaldehyde}}{P_{formaldehyde} + P_{acetaldehyde} + P_{glyoxal} + P_{ozone}} \times 100\%$$

Equation 26

The individual production rates during the midday hours between 12:00 PM and 3:00 PM local time are 13.6%, 0.8% and 6.9% for formaldehyde, acetaldehyde and glyoxal respectively.

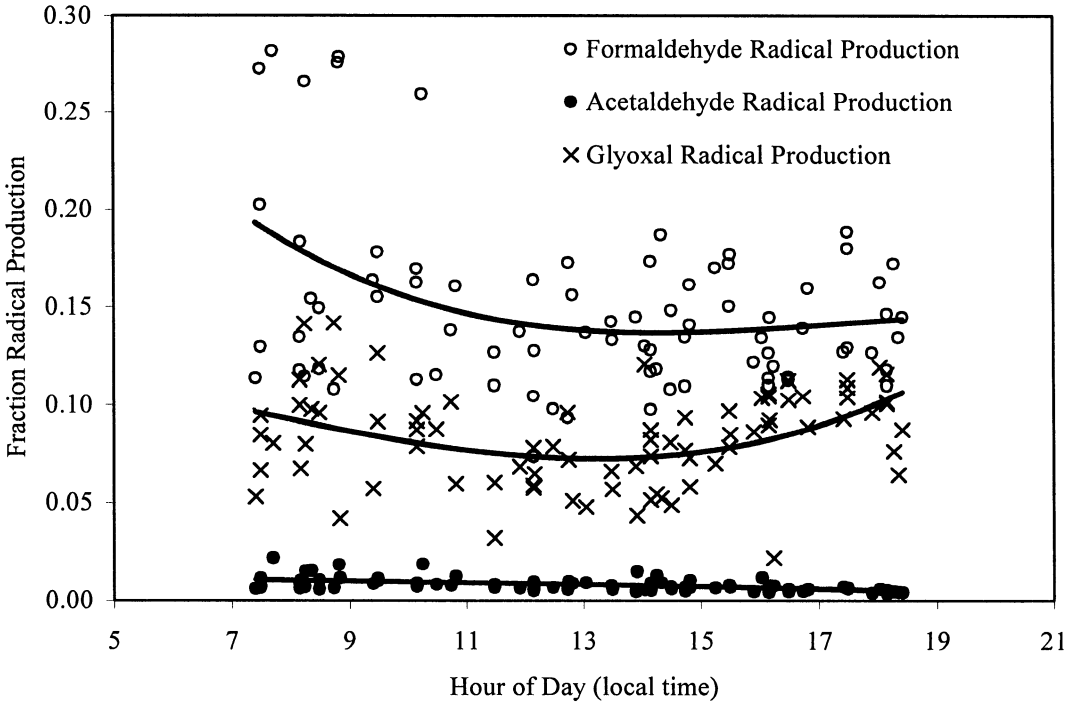

Figure 54. Radical production from formaldehyde, acetaldehyde and glyoxal. Data from between 7:00 AM and 7:00 PM have been included. The solid line is a third order polynomial fit for the carbonyl contribution data. Clear sky conditions have been assumed.

The contribution to radical production from acetone is expected to be minor at this site, since the acetone photolysis rate is low compared to the carbonyls examined here (see Table 1, section 1.4.2). A simple estimation of the importance of acetone relative to acetaldehyde can be made on the basis of their average concentrations, and relative photolysis rates. The photolysis rate for acetone is ~12% that of acetaldehyde, and the average daytime concentration of acetone is ~3.5 times larger than acetaldehyde. The acetone radical source then can be estimated as ~42% as large as the acetaldehyde source. The average acetaldehyde radical source is ~1.1% of the total

carbonyl and ozone radical source, giving an acetone radical contribution of ~0.46% of the total radical source.

Although the contribution of the other carbonyls has been omitted from this analysis, the possibility of significant radical production from other species, carbonyl or otherwise, certainly exists. However, the assumption that ozone is the main radical source is most likely valid, and so the relative contributions of individual carbonyls calculated here will not be significantly affected by the omission of an unknown radical source.

4.2.4. Formaldehyde Budget

The relative contribution of various hydrocarbons to the production of formaldehyde can be estimated using the hydrocarbon data collected during the Simcoe study. Formaldehyde production, P_{form}, is estimated using the following equation,

$$P_{form} = \sum_n k_{n,HO}[HC_n][HO]\gamma_{n,HO} + \sum_n k_{n,O_3}[HC_n][O_3]\gamma_{n,O_3} \qquad \text{Equation 27}$$

where $k_{n,HO}$ and $k_{n,O3}$ are the $HO^{\cdot}$ and O_3 rates for hydrocarbon HC_n respectively, and $\gamma_{n,HO}$ and $\gamma_{n,O3}$ are the formaldehyde yields for $HO^{\cdot}$ and O_3 chemistry with HC_n respectively. For this analysis, only O_3 and $HO^{\cdot}$ chemistry has been considered, and, the reaction rate between O_3 and alkanes is assumed to be negligible (Atkinson, 1994). Also, aromatics are assumed to yield insignificant amounts of formaldehyde. Acetaldehyde has been included in the analysis, assuming a formaldehyde yield of 1 from the reaction of acetaldehyde with $HO^{\cdot}$. A 'steady state' condition is assumed for

the formaldehyde concentration during the day. For formaldehyde this is a reasonable assumption due to its fast photolysis and reaction with $HO^{\cdot}$ at midday (Fried *et al*, 1997). Ozone concentrations measured at the site have been used, and an [$HO^{\cdot}$] of 5×10^6 molecules·cm^{-3} was assumed for the calculations. Only daytime samples taken close to 2:00 PM local time have been included in the analysis. Formaldehyde yields have been calculated by Altshuller, (1993, 1991a, 1991b) based on the mechanisms given by references therein. Values derived at 298 K or 300 K have been used for the calculations here. Also, the NO levels are assumed to be high enough that conversions of the peroxy radicals to alkoxy radicals by NO is the dominant pathway, rather than peroxy-peroxy radical reactions (Altshuller, 1991a). This assumption is valid for conditions where NO > 7×10^8 molecules·cm^{-3}, (> 0.026 ppbV). Although the NO measurements made at the Simcoe site cannot be used to verify this due to a concentration resolution of 1 ppbV, this assumption should be valid over populated regions within the planetary boundry layer (Altshuller, 1991a). The product yields have been adapted for use here from their original form whenever required, and are listed with the other values used in the calculations in Table 9. Reaction rates for both $HO^{\cdot}$ and O_3 reactions were obtained from Atkinson, 1994. Methane concentrations were not measured at the Simcoe site, and so are assumed to be 1800 ppbV. The formaldehyde yields from a few hydrocarbons were not given in the literature, and had to be inferred from similar compounds, or from the mechanistic information given by Atkinson, 1994, and are described below.

The formaldehyde yield values used in the calculations are listed in Table 9. Methane is assumed to react entirely via HO· reaction followed by O_2 addition and NO to NO_2 conversion, followed by H atom abstraction by O_2 to yield formaldehyde. The yield is therefore assumed to be 1. Ethane is assumed to yield no formaldehyde, since the decomposition rate of the ethoxy radical formed, after HO· abstraction of a hydrogen, is negligible compared to the O_2 reaction rate (Altshuller 1991a). Cyclopropane is assumed to have the same formaldehyde yield as propane. The concentration of cyclopropane was small, at < 0.020 ppbV during the Simcoe study, so any assumption made for the yield will have no significant effect on the overall analysis. Cyclopentane is assumed to have the same yield as n-pentane. 2,2-dimethylpropane is assumed to have the same yield as isopentane, but since the concentration of 2,2-dimethylpropane during the Simcoe study was < 0.010 ppbV and generally < 0.005 ppbV, it will also have no significant effect on the outcome of the analysis. The 2-butenes and 2-pentenes yield almost no formaldehyde via HO· reaction based on mechanistic data provided by Atkinson, 1994. The formaldehyde yield is therefore assumed to be 0. The value given for 2-methyl-1-butene by Altshuller, 1991b, is for combined HO· and ozone chemistry under typical atmospheric conditions. Altshuller, 1991b, also estimates that HO· reaction dominates at ~84% of the total reaction rate for 2-methyl-1-butene. The yield is therefore assumed to be equivalent to the HO· yield. The value of 0.92 used is in reasonable agreement with other 1-alkenes such as 1-butene and 1-pentene with yields of 1.0 and 0.875 respectively.

Formaldehyde yields for HO· reactions with isobutene (0.92 ± 0.08), cis-2-butene (0), and 2-methyl-2-butene (0), have been experimentally determined by Tuazon *et al*, 1998, and were found to agree with the values listed in Table 9. Aromatic chemistry has been assumed to be a negligible formaldehyde source. The validity of this assumption is difficult to evaluate however. The production of formaldehyde from some aromatics is certainly a possibility, and given that a significant fraction (~30-50%) of the products of aromatic oxidation remain unaccounted for (Atkinson, 2000), it is likely that at least some formaldehyde is produced from aromatic chemistry. No yield information is available however, and so the yields are assumed to be zero for this analysis.

Formaldehyde yields for several ozone-alkene reactions have also been estimated. 1,3 butadiene (yield of 0.7) is assumed to lie between 1-butene and isoprene (0.5 and 0.9 respectively). Cis-2-butene is assumed to have the same formaldehyde yield as trans-2-butene. Cis-2-pentene is assumed to have the same formaldehyde yield as trans-2-pentene. 2-methyl-1-butene is assumed to have a yield equivalent to 1-pentene. Ethene, propene, and 1-butene values given by Altshuller, 1993, have been compared with the experimentally determined values given by Grosjean *et al*, 1996a, and are found to agree. The trans-2-butene yield of 0.3 given by Altshuller, 1993, is somewhat higher than the value found by Grosjean E. *et al*, 1996a, of 0.13. The 1-pentene yield of 0.5 is in excellent agreement with Grosjean E. and Grosjean D., 1996d, of 0.505. The yield for 1-butene of 0.5 is also in reasonable

agreement with the value given by Grosjean E. *et al*, 1996a, of 0.63. Some difference is seen between the Altshuller value of 0.15 for 2-methyl-2-butene and the Grosjean E., 1996a, of 0.25, however, these discrepancies have no significant effect on the results, due to the low yields, and relatively low reactivities with ozone.

Some uncertainty exists in the yield of formaldehyde from the ozone reaction with iso-butene. Grosjean D. *et al*, 1994, give an experimentally determined yield of 0.31, while Grosjean E. *et al*, 1996a, give an experimental yield of 0.95. Atkinson, 1997, gives a yield of 1.01. Thus three significantly different literature values of 0.31, 0.5 (Altshuller, 1993), and ~1 exist. The value obtained by Tuazon *et al* (unpublished work) given by Atkinson, 1997, of ~1 seems to agree with the Grosjean E., 1996a, value, and is likely the most reliable value. Recalculation of the formaldehyde contributions show that there is no significant change with use of an iso-butene yield of 1 or 0.5, and so the analysis here is not affected by this discrepancy in the literature values.

	HO Reaction Yields	Ozone Reaction Yields	$10^{12} \times k_{HO}$ (molecules·cm^{-3}·s^{-1})	$10^{18} \times k_{O3}$ (molecules·cm^{-3}·s^{-1})
Methane	1[a]		0.00618	
Ethane	0[b]		0.254	
Propane	0.009[b]		1.12	
Cyclo-propane	0.009[a]		0.084	
n-Butane	0[b]		2.44	
Iso-Butane	0.752[b]		2.19	
Cyclo-Pentane	0[a]		5.02	
n-Pentane	0[b]		4	
Iso-Pentane	0.005[b]		3.7	
2,2-Dimethylpropane	0.005[a]		0.85	
Ethene	1.62[c]	1[g]	8.52	1.45
Propene	1[c]	0.65[g]	26.3	9.6
1,3-Butadiene	1[d]	0.7[a]	66.6	6.3
1-Butene	1[c]	0.5[g]	31.4	8.8
Iso-Butene	1[c]	0.5[g]	51.4	10.9
Cis-2-Butene	0[a]	0.3[a]	56.4	123
Trans-2-Butene	0[a]	0.3[g]	64	202
Isoprene	0.7[f]	0.9[e]	101	12.8
1-Pentene	0.875[c]	0.5[c]	31.4	9.2
Cis-2-pentene	0[a]	0.15[a]	65	200
Trans-2-pentene	0[a]	0.15[g]	67	200
2-methyl-1-butene	0.92[a]	0.5[a]	61	400
2-methyl-2-butene	0[a]	0.15[g]	86.9	400

Table 9. Reaction rate constants and formaldehyde yields used in the calculation of the formaldehyde budget. Yields are on a molar basis, and have been adapted from the original references where required. The rate constants have been obtained from Finlayson-Pitts and Pitts, 2000. Notes: a, See text for explanation. b, Altshuler, 1991a. c, Altshuller 1991b. d, Atkinson 1994. e, Aschmann and Atkinson 1994. f, Lee et. al. 1998. g, Altshuller, 1993.

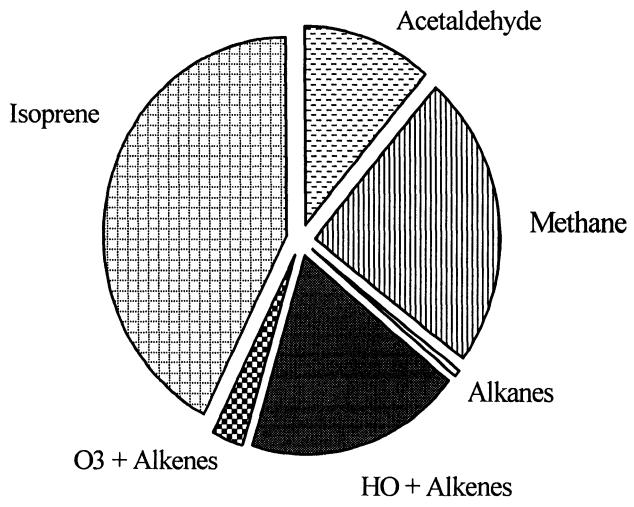

Figure 55. Relative contribution of hydrocarbons to the production of formaldehyde during Simcoe 2000.

The relative contributions of the various hydrocarbon based formaldehyde sources are shown in Figure 55. The contributions from isoprene, methane, alkenes, acetaldehyde and alkanes are estimated as 42.5%, 23.9%, 21.6%, 11.3% and 0.6% respectively. The alkene contribution was found to be dominated by $HO^{\cdot}$ chemistry (~ 87%), with a minor contribution from alkene reactions with ozone (~13%). Isoprene was found to be the single most important species in terms of formaldehyde production, being more important than all the alkanes and alkenes combined. The largest contribution to the isoprene source of formaldehyde was found to be reaction with $HO^{\cdot}$, which represents ~ 97% of the isoprene derived formaldehyde. The isoprene concentrations during the study were relatively low compared to other rural sites with

an average concentration of ~0.27 ppbV, compared to 4.2 ppbV during the 1995 Nashville/Middle Tennessee Ozone Study (Lee et. al., 1998). The formaldehyde production is however dominated by the oxidation of isoprene, even at these lower concentrations, due to its high reactivity with $HO^{\cdot}$, and its high formaldehyde yield. Isoprene then is a significant source of radicals in itself, since formaldehyde photolysis represents ~14% of the total radical production, and about half of the formaldehyde is a direct result of isoprene oxidation.

Knowledge of both the production rate and the removal rate for formaldehyde allows a comparison of the two. The average production rate of formaldehyde from the sources considered here is estimated as 0.78 $ppbV \cdot hr^{-1}$ for midday samples. The removal rate can be estimated from the photolysis rate, and the $HO^{\cdot}$ rate constant, along with the concentration of formaldehyde. Reaction of formaldehyde with $HO^{\cdot}$ is a significant sink for formaldehyde, and must be included. At midday, $[HCHO] \approx 1.0$ ppbV during the Simcoe study. The total photolysis rate has been estimated as $8.0 \times 10^{-5} s^{-1}$ using values given by Jenkin *et al*, 1997, and evaluated for the period and location of the study. As for the production rate calculations, it is assumed that $[HO^{\cdot}] = 5 \times 10^{6}$ $molecules \cdot cm^{-3} \cdot s^{-1}$. The average removal rate of formaldehyde is then estimated as ~ 0.45 $ppbV \cdot hr^{-1}$, giving a ratio of production to removal of ~1.7. The ratio of production to removal is somewhat sensitive to the $[HO^{\cdot}]$ value chosen, since the removal by photolysis is significant, while the production is dominated by $HO^{\cdot}$ chemistry. The removal rate may be somewhat

underestimated, since the deposition of formaldehyde has not been included in the analysis. Including the dry deposition of formaldehyde to the surface, as a removal process will most likely improve the agreement between the values estimated for removal and formation, but the assumed [$HO^{\cdot}$] has the most significant effect on the formaldehyde budget.

Unlike glyoxal, it appears that the hydrocarbon oxidation sources that have been included here can reasonably account for the observed formaldehyde levels. However, this analysis has been performed using only the hydrocarbon data available during this field study. Although extensive, this data set cannot include all hydrocarbon or oxygenated hydrocarbon concentrations. The other uncertainty in this analysis is that formaldehyde yields are simply not known for some hydrocarbons within the data set. The formation of formaldehyde from those sources not included in this analysis, will increase the production to removal ratio. As in the case of glyoxal, a potential loss process that has not been included in the alnalysis is the possibility of losses to atmospheric particles. Little information exists on this process, and so this loss is difficult to estimate. This analysis must be viewed with these limitations in mind.

4.2.5. Acetaldehyde Budget

An analysis similar to the one performed for formaldehyde (section 4.2.4) has been performed for acetaldehyde based on the hydrocarbon data from the Simcoe

study. The yield information used for the calculations is listed in Table 10, and the reaction rates are listed in Table 9. Similar assumptions have been made for the acetaldehyde budget as for the formaldehyde budget. The [HO·] is assumed to be 5×10^6 molecules·cm^{-3}, and the [NO] levels are assumed to be high enough that the reaction of peroxy radicals with NO will dominate over peroxy-peroxy self-reaction. Also, as for formaldehyde, only midday samples have been included in the calculations. Aromatic chemistry has been assumed to be a negligible acetaldehyde source. The validity of this assumption is difficult to evaluate. The production of acetaldehyde from certain aromatics may be a possibility, since a significant fraction (~30-50%) of the products of aromatic oxidation remain unaccounted for but yield information is not available, and so the yields are assumed to be negligible.

Assumptions were required for the acetaldehyde yield for several HO· reactions with hydrocarbons. Cyclo-propane is assumed to have a yield equivalent to propane. Cyclo-pentane has been assumed to have a yield equivalent to n-pentane. 2,2-dimethyl propane is assumed to yield no acetaldehyde. Assumptions made for the ozone reactions with alkenes for which yields were not directly available are as follows. Trans-2-butene is assumed to have the same yield as cis-2-butene. 1-pentene and 2-methyl-1-butene are assumed to have the same yield as 1-butene. Cis-2-pentene is assumed to have the same yield as trans-2-pentene. Acetaldehyde yields for HO· reactions with isobutene (0), cis-2-butene (1.85 ± 0.25), and 2-methyl-2-butene

(0.98 ± 0.10), have been experimentally determined by Tuazon *et al*, 1998, and were found to agree with the values listed in Table 10.

The resulting production rates for acetaldehyde from the hydrocarbons during Simcoe 2000 are shown in Figure 56. The hydrocarbons, which yielded the highest production rates, were propene and trans-2-butene. The majority of the acetaldehyde production was found to be from $HO^{\cdot}$ reactions with alkenes, as shown in Figure 57. The distributions between the sources examined here are 19%, 64%, and 17% for the alkanes, $HO^{\cdot}$ with alkenes, and O_3 with alkenes respectively. Alkenes represent a combined contribution of 81% of the total acetaldehyde production.

	HO Reaction Yields	Ozone Reaction Yields
Methane	0[a]	
Ethane	1.0[b]	
Propane	0[b]	
Cyclo-propane	0[a]	
n-Butane	0.389[b]	
Iso-Butane	0[b]	
Cyclo-Pentane	0.326[a]	
n-Pentane	0.326[b]	
Iso-Pentane	1.3[b]	
2,2-Dimethylpropane	0[a]	
Ethene	0[c]	0[c]
Propene	1.0[c]	0.5[c]
1,3-Butadiene	0[d]	0[d]
1-Butene	0[c]	0.15[c]
Iso-Butene	0[c]	0[c]
Cis-2-Butene	2.0[a]	1.0[f]
Trans-2-Butene	2.0[a]	1.0[a]
Isoprene	0[d]	0[e]
1-Pentene	0[a]	0.15[a]
Cis-2-pentene	1.0[a]	0.625[a]
Trans-2-pentene	1.0[a]	0.625[f]
2-methyl-1-butene	0[c]	0.15[a]
2-methyl-2-butene	1.0[a]	0.5[f]

Table 10. Acetaldehyde yields used in the calculation of the acetaldehyde budget. Yields are on a molar basis, and have been adapted from the original references where required. Notes: a, See text for explanation. b, Altshuler, 1991a. c, Altshuller 1991b and Atkinson and Loyd, 1984. d, Atkinson 1994. e, Aschmann and Atkinson 1994. f, Altshuller, 1993.

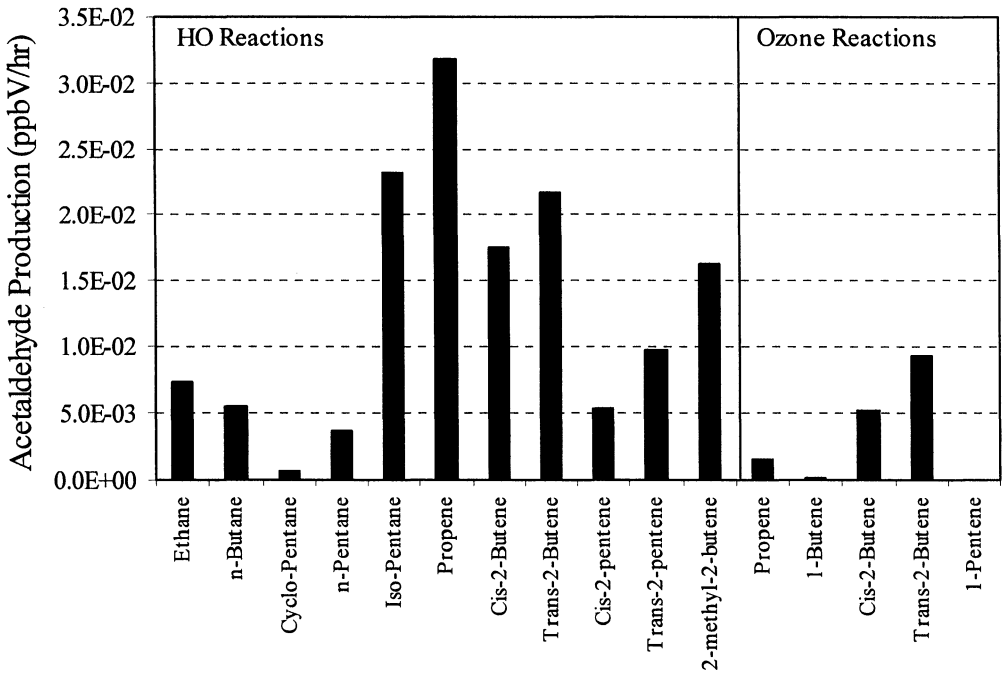

Figure 56. Acetaldehyde production rates from hydrocarbons for midday samples taken during Simcoe 2000.

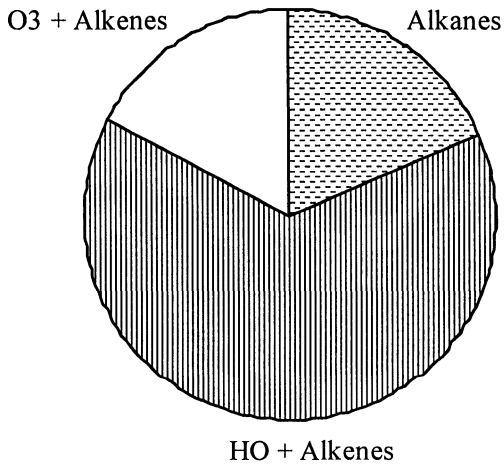

Figure 57. Distribution of acetaldehyde sources during the Simcoe 2000 study.

The total acetaldehyde production rate is estimated to be ~0.19 ppbV/hr. The removal rate for acetaldehyde can be estimated using the photolysis rate and the $HO^{\cdot}$ reaction rate. A photolysis rate of $4.4 \times 10^{-6} s^{-1}$ has been estimated for midday at the Simcoe site, and a $HO^{\cdot}$ rate of 1.58×10^{-11} molecules$\cdot cm^{-3} \cdot s^{-1}$ has been used for the calculation. The midday average acetaldehyde concentration was found to be ~0.35 ppbV during the study, giving a total removal rate of ~0.11 ppbV/hr. The ratio of production to removal is then ~1.7. As with formaldehyde, dry deposition has not been included as a removal process, which if included would bring the removal closer to the production rate. Unlike formaldehyde, the resulting ratio of production to removal should be relatively insensitive to the assumed $[HO^{\cdot}]$. The main production mechanism appears to be the reaction of $HO^{\cdot}$ with both alkanes and alkenes, accounting for ~83% of the total acetaldehyde production. The removal mechanism is also dominated by $HO^{\cdot}$, at ~95% of the removal at a $[HO^{\cdot}] \approx 5 \times 10^{6}$ molecules$\cdot cm^{-3}$. Calculating the ratio of production to removal at $[HO^{\cdot}] \approx 1 \times 10^{6}$ molecules$\cdot cm^{-3}$ yields a ratio of ~1.6, thus the assumed $[HO^{\cdot}]$ has little effect on the ratio. The most probable reason for the difference between the production and removal is the uncertainty in the production rate, created by uncertainties in the yields. While the production rate is higher than the removal rate, the possibility of omitted sources of acetaldehyde is a possibility. The yields in many cases are not based on experimental values, but rather on estimation methods developed based on results and mechanistic information from other hydrocarbons (Atkinson, 1994), and although generally useful for predicting product

yields, these methods may give yields significantly different from the true yields. Also as for formaldehyde, yields from many hydrocarbons are not known.

4.2.6. Acetone Budget

The acetone budget has been calculated using methods similar to those for formaldehyde and acetaldehyde in sections 4.2.4 and 4.2.5. The formation yields for acetone from the hydrocarbons measured during Simcoe 2000 are listed in Table 11, and the reaction rate constants are listed in Table 9. Acetone presents a somewhat different analysis situation compared to formaldehyde and acetaldehyde, in that the lifetime of acetone is relatively long, and so it is not reasonable to assume that it is at a 'steady state' concentration during the daytime hours. For a photolysis rate of $5.7 \times 10^{-7} s^{-1}$ at midday (Jenkin *et al*, 1997), and a $HO^{\cdot}$ reaction rate of $2.3 \times 10^{-13} molecules^{-1} \cdot cm^3 s^{-1}$ (Atkinson, 1990), and assuming $[HO^{\cdot}] = 5 \times 10^6$ molecules$\cdot cm^{-3}$ the lifetime of acetone is ~166 hours. This is certainly not a short lifetime for the time scales of interest here, and so must be considered in the analysis. The yields which were not available in the literature, and have been assumed are as follows. Methane and ethane are assumed to yield no acetone. Cyclo-propane and 2,2-dimethylpropane are also assumed to yield no acetone. Cyclo-pentane is assumed to have the same acetone yield as n-pentane.

	HO Reaction Yields	Ozone Reaction Yields
Methane	0[a]	
Ethane	0[a]	
Propane	0.661[b]	
Cyclo-propane	0[a]	
n-Butane	0[b]	
Iso-Butane	0.75[b]	
Cyclo-Pentane	0[a]	
n-Pentane	0[b]	
Iso-Pentane	0.605[b]	
2,2-Dimethylpropane	0[a]	
Ethene	0[c]	0[c]
Propene	0[c]	0[c]
1,3-Butadiene	0[d]	0[d]
1-Butene	0[c]	0[c]
Iso-Butene	1[c]	0.5[c]
Cis-2-Butene	0[c]	0[c]
Trans-2-Butene	0[c]	0[c]
Isoprene	0[d]	0[e]
1-Pentene	0[c]	0[c]
Cis-2-pentene	0[c]	0[c]
Trans-2-pentene	0[c]	0[c]
2-methyl-1-butene	0[c]	0[c]
2-methyl-2-butene	0.9[f]	0.30[g]

Table 11. Acetone yields used in the calculation of the acetone budget. Yields are on a molar basis, and have been adapted from the original references where required. Notes: a, See text for explanation. b, Altshuler, 1991a. c, Altshuller 1991b. d, Atkinson 1994. e, Aschmann and Atkinson 1994. f, Tuazon, 1998. g, Grosjean *et. al.* 1996a.

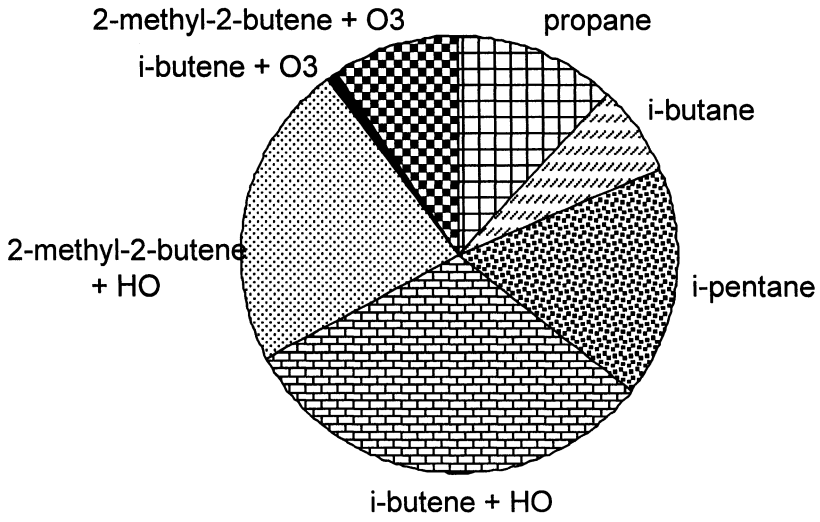

Figure 58. Relative contributions of the hydrocarbons to the acetone production during Simcoe 2000.

The relative contributions of the hydrocarbons to the production of acetone are shown in Figure 58. Acetone production is dominated by HO· chemistry at the assumed HO· of 5×10^6 molecules·cm^{-3}, representing 90% of the production rate. The total production rate based on the average daytime hydrocarbon concentrations is 0.064 ppbV/hr. It is interesting to note that the two most important acetone producing hydrocarbons are two alkenes, which represent 64% of the total acetone production. The concentrations of i-butene and 2-methyl-2-butene are 0.022 and 0.010 ppbV respectively. The high acetone production from these alkenes is due to their high reactivities and their high acetone yields. At the production rate estimated for acetone, these two compounds contribute significantly, despite their low levels. Propane

although much higher in concentration at ~0.58 ppbV, and with a significant acetone yield of 0.661, represents only ~12% of the total acetone production, since its $HO^{\cdot}$ reaction rate is fairly slow (~50 to 100 times slower than the alkenes). These results suggest that propane oxidation is a relatively small source of acetone production at this site. These results also agree with the speculation made by Goldstein and Schade, 2000, that the secondary anthropogenic contributions to the acetone levels in a forest were most likely minor from propane, and highest from isobutene and isopentene, although the measurement of these hydrocarbons was not performed.

The midday removal rate for acetone can be estimated based on the overall midday lifetime with respect to $HO^{\cdot}$ and photolysis of 166 hours, and the median midday concentration of 1.2 ppbV, giving a midday removal rate of 0.007 ppbV/hr. Compared to the midday production rate of 0.064 ppbV/hr, the removal rate is relatively minor. The net midday acetone production rate can be estimated as the difference between the production and removal rates, giving ~0.057 ppbV/hr. The measurements of acetone can be used to compare the estimated acetone daytime net production rate to the real acetone values. The diurnal acetone concentrations are potted in Figure 59. Each point represents the average of all data collected during the study in the two hour period centered at the time plotted. The daytime net production observed has been estimated by fitting a line to the daytime data. The data used in this calculation has been indicated as open circles on the plot. The resulting acetone

production rate is 0.051 ± 0.008 ppbV/hr. This is in agreement with the estimated net production rate from hydrocarbon oxidation of 0.057 ppbV/hr.

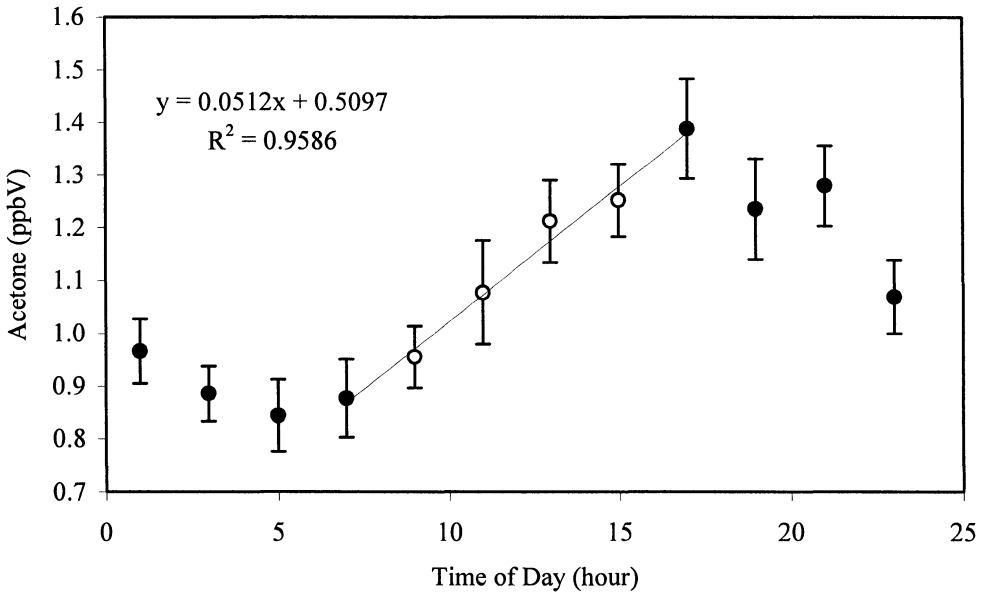

Figure 59. Midday acetone growth rate during Simcoe 2000. Points represent the average concentration for the two hour period centered at the time plotted for the entire study. The open circles show the data used in the calculation of the best fit line to estimate the net acetone production rate observed during the study. The error bars represent the 1σ uncertainty in the average values.

The possibility of significant above background acetone contribution from vehicle exhaust can be explored by examining the relationship between acetone and acetylene during the study. Acetylene can be used as a tracer for vehicle exhaust (Henry *et al*, 1994), and so a significant correlation between acetone and acetylene would suggest a local contribution from vehicle exhaust. The regression coefficient (r^2) for a plot of acetone vs. acetylene found for samples taken at ~2:00 PM local time

is ~0.1, and so these species are not well correlated. This suggests that no significant local source of acetone from vehicle exhaust existed during the time of the Simcoe 2000 study. Although some vehicle exhaust contribution to the background acetone level is certainly present, the relative amount is expected to be minor, since the ratio of acetone to acetylene on a molar basis in vehicle exhaust is small, at ~0.03 (Kirchstetter *et al*, 1999).

The above acetone budget analysis is highly dependant on the assumed [HO·], since the production rate is dominated by HO· reactions. At a [HO·] of 10^6 molecules·cm^{-3} the production of acetone becomes ~0.008 ppbV/hr, which is of course significantly lower than the daytime acetone increase. The analysis here must be viewed with this in mind. While it is likely that the majority of the above background acetone sources have been accounted for, reliable [HO·] estimates are required to determine this with greater certainty. The possibility of contribution to the acetone levels by biogenic emissions is known to be significant (Kotzias *et al*, in Helas *et al*, 1997), and is certainly not ruled out by this analysis.

4.2.7. Diurnal Profiles of Other Carbonyls

For comparison with the acetone diurnal profile, the profiles of formaldehyde, acetaldehyde and glyoxal have been plotted, and are shown in Figure 60. Formaldehyde shows a distinct day to night difference of ~0.4 ppbV, and a fairly stable

midday concentration of ~0.7 ppbV on average. Acetaldehyde shows little day to night variation on average, with a level of ~0.35 ppbV. Glyoxal, like formaldehyde shows a distinct day to night difference of ~0.4 ppbV. Peak concentrations occur in the 8 PM to 10 PM time period.

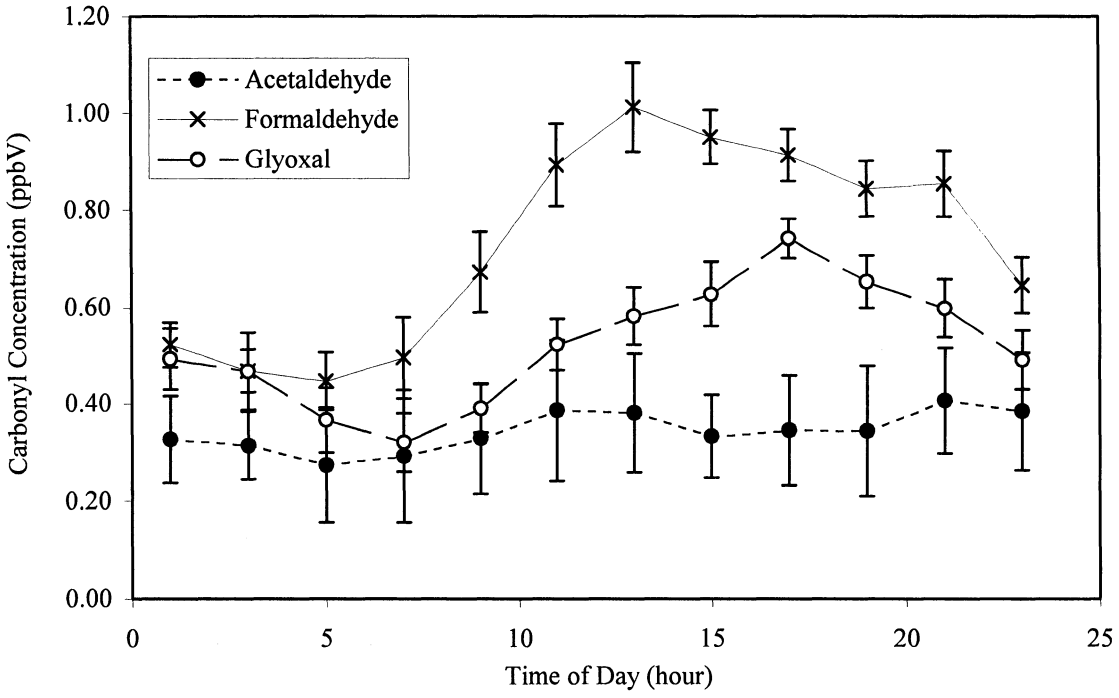

Figure 60. Diurnal profile of formaldehyde, acetaldehyde and glyoxal during Simcoe 2000. Points represent the average concentration for the two hour period centered at the time plotted for the entire study. Error bars represent the 1σ uncertainty in the average values.

4.2.8. Relationship Between Formaldehyde and Acetaldehyde

Since formaldehyde and acetaldehyde both have similar sources in hydrocarbon oxidation, and similar overall daytime lifetimes due to removal by $HO^{\cdot}$ and photolysis, some comparison can be made between these species. Based on the production rates calculated for formaldehyde and acetaldehyde (sections 4.2.4 and 4.2.5), and their lifetimes, it is possible to calculate the theoretical ratio of formaldehyde to acetaldehyde expected during Simcoe 2000. Assuming $[HO^{\cdot}] = 5 \times 10^6$ molecules·cm^{-3}, and for midday photolysis rates for Simcoe, the lifetimes of formaldehyde and acetaldehyde are estimated as 2.2 hours, and 3.3 hours respectively. The theoretical ratio of formaldehyde to acetaldehyde can be estimated as,

$$\frac{[formaldehye]}{[acetaldehyde]} = \frac{P_{form}\tau_{form}}{P_{acetal}\tau_{acetal}} \qquad \text{Equation 28}$$

where P_{form} and P_{acetal} are the production rates for formaldehyde and acetaldehyde respectively, as calculated in sections 4.2.4 and 4.2.5, and τ_{form} and τ_{acetal} are the lifetimes of formaldehyde and acetaldehyde respectively. The theoretical ratio calculated is then ~2.6 for these conditions.

The ratio of formaldehyde to acetaldehyde during Simcoe 2000 can be estimated in different ways for the ambient measurements. The ratio can be obtained by simply dividing the concentrations for each sample to determine the ratio for a

given sample, and averaging the ratios. This results in a ratio of 2.8 ± 0.6 for samples collected between 12:00 PM and 5:00 PM local time. The error in the ratio represents the 1σ standard deviation. This value appears to be in reasonable agreement with the theoretical estimated ratio of 2.6. A plot of acetaldehyde vs. formaldehyde is given in Figure 61, with the least squares regression best fit line shown. If the formaldehyde to acetaldehyde ratio is calculated as the reciprocal of the slope of this line, then the ratio determined is 4.2 ± 0.8 where the error is determined by the 1σ standard error in the slope. This ratio is somewhat higher than the theoretically calculated one.

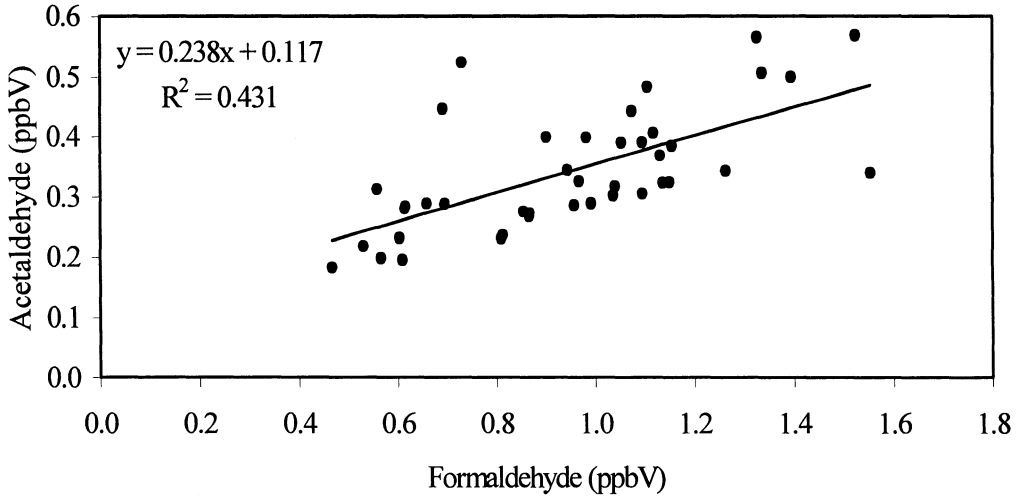

Figure 61. Acetaldehyde vs. formaldehyde during Simcoe 2000.

While a positive intercept in the acetaldehyde data may suggest a source of acetaldehyde, which is not a source of formaldehyde, the situation may be more complex than this. If the regression analysis is presumed to represent local secondary chemistry, then at steady state, the net production of formaldehyde is ~4 times higher than acetaldehyde from secondary sources. This suggests a gas phase photochemical source of formaldehyde, which has not been included in the analysis, or possibly an acetaldehyde sink has been omitted. Since the deposition of both to the surface is unknown, it is possible that this loss mechanism is significantly larger for acetaldehyde than for formaldehyde. Unknown formaldehyde sources may be biogenic in nature, although emission rates for the plant species in the region of Simcoe would have to be evaluated specifically. High biogenic formaldehyde emitters may create the same effect as an increased production of formaldehyde at steady state. The uncertainties in the aldehyde yields from some hydrocarbons, and the production from unmeasured hydrocarbons could possibly account for this difference.

4.2.9. Nighttime Carbonyl Decay

Inspection of Figure 42, Figure 43 and Figure 45 shows that there are a few nights when a significant decrease in the concentrations of the carbonyls and ozone are seen. The production of the carbonyls at night will be reduced, since the main production route is through HO· chemistry, and the HO· is expected to be very low at night. The removal rates by HO· chemistry and by photolysis will obviously also be insignificant at night as well. Thus the carbonyl concentrations are relatively unaffected at night by most production sources, and by most removal mechanisms other than deposition. A comparison can be made between the ozone deposition rate and the carbonyl deposition rates to estimate the relative rate of deposition at night for the carbonyls. The first order rate constant (k_{dep}) for deposition to the surface is given by:

$$k_{dep} = \frac{v_{dep}}{H} \qquad \text{Equation 29}$$

where v_{dep} is the deposition velocity, and H is the height of the mixed layer.

$$\frac{k_i}{k_{O_3}} = \frac{v_{dep_i} / H}{v_{dep_{O_3}} / H} = \frac{v_{dep_i}}{v_{dep_{O_3}}} \qquad \text{Equation 30}$$

The nighttime decay rates for ozone can then be used to estimate the deposition velocities of the carbonyls. Three nights during the study will be explored in this

respect. These are July 11th to 12th, July 17th to 18th, and July 19th to 20th. The concentrations from these nights are shown in Figure 62. The nights chosen for this analysis were subject to low wind speeds of ~1 to 3 km/hr, from the northwest, allowing the deposition process to dominate over either transport or mixing. Removal of ozone via reaction with NO is assumed to be minor for this analysis. The lifetime of NO with respect to O_3 is on the order of 1 minute for an ozone level of 30 ppbV (Shepson *et al*, 1992). The removal of ozone will then be insignificant as long as there is no ground source of NO. The validity of this assumption is difficult to estimate since no there is no NO emission data from the Simcoe site. NO values obtained were roughly 0.0 ppbV with a measurement resolution of 1.0 ppbV, so that the NO concentrations can only be estimated as <1 ppbV. This does not rule out significant removal of ozone through NO reactions, and so this analysis will be affected by this uncertainty.

NO_3 chemistry can be significant at night, and so should be examined to ensure it does not have a significant effect on the loss rates of the carbonyls of interest. The effect of NO_3 on the nighttime decay rates can be estimated using the second order rate constants, and the approximate concentrations of the species involved. Reaction of acetone with NO_3 is unimportant in the troposphere, and so NO_3 chemistry will not be significant as a sink for acetone in this analysis (Atkinson, 2000). Estimating typical NO_3 night time levels to be about 0.02 ppbV (McLaren *et al*, in press), and given a second order rate constant of 6×10^{-16} cm^3 molecule^{-1} s^{-1} and

2.7×10^{-15} cm^3 $molecule^{-1}$ s^{-1} for formaldehyde and acetaldehyde respectively (Atkinson, 1990), the approximate removal rate for formaldehyde and acetaldehyde are 10 pptV and 20 pptV with respect to NO_3 chemistry over 8 hours. Decays for formaldehyde and acetaldehyde of about 400 pptV and 150 pptV respectively, were seen on the three nights used in this analysis. NO_3 chemistry is therefore negligible as a nighttime loss process for these species. No kinetic data are available for reaction of glyoxal with NO_3 (Atkinson, 2000), and so it is difficult to estimate the effects on its decay rate. NO_3 is assumed to have no effect for the purpose of this analysis.

If deposition is the main removal mechanism, then the concentration change with time should be consistent with a first order removal, since deposition is a first order process. The expected relationship is then,

$$\ln \frac{[carbonyl]_t}{[carbonyl]_o} = -kt \qquad \text{Equation 31}$$

and a plot of $\ln([carbonyl]_t/[carbonyl]_o])$ vs. t should yield a straight line of slope –k.

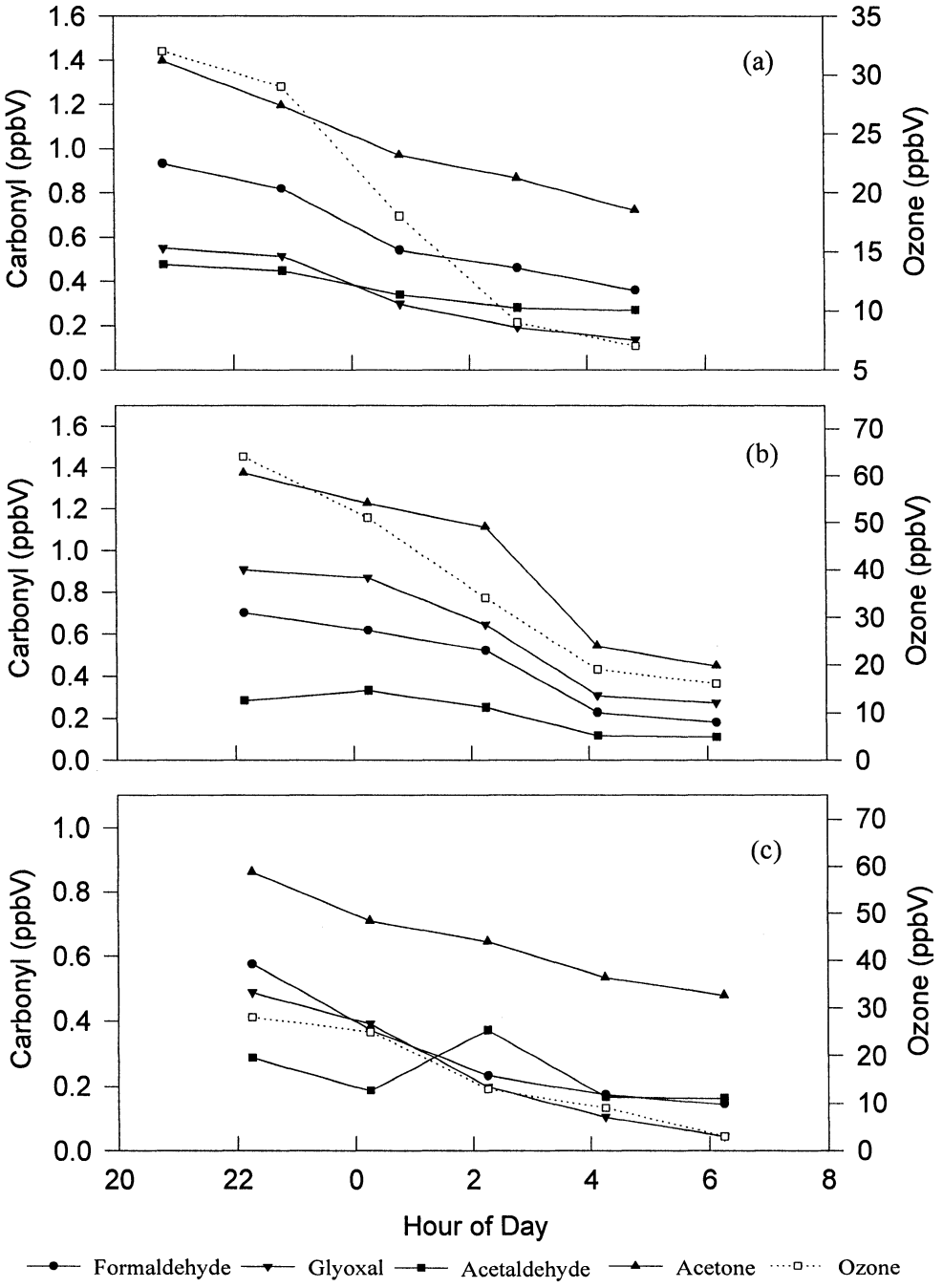

Figure 62. Carbonyl and ozone nighttime decays for (a) July 11th to 12th, (b) July 17th to 18th and (c) July 19th to 20th.

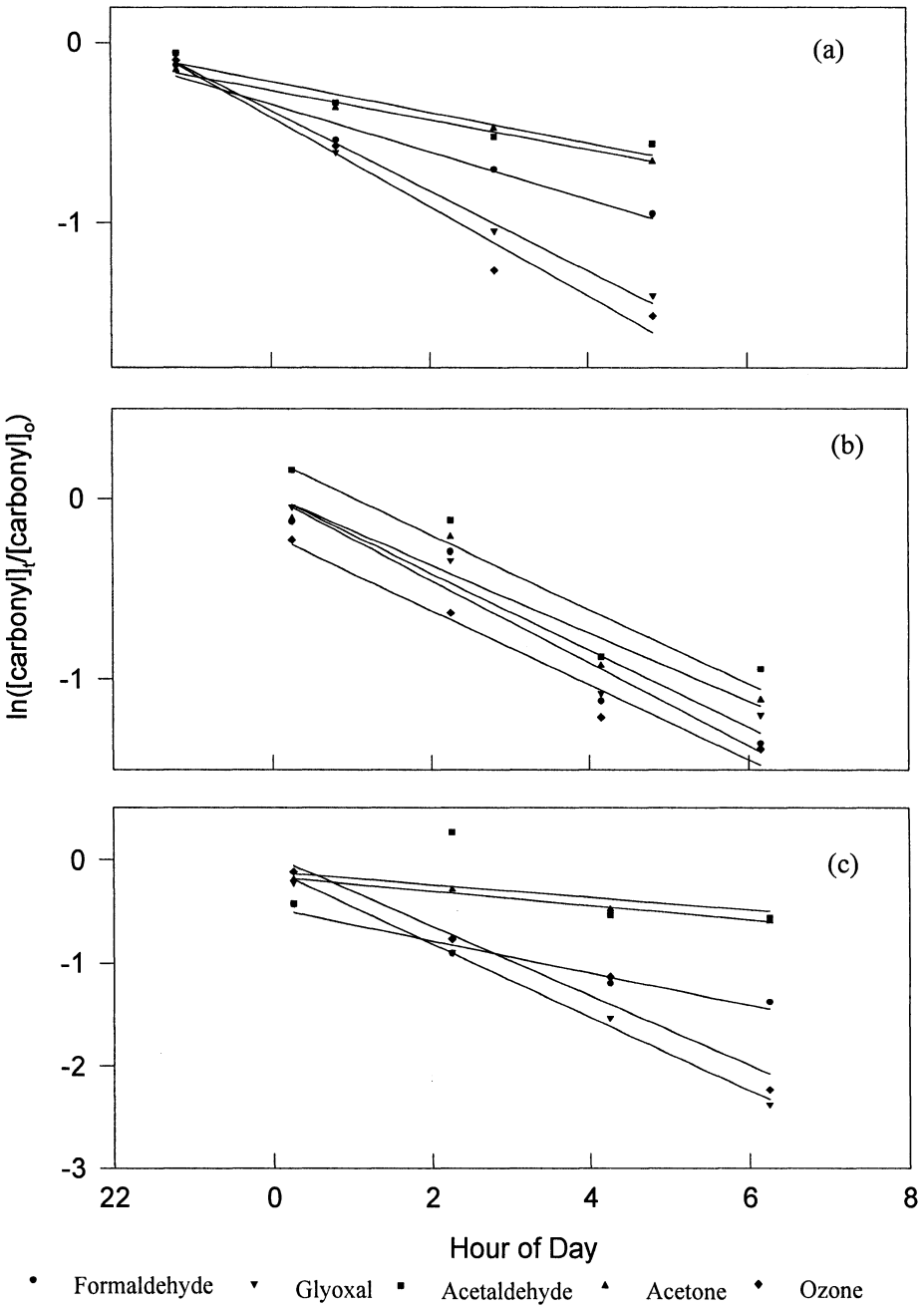

Figure 63. Plots of $\ln([carbonyl]_t/[carbonyl]_o])$ vs. time for (a) July 11th to 12th, (b) July 17th to 18th, and (c) July 19th to 20th. The lines represent the least squares best fit.

The plots of $\ln([carbonyl]_t/[carbonyl]_o])$ vs. time are shown in Figure 63. In general, the plots show linear results, with regression coefficients (R^2) of >0.9, with the exception of the acetaldehyde results for July 19th to 20th (Table 12). The poor regression coefficient for acetaldehyde is caused by one point, which significantly deviated from the linear fit. The point has not been removed from the calculations. The reasonably linear fit in most cases indicates that the decays are due to some first order process, most likely deposition to the surface. The results are summarized in Table 12.

	Formaldehyde	Acetaldehyde	Acetone	Glyoxal	O_3
July 11th-12th					
Slope	-3.7E-5	-2.4E-5	-2.3E-5	-6.2E-5	-6.9E-5
R^2	0.96	0.91	0.99	0.99	0.97
July 17th-18th					
Slope	-6.3E-5	-5.6E-5	-5.2E-5	-5.8E-5	-5.6E-5
R^2	0.93	0.91	0.91	0.93	0.96
July 19th-20th					
Slope	-4.4E-5	-1.7E-5	-1.9E-5	-9.9E-5	-9.4E-5
R^2	0.96	0.16	0.98	0.996	0.96
Average slope ($\times 10^5$ s^{-1})	-4.8 ± 1.4	-3.2 ± 2.1	-3.1 ± 1.8	-7.3 ± 2.2	-7.3±1.9

Table 12. Results of the least squares best fit regression analysis performed on the data in Figure 63. The errors for the average slope are the 1σ standard deviation of the three slopes obtained.

The ratio of k_i to k_{O3} (Equation 30) has been calculated for each night examined. The results are given in Table 13.

	Formaldehyde	Acetaldehyde	Acetone	Glyoxal
July 11^{th}-12^{th}	0.53	0.34	0.33	.90
July 17^{th}-18^{th}	1.11	1.0	.92	1.0
July 19^{th}-20^{th}	0.47	0.18	0.20	1.1
Average k_i/k_{O3}	0.7 ± 0.4	0.5 ± 0.4	0.5 ± 0.4	1.0 ± 0.1

Table 13. k_i to k_{O3} ratios calculated for each night. Errors are the 1σ standard deviations of the three values.

It is important to note that the area surrounding the Simcoe site is relatively flat, since Wesely and Hicks, 2000, discuss significant uncertainties created by non-uniform terrain. Also, it is assumed that the measurement height of ~4 m is at a height at which the vertical concentration gradients are insignificant (*i.e.* within the mixed layer). For a species with deposition velocity of 0.2 $cm \cdot s^{-1}$, under neutral conditions, the difference in concentrations at 2 m and 4 m will be < 1% (Seinfeld and Pandis, 1998).

The ozone deposition velocities can be quite variable, and difficult to predict, and in general must be measured for the site and conditions of interest. While there is significant uncertainty in the absolute ozone deposition, the literature value of 0.2 cm/s given by Wesely and Hicks, 2000, for midsummer range land and agricultural land at night, can be used to estimate the absolute deposition velocity for the carbonyls. Formaldehyde, acetaldehyde, acetone and glyoxal are then estimated to have deposition velocities of 0.14 ± 0.07, 0.1 ± 0.09 and 0.1 ± 0.08 and 0.2 ± 0.02 cm/s

respectively. The errors given are the standard deviations of the deposition velocities determined, and are not meant as overall uncertainties. Considering the number of uncertainties in this analysis, the deposition velocities presented here are likely within a factor of 2, at best, of the true values. The deposition velocity ratios presented in Table 13 are somewhat more reliable than the final deposition velocities presented here. Use of the relative numbers for studies where ozone deposition is being monitored will give a better estimate of the carbonyl deposition velocities. If the assumption that there is no significant NO emission from the ground is not correct, then the relative deposition velocities given here will be underestimated.

Limited experimental data on the deposition velocities of carbonyls is available in the literature. Formaldehyde has been measured to have a nighttime deposition velocity of 0.5 cm/s in one study at a deciduous forest in summer, and no data are available for the other carbonyls examined in this analysis (Zhang et al, 2002). Limited comparisons can be made for formaldehyde, and no comparisons with other measurements are possible for the other species. The result of 0.5 cm/s given for formaldehyde deposition was obtained over deciduous forest, and is therefore not representative of the site in this study, which was agricultural.

In the case of glyoxal, the results here are difficult to interpret, since the source of glyoxal may be related to ozone induced surface emissions. The rate constants obtained from the plots are very similar for ozone and glyoxal. The close relationship

during the nighttime decay may be due to a more complicated situation however, and the deposition value obtained here should be viewed with this in mind.

4.3 Comparison Between Hamilton 1999 and Simcoe 2000

Since the areas surrounding the Hamilton 1999 site and the Simcoe 2000 site are different in nature, some comparisons can be made between the studies. The Hamilton study site was reasonably urban in nature, while the Simcoe site was more rural in nature. Median daytime carbonyl concentrations from the two studies have been plotted in Figure 64.

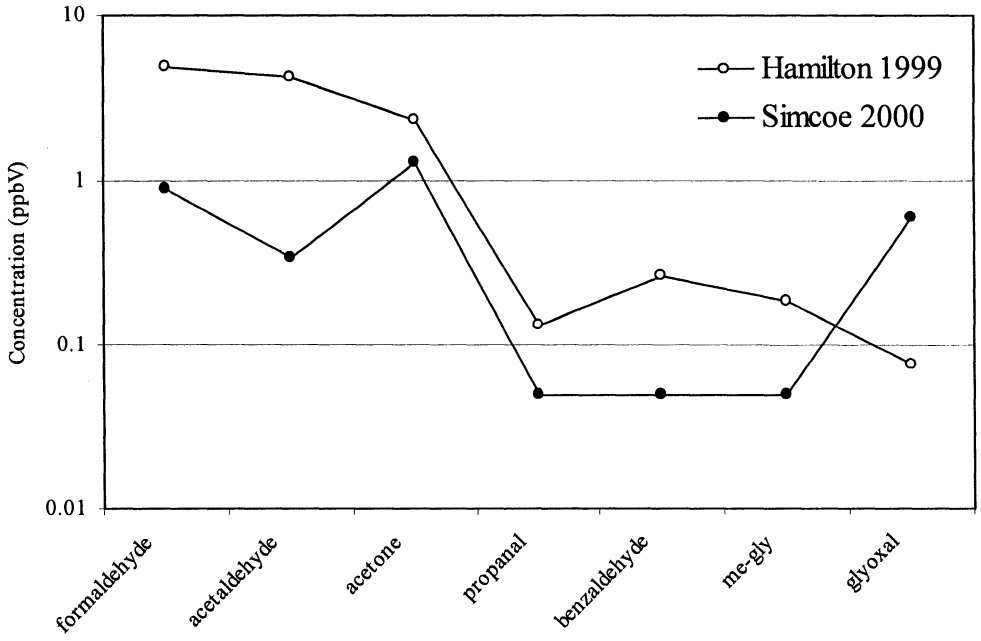

Figure 64. Daytime median carbonyl concentrations during Hamilton 1999 and Simcoe 2000.

The concentrations of benzaldehyde, methylglyoxal, and propanal, have all been assumed to be at the detection limit for the Simcoe study in Figure 64. Formaldehyde, acetaldehyde, propanal, benzaldehyde and methylglyoxal have similar distributions at the two sites, with lower concentrations at the Simcoe site. The exception to this is glyoxal, where higher concentrations were seen in Simcoe. Also, acetone deviates from the distribution for the other carbonyls, and shows a smaller difference between Hamilton and Simcoe. The fact that the acetone was higher at the urban site, as with most other species, suggests that there was some urban impact on the Hamilton sampling site during the field study. The smaller difference between the two sites for acetone is most likely due to the long lifetime of acetone in the atmosphere, giving an more even distribution over these two sites.

Glyoxal was the only carbonyl with higher concentrations at the Simcoe site. This again suggests a source of glyoxal from a source other that aromatic oxidation chemistry, since the aromatic hydrocarbon concentrations were higher in the Hamilton area. An analysis of the Hamilton data shows that the glyoxal concentrations were highest during the episode period of July 14th to 16th 1999, which coincided with high ozone levels and southwest winds, coming from the Simcoe area. These are consistent with a source of glyoxal which is relatively close to the Simcoe area, and is fairly widespread. If the glyoxal concentrations seen at the Simcoe site were due to a small source located very close to the sampling location, then it is unlikely that this source would have an impact on the glyoxal concentrations at the Hamilton site. The

effects of dilution and the short lifetime of glyoxal combined with the distance between the sites would make a small glyoxal source located at the Simcoe site an insignificant source of glyoxal at the Hamilton site.

5. CONCLUSIONS AND FUTURE WORK

The development of a highly innovative sampling and injection method for the determination of ambient carbonyls has been described in this thesis. This development is significant in the field of analytical chemistry as a whole, in that it describes an analytically sound technique by which a gas phase analyte can be quantified using a liquid phase technique. The application of this sampling/injection system utilizing the 'direct injection' method, need not be limited to the analysis of carbonyls, but can be applied to the analysis of any gas phase species which can be derivatized. A robust, useful technique has proven its usefulness in the field, especially in its application towards quantifying otherwise difficult analytes. The goal of automating the DNPH method was fulfilled with the instrument developed here. Improvements in detection limits and sampling times have been realized with close to an order of magnitude improvement over the standard DNPH cartridge technique, and with some minor modifications, this system can still realize significant improvements.

A micro scale UV absorbance detection system has been developed and used in this project with success. Full spectra can be collected for the hydrazone analytes with sufficient frequency, so that qualitative identification can be made, and possible interferences discovered. The acetaldehyde data collected during Hamilton 1999 is a good example of the usefulness of collecting full spectra, rather than a single wavelength. In short, the spectral data adds significant certainty to the identification

of analyte peak in real samples, where unknown interferences may exist. The 30 nL flow cell exceeds the volume requirements by about 10 times, and leaves a potential signal improvement by about 1 order of magnitude. This improvement can be realized by simply increasing the length of the flow cell, while maintaining the same cross sectional area. The effect on signal to noise realized would have to be experimentally determined, and will in principle depend on the experimental setup, light source used, and the spectrometer.

Some of the most interesting data collected during this project includes the substantial glyoxal data set obtained during Simcoe 2000. While the source of the observed glyoxal remains uncertain, the fact that an unknown source exists is significant for such a highly reactive species. The radical source in glyoxal may be significant over continental regions if the source is related to ozone induced biogenic emissions. Measurements at more sites, with diverse vegetation, under carefully designed measurement conditions are required to obtain a more representative picture of the overall glyoxal source strength. The glyoxal results here are significant in that the levels seen were higher than expected, and did not clearly follow known gas phase mechanisms. As such, these results are a reminder that known gas phase mechanisms may not describe the complete picture, and that compounds which may be important to atmospheric chemistry may not yet have received the attention they deserve. Development and validation of analytical methods aimed at the somewhat analytically difficult class of oxygenated hydrocarbons remains important work for future

researchers. Development of reliable, robust methods for these compounds, is a challenging task, since many are highly water soluble, sometimes thermally unstable, and present at trace levels in the atmosphere. Traditional methods using cryogenic trapping and thermal desorption are often unsuited to these analytes, and new methods must be developed to make useful measurements in the atmosphere.

The contribution of the low molecular weight carbonyls to the production of radicals has been estimated for the Simcoe 2000 study. Radical levels have often been estimated through modeling methods, based on known mechanisms, and the measurement information available. Knowledge of the carbonyl levels, which represent a significant fraction of the total radical source, allows more accurate estimates to be made, than what would be possible without carbonyl measurements. Most notably, the glyoxal levels, which are estimated to contribute ~75% as many radicals as formaldehyde, could not be explained with known gas phase mechanisms. In this case, the measurements are needed to estimate the total radical production.

An analysis of the gas phase budget for the carbonyls yielded some interesting information about the sources of the carbonyls. Formaldehyde and acetaldehyde were essentially accounted for by known gas phase mechanisms, with the greatest uncertainty being in the assumed $HO^{\cdot}$ level. An analysis of acetone showed a somewhat unexpected result, showing two relatively minor alkene species, in terms of absolute concentrations, being the most important contributors to the daytime production of acetone. 2-methyl-2-butene and iso-butene combined represent ~64% of

the total acetone production rate. The importance of propane in the production of acetone was found to be relatively minor at ~12%. Any acetone analysis which is to be undertaken in future field studies must include the two alkenes 2-methyl-2-butene and iso-butene. This case shows the importance of having hydrocarbon measurements for many carbonyl precursors, rather than the ones of highest concentration, or the ones for which the methodology is easiest.

Future improvements using this instrument, and the methodology developed here are possible, with relatively simple modifications to the current instrument. These involve two main improvements, one in the sampling system, and one in the detection system. Improvement in the sampling system can be realized by increasing the sampling flow rate and thereby increasing the sample size while maintaining the same cycle time. It has been shown in section 3.4 that complete trapping is seen for many analytes at flow rates ~4 times higher than those currently used. The flow rate selected was based on the maximum flow possible using the sampling cartridge in its present geometry. Increasing the diameter of the packed cartridge by a factor of 2, and decreasing its length by a factor of 4 will maintain the same packed volume, but will allow an increase in sampling flow rate by ~4 times. This will result in an increase in sample volume, and an equivalent decrease in detection limits. For analytes such as acetaldehyde, with detection limits of ~50-60 pptV (section 3.5), this would result in a detection limit of ~14 pptV for the same sampling time. For formaldehyde, a detection limit of ~22 pptV could be obtained, without increasing the total cycle time.

Improvements in the detector system will potentially yield significant improvements for species whose detection limit is instrument noise limited. For such species, detection limits are not dependant on the variability in the blank, but rather on the instrumental detection limit. Increasing the length of the flow cell will yield an equivalent increase in the response for analyte peaks. This increase could potentially provide another order of magnitude improvement in detection limits for many analytes.

The future of this analytical method may be in a somewhat different direction. Once improvements in the blank variability have been dealt with, improvements should be in the speed of analysis, allowing greater amounts of time to be dedicated to sample collection, rather than analysis. Significantly improved separation methods in the liquid phase have recently become available. These include Capillary Electrophoresis (CE), and its variations, and Capillary Electrochromatography (CEC). While both of these methods achieve significantly improved separations, and potentially shorter analysis times over conventional HPLC methods, the amount of sample which can be analysed remains quite small. Also, coupling the separation system to a more selective detection system could possibly eliminate some of the separation power required for the analysis of multiple carbonyls. LC-MS/MS provides a technique capable of significantly improved analyte identification, and could significantly reduce separation times, while improving the reliability of the data collected. While robust, the field portability of an LC-MS/MS system may be a

shortcoming of this direction in development. As the cost and portability of these systems improves in the future, their use may become more common in the field.

6. REFERENCES

Altshuller, A. P. Chemical Reactions and Transport of Alkanes and Their Products in the Troposphere. Journal of Atmospheric Chemistry. 1991a; 12:19-61.

Altshuller, A. P. Estimating Product Yields of Carbon-Containing Products from the Atmospheric Photooxidation of Ambient Air Alkenes. Journal of Atmospheric Chemistry. 1991b; 13:131-154.

Altshuller, A. P. Production of Aldehydes as Primary Emissions and from Secondary Atmospheric Reactions of Alkenes and Alkanes During the Night and Early Morning Hours. Atmoshperic Environment . 1993; 27A(1):21.

Anderson, L. G.; Lanning, J. A.; Barrell, R.; Miyagishima, J.; Jones, R. H., and Wolfe, Pamela. Sources and Sinks of Formaldehdye and Acetaldehyde: An Analysis of Denver's Ambient Concentration Data. Atmoshperic Environment. 1996; 30(12):2113-2123.

Apel, E. C.; Calvert, J. G.; Reimer, D.; Pos, W.; Zika, R.; Kleindienst, T. E.; Lonneman, W. A.; Fung, K.; Fujita, E.; Shepson, P. B.; Starn, T. K., and Roberts, P. T. Measurements Comparison of Oxygenated Volatile Organic Compounds at a Rural Site During the 1995 SOS Nashville Intensive. Journal of Geophysical Research. 1998; 103(D17):22295.

Arlander, D. W.; Bruning, D.; Schmidt, U., and Ehhalt, D. H. The Distribution of Acetaldehyde in the Lower Troposphere During TROPOZ II. Journal of Atmospheric Chemistry. 1995a; 22(3):243-249.

Arlander, D. W.; Bruning, D.; Schmidt, U., and Ehhalt, D. H. The Tropospheric Distribution of Formaldehyde during TROPOZ II. Atmospheric Chemistry. 1995b; 22(3):251-268.

Arnts, R.R and Tejada S.B. 2,4-Dinitrophenylhydrazine-coated Silica Gel Cartridge Method for Determination of Formaldehyde in Air: Identification of an Ozone Interference. Environmental Science and Technology. 1989; 22: 251-268.

Aschmann, Sara M. and Atkinson, Roger. Formation Yields of Methyl Vinyl Ketone and Methacrolein from the Gas-Phase Reaction of O_3 with Isoprene. Environmental Science and Technology. 1994; 28:1539.

Atkinson, R. Gas-phase Tropospheric Chemistry of Organic Compounds: A Review. Atmospheric Environment, Part A: General Topics. 1990; 24A(1):1-41.

Atkinson, R. Gas-phase Tropospheric Chemistry of Organic Compounds. Journal of Physical and Chemical Reference Data, Monograph No. 2. 1994.

Atkinson, R. Gas-Phase Tropospheric Chemistry of Volatile Organic Compounds: 1. Alkanes and Alkenes. Journal of Physical and Chemical Reference Data. 1997; 26(2):215-272.

Atkinson, R. Atmospheric Chemistry of VOCs and NO_x. Atmospheric Environment. 2000; 34:2063-2102.

Atkinson, R. and Lloyd, A. C. Evaluation of Kinetic and Mechanistic Data for Modelling of Photochemical Smog. Journal of Physical and Chemical Reference Data. 1984; 13(2):315.

Benning, L. and Wahner, A. Measurements of Atmospheric Formaldehyde (HCHO) and Acetaldehyde (CH_3CHO) during POPCORN 1994 using 2,4-DNPH Coated Silica Cartridges. Journal of Atmospheric Chemistry. 1998; 31(1-2):105.

Biesenthal, T. A.; Wu, Q.; Shepson, P. B.; Wiebe, H. A.; Anlauf, K. G., and MacKay, G. I. A Study of Relationships Between Isoprene, its Oxidation Products, and Ozone, in the Lower Fraser Valley, BC. Atmoshperic Environment. 1997; 31(14):2049-2058.

Biesenthal, T. A. The role of Carbonyl Compounds in Tropospheric Ozone Chemistry. Toronto: York University; 1997; c1997.

Biesenthal, T. A.; Bottenheim, J. W.; Shepson, P. B.; Li, S. M., and Brickell, P. C. The Chemistry of Biogenic Hydrocarbons at a Rural Site in Eastern Canada. Journal of Geophysical Research. 1998; 103(D19):25487.

Cardenas, L. M.; Brassington, D. J.; Allan, B. J.; Coe, H.; Alicke, B.; Platt, Urlich; Wilson, K. M.; Plane, J. M. C., and Penkett, S. A. Intercomparison of Formaldehyde Measurements in Clean and Polluted Atmospheres. Journal of Atmospheric Chemistry. 2000; 37:53-80.

Carey, M. A. and Persinger, H. E. Liquid Chromatographic Determination of Traces of Aliphatic Carbonyl Compounds and Glycols as Derivatives That Contain the Dinitrophenyl Group. Journal of Chromatographic Science. 1972; 10:537.

Carlier, P.; Hannachi, H., and Mouvier, G. The chemistry of carbonyl compounds in the atmosphere-a review. Atmospheric Environment, Part A: General Topics. 1986; 20(11):2079-2099.

Chance, K.; Palmer, P. I.; Spurr, R. J. D.; Martin, R. V.; Kurosu, T. P., and Jacob, D. J. Satellite Observations of Formaldehyde over North America from Gome. Geophysical Research Letters. 2000; 27(21):3461-3464.

Christensen, C. S.; Skov, H.; Nielsen, T., and Lohse, C. Temporal Variation of Carbonyl Compound Concentrations at a Semi-rural Site in Denmark. Atmoshperic Environment. 2000; 34:287-296.

Ciccioli, P.; Brancaleoni, E.; Frattoni, M..; Cecinato, A., and Brachetti, A. Ubiquitous Occurrence of Semi-Volatile Carbonyl Compounds in Tropospheric Samples and Their Possible Sources. Atmospheric Environment. 1993; 27A(12):1891-1901.

Ciccioli, P.; Fabozzi, C.; Brancaleoni, E.; Cecinato, A.; Frattoni, M..; Cieslik, S.; Kotzias, D.; Seufert, G.; Foster, P., and Steinbrecher, R.. Biogenic Emission from the Mediterranean Pseudosteppe Ecosystem Present in Castelporziano. Atmospheric Environment. 1997; 31(SI):167-175.

Dasgupta, P.; Zhang, G.; Schulze, S., and Marx, J. N. Measurement of Carbonyl Compounds as the 2,4-dinitrophynlhydrazonate Anion. Reaction Mechanism and an Automated Measurement System. Analytical Chemistry. 1994; 66:1965-1970.

Druzik, C. M.; Grosjean, D.; Van Neste, A., and Parmar, S. S. Sampling of Atmospheric Carbonyls with Small DNPH-coated C18 Cartridges and Liquid Chromatography Analysis with Diode Array Detection. International Journal of Environmental Analytical Chemistry. 1990; 38:495-512.

Dumdei, B. E. and O'Brien, R. J. Toluene Degradation Products in Simulated Atmospheric Conditions. Letters to Nature. 1984; 311(20):248-250.

Finlayson-Pitts, B. J. and Pitts, J. N. Jr. Chemistry of the Upper and Lower Atmosphere: Theory, Experiments and Applications. London: Academic Press; 2000.

Forstner, H. J.; Flagan, R. C., and Seinfeld, J. H. Secondary Organic Aerosol from the Photooxidation of Aromatic Hydrocarbons: Molecular Composition. Environmental Science and Technology. 1997; 31(5):1345-1358.

Fraser, M. P.; Cass, G. R., and Simoneit, B. R. T. Gas-Phase and Particle-Phase Organic Compounds Emitted from Motor Vehicle Traffic in a Los Angeles Roadway Tunnel . Environmental Science and Technology. 1998; 32:2051.

Fried, A.; McKeen, S.; Sewell, S.; Harder, J.; Henry, B.; Goldan, P.; Kuster, W.; Williams, E.; Baumann, K.; Shetter, R., and Cantrell, C.. Photochemistry of formaldehyde during the 1993 Tropospheric OH Photochemistry Experiment. Journal of Geophysical Research. 1997; 102(D5):6283.

Fruekilde, P.; Hjorth, J.; Jensen, N. R.; Kotzias, D., and Larsen, B. Ozonolysis at Vegetation Surfaces: A Source of Acetone, 4-Oxopentanal, 6-Methyl-5-hepten-2-one, and Geranyl Acetone in the Troposphere. Atmoshperic Environment. 1998; 32(11):1893-1902.

Fuchs, N. A. The Mechanics of Aerosols. New York: The Macmillan Company; 1964.

Fung, K. and Grosjean, D.. Determination of Nanagram Amonts of Carbonyls as 2,4-Dinitrophenylhydrazones by High-Performance Liquid Chromatography. Analytical Chemistry. 1981; 53(2):168-171.

Gilpin, T.; Apel, E.; Fried, A.; Wert, B.; Calvert, J.; Genfa, Z.; Dasgupta, P.; Harder, J. W.; Heikes, B.; Hopkins, B.; Westberg, H.; Kleindienst, T.; Lee, Y.-N.; Zhou, X.; Lonnenman, W., and Sewell, S.. Intercomparison of six ambient [CH_2O] measurement techniques. Journal of Geophysical Research. 1997; 102(D17):21161-21188.

Goldan, Paul D.; Kuster, William C.; Fehsenfeld, Fred C., and Montzka, Stephen A. Hydrocarbon measurements in the southeastern United Sates: The Rural Oxidants in the Southern Environment (ROSE) Program 1990. Journal of Geophysical Research. 1995; 100(D12):25945-25963.

Goldstein, Allen H. and Schade, Gunnar W. Quantifying Biogenic and Anthropogenic Contributions to Acetone Mixing Ratios in a Rural Environment. Atmoshperic Environment. 2000; 34:4997-5006.

Goschnick, J. and Schuricht, J. Surface and Depth Analysisof Pollen Treated with Atmospheric Trace Gases. Journal of Aerosol Science. 1996; 27(Supplement 1):S229-S230.

Grosjean, D. Formaldehyde and other Carbonyls in Los Angeles Ambient Air. Environmental Science and Technology. 1982; 16:254.

Grosjean, D. and Fung, K. Collection Efficiencies of Cartridges and Microimpingers for Sampling of Aldehydes in Air as 2,4-Dinitrophenylhydrazones. Analytical Chemistry. 1982; 54:1221.

Grosjean, D.; Grosjean, E., and Gertler, A. W. On-Road Emissions of Carbonyls from Light-Duty and Heavy-Duty Vehicles. Environmental Science and Technology. 2001; 35(1):45-53.

Grosjean, D.; Grosjean, E., and Williams, E. L. II. Atmospheric Chemistry of Olefins: A Product Study of the Ozone-Alkene Reaction with Cyclohexane Added to Scavenge OH. 1994; 28, (1): 186-196.

Grosjean, E.; De Andrade, J. B., and Grosjean, D. Carbonyl Products of the Gas-Phase Reaction of Ozone with Simple Alkenes. Environmental Science and Technology. 1996a; 3:975-983.

Grosjean, E. and Grosjean, D. Liquid Chromatographic Analysis of C_1-C_{10} Carbonyls. International Journal of Environmental Analytical Chemistry. 1995; 61:47-64.

Grosjean, E. and Grosjean, D. Carbonyl Collection Efficiency of the DNPH-coated C18 Cartridge in Dry Air and in Humid Air. Environmental Science and Technology. 1996b; 30(3):859-863.

Grosjean, E. and Grosjean, D. Carbonyl Products of the Gas-Phase Reaction of Ozone with 1-Alkenes. Atmospheric Environment. 1996c; 30(24):4107-4113.

Grosjean, E. and Grosjean, D. Carbonyl Products of the Gas Phase Reaction of Ozone with C_5-C_7 Alkenes. Environmental Science and Technology. 1996d; 30(4):1321-1327.

Grosjean, E. and Grosjean, D. Carbonyl Products of the Gas Phase Reaction of Ozone with Symmetrical Alkenes. Environmental Science and Technology. 1996e; 30(6):2036-2044.

Grosjean, E. and Grosjean, D. The Gas Phase Reaction of Unsaturated Oxygenates with Ozone: Carbonyl Products and Comparison with the Alkene-ozone Reaction. Journal of Atmospheric Chemistry. 1997; 27:271.

Grosjean, E; Grosjean, D.; Fraser, M. P., and Cass, G. R. Air Quality Model Evaluation Data for Organics. 2. C1-C14 Carbonyls in Los Angeles Air. Environmental Science and Technology. 1996f; 30(9):2687-2703.

Harley, R. A.; Hannigan, M. P., and Cass, G. R. Respeciation of Organic Gas Emissions and the Detection of Excess Unburned Gasoline in the Atmosphere. Environmental Science and Technology. 1992; 26(12):2395-2408.

Heiden, A. C.; Kobel, K.; Wildt, J. Einfluß verschiedener Streßfaktoren auf die Emission pflanzlicher flüchtiger organischer Verbindungem. Forschungszentrum Jülich. 1999

Heikes, B.; McCully, B.; Zhou, X.; Lee, Y. N.; Mopper, K.; Chen, X.; Mackay, G.; Karecki, D.; Campos, T., and Atlas, E. Formaldehyde Methods Comparison in the Remote Lower Troposphere During the Mauna Loa Photochemistry Experiment 2. Journal of Geophysical Research. 1996; 101(D9):14741-14755.

Heikes, B. G. Formaldehyde and Hydroperoxides at Mauna Loa Observatory. Journal of Geophysical Research. 1992; 97(D16):18001-18013.

Helmig, Detlev. Ozone Removal Techniques in the Sampling of Atmospheric Volatile Organic Trace Gases. Atmospheic Environment. 1997; 31(21):3635-3651

Henry, R. C.; Lewis, C. W., and Collins, J. F. Vehicle-Related Hydrocarbon Source Compositions from Ambient Data: The GRACE/SAFER Method. Environmental Science and Technology. 1994; 28:823-832.

Houdier, S.; Perrier, S.; Defrancq, E., and Legrand, M. A New Fluorescent Probe for Sensitive Detection of Carbonyl Compouds: Sensitivity Improvement and Application to Environmental Water Samples. Analytica Chimica Acta. 2000; 412:221-233.

Isidorov, V. A.; Zenkevich, I. G., and Ioffe, B. V. Volatile Organic Compounds in the Atmosphere of Forests. Analytical Chemistry. 1985; 19(1):1.

Jenkin, M. E.; Saunders, S. M., and Pilling, M. J. The Tropospheric Degradation of Volatile Organic Compounds: A Protocol for Mechanism Development. Atmoshperic Environment. 1997; 31(1):81.

Kesselmeier, J.; Bode, K.; Hofmann, U.; Muller, H.; Schafer, L.; Wolf, A.; Ciccioli, P.; Brancaleoni, E.; Cecinato, A.; Frattoni, M.; Foster, P.; Ferrari, C.; Jacob, V.; Fugit, J. L.; Dutaur, L.; Simon, V., and Torres, L. Emission of Short Chained Organic Acids, Aldehydes and Monoterpenes from *Quercus Ilex* L. and *Pinus Pinea* L. in Relation to Physiological Activities, Carbon Budget and Emission Algorithms. Atmoshperic Environment. 1997; 31(SI):119-133.

Kesselmeier, J.; Kuhn, U.; Wolf, A.; Andreae, M. O.; Ciccioli, P.; Brancaleoni, E.; Frattoni, M.; Guenther, A.; Greenberg, J.; Vasconecellos, P. D.; de Oliva, T.; Tavares, T., and Artaxo, P. Atmospheric Volatile Organic Compounds (VOC) at a Remote Tropical Forest Site in Central Amazonia. Atmospheric Environment. 2000; 34:4063-4072.

Kesselmeier, J. and Staudt, M. Biogenic Volatile Organic Compounds (VOC): An Overview on Emission, Physiology and Ecology. Journal of Atmospheric Chemistry. 1999; 33:23-88.

Kirchstetter, K. W.; Singer, B. C.; Harley, R. A.; Kendall, G. R., and Hesson, J. M. Impact of California Reformulated Gasoline on Motor Vehicle Emmissions. 2. Volatile Organic Compound Speciation and Reactivity. Environmental Science and Technology. 1999; 33:329-336.

Kirstine, W.; Galbally, I.; Ye, Y., and Hooper, M. Emmisions of Volatile Organic Compounds (Primarily Oxygenated Species) from Pasture. Journal of Geophysical Research. 1998; 103(D9):10605-10619.

Kleindienst, T. E.; Coarse, E. W.; Blanchard, F. T., and Lonneman, W. A. Evaluation of the Performance of DNPH-Caoted Silica Gel and C_{18} Cartridges in the Measurement of Formaldehyde in the Presence and Absence of Ozone. Environmental Science and Technology. 1998; 32(1):124-130.

Kleindienst, T. E.; Shepson, P. B.; Nero, C. M.; Arnts, R. R.; Tejada, S. B.; Mackay, G. I.; Mayne, L. K.; Schiff, H. I.; Lind, J. A.; Kok, G. L.; Lazrus, A. L.; Dasgupta, P. K., and Dong, S. An Inercomparison of Formaldehyde Measurement Techniques at Ambient Concentration. Atmoshperic Environment . 1988; 22(9):1931.

Klotz, Bjorn; Sørensen, Søren; Barnes, Ian; Becker, Karl H.; Etzkorn, Thomas; Volkamer, Rainer; Platt, Ulrich; Wirtz, Klaus, and Martin-Reviejo, Montserrat. Atmospheric Oxidation of Toluene in a Large-Volume Outdoor Photoreactor: In Situ Determination of Ring-Retaining Product Yields. Journal of Physical Chemistry A. 1998; 102(50):10289.

Kotzias, D.; Konidari, C., and Sparta, C. Volatile carbonyl compounds of biogenic origin - Emission and concentration in the atmosphere. Helas, G.; Salina, S., and Steinbrecher, R. editors. Biogenic Volatile Organic Compounds in the Atmosphere. Amsterdam, The Netherlands: SPB Academic Publishers; 1997.

Kuntz, R.; Lonneman, W. A.; Namie, G., and Hull, L. A. Rapid Determination of Aldehydes in Air Analyses. Analytical Letters. 1980; 13(A16):1409-1415.

Kuwata, Kazuhiro; Uebori, Michiko, and Yamasaki, Yoshiaki. Determination of Aliphatic and Aromatic Aldehydes in Polluted Airs as their 2,4-Dinitophenylhydrazones by High Performance Liquid Chromatography. Journal of Chromatographic Science. 1979; 17:264.

Lary, D. J. and Shallcross, D. E. Central Role of Carbonyl Compounds in Atmospheric Chemistry. Journal of Geophysical Research. 2000; 105(D15):19771-19778.

Latrasse, A.; Sémon, E., and Quéré, .J. Composition and Major Odorous Compounds of the Essential Oil of *Bifor radians*, an Aldehyde-Producing Weed. Journal of High Resolution Chromatography. 1991; 14:549-553.

Le Lacheur, R. M.; Sonnenberg, L. B.; Singer P. C.; Christman, R. F., and Charles, M. J. Identification of Carbonyl Compounds in Environmental Samples. Environmental Science and Technology. 1993; 27(13):2745-2753.

Lee, Y. N.; Zhou, X.; Kleinman, L. I.; Nunnermacker, L. J.; Springston, S. R.; Daum, P. H.; Newman, L.; Keigley, W. G.; Holdren, M. W.; Spicer, C. W.; Young, V.; Fu, B.; Parrish, D. D.; Holloway, J.; Williams, J.; Roberts, J. M.; Ryerson, T. B., and Fehsenfeld, F. C. Atmospheric Chemistry and Distribution of Formaldehyde and Several Multioxygenated Carbonyl Compounds During the 1995 Nashville/Middle Tennessee Ozone Study. Journal of Geophysical Research. 1998; 103(D17):22449.

Lee, Y.-N.; Zhou, X., and Hallock, K.. Atmospheric Carbonyl Compounds at a Rural Southeastern United States Site. Journal of Geophysical Research. 1995; 100(D12):25,933-25,944.

Lee, Y.-N.; Zhou, X.; Leaitch, W. R., and Banic, C. M. An Aircraft Measurement Technique for Formaldehyde and Soluble Carbonyl Compounds. Journal of Geophysical Research. 1996; 101(D22):29075-29080.

Leibrock, E. and Slemr, J. Method for Measurement of Volatile Oxygenated Hydrocarbons in Ambient Air. Atmoshperic Environment. 1997; 31(20):3329-3339.

Lipari, F. and Swarin, S. 2,4-Dinitrophenylhydrazine-coated Florisil Sampling Cartridges for the Determination of Formaldehyde in Air. Environmental Science and Technology. 1985; 19(1):70-74.

Lowe, D. C. and Schmidt, U. Formaldehyde Measurements in the Non-Urban Atmosphere. Journal of Geophysical Research. 1983; 88(C15):10844-10858.

Lowe, D. C.; Schmidt, U.; Ehhalt, D. H.; Frischkorn, C. G B., and Nurnberg, H. W. Determination of Formaldehyde in Clean Air. Environmental Science and Technology. 1981; 15(7):819.

Mackay, G. I.; Karecki, D. R., and Schiff, H. I. Tunable Diode Laser Absorption Measurements of H_2O_2 and HCHO During the Mauna Loa Observatory Photochemistry Experiment. Journal of Geophysical Research. 1996; 101(D9):14721-14728.

Martin, R. S.; Villanueva, I.; Zhang, J., and Popp, C. J. Nonmethane Hydrocarbon, Monocarboxylic Acid, and Low Molecular Weight Aldehyde and Ketone Emissions from Vegetation in Central New Mexico. Environmental Science and Technology. 1999; 33(13):2186-2192.

McLaren, R.; Salmon, R. A.; Liggio, J.; Hayden, K. L.; Anlauf, K. G.; Leaitch, R. Nighttime Chemistry at a Rural Site in the Lower Fraser Valley. Atmospheric Environment, In Press

Moise, T; Rudich, Y. Reactive uptake of ozone by proxies for organic aerosols: Surface versus bulk processes. Journal of Geophysical Research, [Atmospheres]. 2000, 105(D11), 14667-14676.

Mopper, K.; Stahovec, W. L., and Johnson, L. Trace Analysis of Aldehydes By Reversed Phase High Performance Liquid Chromatography and Precolumn fluorogenic Labeling with 5,5-Dimethyl-1,3-Cylcohexanedione. Journal of Chromatography. 1983; 256:243-252.

Neitzert, V. and Seiler, W. Measurement of Formaldehyde in Clean Air. Geophysical Research Letters. 1981; 8(1):79-82.

Nondek, L.; Milofsky, R. E., and Birks, J. W. Determination of Carbonyl Compounds in Air by HPLC Using On-line Analyzed Microcartridges, Fluorescence and Chemiluminescence Detection. Chromatographia. 1991; 32:33-39.

Nondek, L.; Rodier, D. R., and Birks, J.W. Measurement of Sub-ppbv Concentrations of Aldehydes in a Forest Atmosphere Using a New HPLC technique. Environmental Science and Technology. 1992; 26:1174.

Papa, L. J. and Turner, L. P. Chromatorgraphic Determination of Carbonyl Compounds as their 2,4-Dinitrophenylhydrazones. I Gas Chromatography. Journal of Chromatographic Science. 1972a; 10:744.

Papa, L. J. and Turner, L. P. Chromatorgraphic Determination of Carbonyl Compounds as their 2,4-Dinitrophenylhydrazones. II High pressure Liquid Chromatography. Journal of Chromatographic Science. 1972b; 10(747).

Paulson, S. E. and Seinfeld, J. H. Development and Evaluation of a Photooxidation Mechanism for Isoprene. Journal of Geophysical Research. 1992; 97(D18):20703-20715.

Pires, M. and Carvalho, L. R. F. An Artifact in Air Carbonyls Sampling Using C_{18} DNPH-coated Cartridge. Analytica Chimica Acta. 1998; 367:223-231.

Plum, Christopher N.; Sanhueza, Eugenio; Atkinson, Roger; Carter, William P. L., and Pitts, James N. Jr. OH Radical Rate Constant and Photolysis Rates of α-Dicarbonyls. Environmental Science and Technology. 1983; 17(8):479-484.

Poole, C. F. and Poole, S. K. Chromatography Today. 5th ed. Amsterdam: Elsevier Science; 1997.

Possanzini, M.; Di Palo, V.; Petricca, M.; Fratarcangeli, R., and Brocco, D. Measurements of Lower Carbonyls in Rome Ambient Air. Atmospheric Environment . 1996; 30(22):3757.

Possanzini, Massimiliano.; Di Palo, Vincenzo; Brancaleoni, Enzo; Frattoni, Massimiliano., and Ciccioli, Paolo. A Train of Carbon and DNPH-coated Cartridges for the Determination of Carbonyls from C_1 to C_{12} in Air and Emission Samples. Atmospheric Environment. 2000; 34:5311-5318.

Puxbaum, Hans. Biogenic emissions of alcohols, ester, ether and higher aldehydes. Helas, G.; Salina, S., and Steinbrecher, R. editors. Biogenic Volatile Organic Compounds in the Atmosphere. Amsterdam, The Netherlands: SPB Academic Publishers; 1997.

Rappaport, Z. CRC Handbook of tables for Organic Compound Identification. Third Edition ed. Boca Raton, Florida: CRC Press, Inc.; 1967.

Rodier, D. R. and Birks, J. W. Evaluation of Isoprene Oxidation as an Interference in the Cartridge Sampling and Derivatization of Atmosopheric Carbonyl Compounds. Environmental Science and Technology. 1994; 28:2211.

Rodier, D. R.. Measurement of Tropospheric Aldehydes and Ketones by Derivatization with Dansyl Hydrazine and 2,4-dinitrophenylhydrazine: University of Colorado at Boulder; 1993.

Saito, K.; Kakumoto, T., and Murakami, I.. Thermal Unimolecular Decomposition of Glyoxal . Journal of Physical Chemistry. 1984; 88:1182-1187.

Seinfeld, J. H. and Pandis, N. Spyros. Atmospheric Chemistry and Physics. New York: John Wiley & Sons, Inc.; 1998.

Shepson, P. B.; Hastie, D. R.; Schiff, H. I.; Polizzi, M.; Bottenheim, J. W.; Anlauf, K.; Mackay, G. I., and Karecki, D. R. Atmospheric Concentrations and Temporal Variations of C1-C3 Carbonyl Compounds at Two Rural Sites in Central Ontario. Atmospheric Environment. 1991; 25A(9):2001-2015.

Shepson, P.B.; Bottenheim, J.W.; Hastie, D.R., and Venkatram, A. Determination of the Relative Ozone and PAN Deposition Velocities at Night. Geophysical Research Letters. 1992; 19 (11): 1121-1124.

Shimanouchi, T. Tables of Molecular Vibrational Frequencies Consolidated Volume II. Journal of Physical and Chemical Reference Data. 1972; 6(3):993-1102.

Singh, H. B.; Kanakidou, M.; Crutzen, P. J., and Jacob, D. J. High Concentration and Photochemical Fate of Oxygenated Hydrocarbons in the Global Troposphere. Letters to Nature. 1995; 378(50-54).

Sirju, A. and Shepson, P. B. Laboratory and Field investigation of the DNPH Cartridge Technique for the Measurement of Atmospheric Carbonyl Compounds. Environmental Science and Technology. 1995; 29(2):384-392.

Skoog, D and Leary, J. Principles of Instrumental Analysis . 4th Edition ed. Saunders Publishing Company; 1992.

Slemr, J.; Junkermann, W., and Volz-Thomas, A. Temporal Variations in Formaldehyde, Acetaldehyde and Accetone at a Rural Site in Southern Germany. Atmospheric Environment. 1996; 30(21):3667-3676.

Slemr, J. Determination of Volatile Carbonyl Compounds in clean air. Fresenius Journal of Analytical Chemistry. 1991; 340:672.

Smith, D.; Kleindienst, T., and Hudgens, E. E. Improved High-performance Liquid Chromatographic Method for Artifact-free Measurements of Aldehydes in the Presence of Ozone using 2,4-dinitrophenylhydrazine. Journal of Chromatography. 1989; 483:431-436.

Solberg, S.; Dye, C.; Walker, S.-E., and Simpson, D. Long-term Measurements and Model Calculations of Formaldehyde at Rural European Monitoring Sites . Atmospheric Environment. 2001; 35:195-207.

Spaulding, R. S.; Frazey, P.; Rao, X., and Charles, J.M. Measurement of Hydroxy Carbonyls and Other Carbonyls in Ambient Air Using Pentafluorobenzyl Alcohol as a Chemical Ionization Reagent. Analytical Chemistry. 1999; 71:3420-3427.

Steacie, E. W. R.; Hatcher, W. H., and Horwood, J. F. The Kinetics of the Decomposition of Gaseous Glyoxal. Journal of Chemical Physics. 1935; 3:291.

Swarin, S. J. and Lipari, F. Determination of Formaldehyde and Other Aldehydes by High Performance Liquid Chromatography with Fluorescence Detection. Journal of Liquid Chromatography. 1983; 6(3):425.

Tanner, R. L. and Meng, Z. Seasonal Variations in Ambient Atmospheric Levels of Formaldehyde and Acetaldehyde. Environmental Science and Technology. 1984; 18(9):723-726.

Tejada, S. B. Evaluation of Silica Gel Cartridges *In Situ* with Acidified 2,4-Dinitrophenylhydrazine for Sampling Aldehydes and Ketones in Air. International Journal of Environmental Analytical Chemistry. 1986; 26:167-185.

Thompson, A. M. Wet and Dry Removal of Tropospheric Formaldehyde at a Costal Site. Tellus. 1980; 32: 376-383.

Tuazon, E. C.; Aschmann, S. M.; Arey, J., and Atkinson, R. Products of the Gas-Phase Reactions of a series of Methyl-substituted Ethenes with the OH Radical. Environmental Science and Technology. 1998; 32:2106.

Vairavamurthy, A.; Roberts, J. M., and Newman, L. Methods for the Determination of Low Molecular Weight Carbonyl Compounds in the Atmosphere: A Review. Atmoshperic Environment. 1992; 26A(11):1965.

Viskari, E.-L.; Vartiainen, M., and Pasanen, P. Seasonal and Diurnal Variation in Formaldehyde and Acetaldehyde Concentrations Along a Highway in Eastern Finland. Atmospheric Environment. 2000; 34:917-923.

Wesely, M. L. Parameterization of Surface Resistances to Gaseous Dry Deposition in Regional-Scale Numerical Models. Atmospheric Environment. 1989; 23:1293-1304

Wesely, M. L. and Hicks, B. B. A Review of the Current Status of Knowledge on Dry Deposition. Atmospheric Environment. 2000; 34:2261-2282.

Yang, F. J. On-Column Detection Using a Fused Silica Column. Journal of High Resolution Chromatography & Chromatography Communications. 1981; 4:83-85.

Yu, J.; Jeffries, H. E., and Sexton, K. G. Atmospheric Photooxidation of alkylbenzenes-I. Carbonyl Product Analyses. Atmospheric Environment. 1997; 31(15):2261-2280.

Zhang, L.; Moran, M. D.; Makar, P. A.; Brook, J. R.; Gong, S. Modelling Gaseous Dry Deposition in AURAMS: A Unified Regional Air-quality Modelling System. Atmospheric Environment, 2002, 36: 537-560

7. APPENDIX

7.1. Appendix A- Data Collection software

The software used to collect chromatograms and spectral data using the Ocean Optics CCD spectrometer is given below. The program was written in Visual Basic 4.0, and consists of 5 separate files named hplcauto.vbp, module1.bas, vbsamp32.frm, form1.frm and form2.frm. An executable file was created based from this source code, and used in the field. The version given here controlled the automated instrument in Simcoe 2000. The version used in Hamilton 1999 was based on the same program, without the later added automation code. Minor modifications have been made to the software to remove some problems found during operation at Simcoe, and are included in the version below.

Hplcauto.Vbp

```
Form=VBSAMP32.frm
Module=Module1; Module1.bas
Form=Form1.frm
Form=Form2.frm
ProjWinSize=76,602,194,128
ProjWinShow=2
IconForm="C"
Title="VBSAMP32"
ExeName32="hplcauta.exe"
Path32="C:\chroma"
ExeName="VBSAMP32.EXE"
Name="VBSamp32"
HelpContextID="0"
StartMode=0
VersionCompatible32="0"
```

```
MajorVer=1
MinorVer=0
RevisionVer=0
AutoIncrementVer=0
ServerSupportFiles=0
VersionCompanyName="Ocean Optics, Inc."
```

Module1.Bas

```
Attribute VB_Name = "Module1"
'////////////////////////////////////////////////////////////////////////////
'//// SCANPARM structure for DoScan acquisition mode
'////////////////////////////////////////////////////////////////////////////
Type SCANPARM
  cmd As Integer           ' command, use CMD_ constants
  fdc As Integer           ' flash delay in msec
  dsf As Integer           ' sampling frequency (kHz - S1000, msec - S2000)
  boxcar As Integer        ' boxcar smoothing width
  average As Integer       ' samples to average
  chan_ena(3) As Integer   ' spectrometer channel enabled array
  scan_dark As Integer     ' scan dark
  correct_dark As Integer  ' correct for electrical dark signal
  extrig As Integer        ' external trigger mode
  upper4chan As Integer    ' flag true if want data from S2000 channels 4-7
  sdat(2047, 3) As Single  ' spectral data arrays
End Type

Public ref()
Public ref1()
Public datta() As Single
Global zeroval
Global stopscanning As Boolean
Global n As Integer
Global dint As Integer
Global startpixel As Integer
Global endpixel As Integer
Global boxcar As Integer
Global yscal As Single
Global x As Integer
Global path1 As String
```

```
Global driv1 As String
Global runtime As Integer
Global Directoryname As String
Global runnum As Integer
Global runnumb As Integer
Global starttime
Global stoptime
Global first As String
Global methods As String
Global datastart As Integer
Global datastart1 As Integer
Declare Function OOI_DoScan_32 Lib "OOIDRV32.DLL" Alias "#18" (sp As
SCANPARM) As Integer
Declare Sub OOI_Config_32 Lib "OOIDRV32.DLL" Alias "#19" (ByVal spec As
Integer, ByVal adc As Integer, ByVal irq As Integer, ByVal base As Integer)
' the coefs single must be the first element of a 8 member array of coefficients
Declare Sub OOI_SetNLCoefs_32 Lib "OOIDRV32.DLL" Alias "#24" (ByVal chan
As Integer, coefs As Single)
Declare Sub OOI_SetSLCoef_32 Lib "OOIDRV32.DLL" Alias "#25" (ByVal chan As
Integer, ByVal coef As Single)
Declare Sub OOI_EnableNLCorrection_32 Lib "OOIDRV32.DLL" Alias "#26"
(ByVal chan As Integer, ByVal ena As Integer)
Declare Sub OOI_EnableSLCorrection_32 Lib "OOIDRV32.DLL" Alias "#27"
(ByVal chan As Integer, ByVal ena As Integer)
Declare Sub OOI_ConfigEx_32 Lib "OOIDRV32.DLL" Alias "#28" (ByVal spec As
Integer, ByVal adc As Integer, ByVal irq As Integer, ByVal base As Integer, ByVal
port As Integer, ByVal NIDAQ As Integer)
Declare Function OOI_GetSpectrometerType_32 Lib "OOIDRV32.DLL" Alias "#29"
() As Integer
Declare Function OOI_GetADCType_32 Lib "OOIDRV32.DLL" Alias "#30" () As
Integer
Declare Function OOI_GetBaseAddress_32 Lib "OOIDRV32.DLL" Alias "#31" () As
Long
Declare Function OOI_GetIRQ_32 Lib "OOIDRV32.DLL" Alias "#32" () As Integer
Declare Function OOI_GetSerialPort_32 Lib "OOIDRV32.DLL" Alias "#33" () As
Integer
Declare Function OOI_GetNIDAQCardID_32 Lib "OOIDRV32.DLL" Alias "#34" ()
As Integer
Declare Function OOI_GetIntegrationTime_32 Lib "OOIDRV32.DLL" Alias "#35" ()
As Integer
```

```
Declare Function OOI_GetNumberOfPixels_32 Lib "OOIDRV32.DLL" Alias "#38"
() As Integer
Declare Sub OOI_EnableMultichannelSpectra_32 Lib "OOIDRV32.DLL" Alias
"#36" (ByVal chan As Integer)
Declare Sub OOI_DisableMultichannelSpectra_32 Lib "OOIDRV32.DLL" Alias
"#37" ()
Declare Sub OOI_S2000StrobeEnable_32 Lib "OOIDRV32.DLL" Alias "#39"
(ByVal ean As Integer)
```

Form1.Frm

```
VERSION 4.00
Begin VB.Form Form1
  Caption       =  "Sample info"
  ClientHeight  =  5940
  ClientLeft    =  2700
  ClientTop     =  1830
  ClientWidth   =  7665
  Enabled       =  0  'False
  Height        =  6345
  Left          =  2640
  LinkTopic     =  "Form1"
  ScaleHeight   =  5940
  ScaleWidth    =  7665
  Top           =  1485
  Visible       =  0  'False
  Width         =  7785
  Begin VB.TextBox Text11
    Height        =  285
    Left          =  5520
    TabIndex      =  21
    Text          =  "Text11"
    Top           =  1320
    Width         =  2055
  End
  Begin VB.TextBox Text10
```

```
  Height        =  285
  Left          =  5520
  TabIndex      =  20
  Text          =  "Text10"
  Top           =  4200
  Width         =  1695
End
Begin VB.TextBox Text9
  Height        =  285
  Left          =  5520
  TabIndex      =  17
  Text          =  "Text9"
  Top           =  3840
  Width         =  2055
End
Begin VB.TextBox Text8
  Height        =  285
  Left          =  5520
  TabIndex      =  15
  Text          =  "Text8"
  Top           =  960
  Width         =  2055
End
Begin VB.DirListBox Dir1
  Height        =  2280
  Left          =  120
  TabIndex      =  14
  Top           =  2280
  Width         =  3255
End
Begin VB.TextBox Text6
  Height        =  285
  Left          =  1680
  TabIndex      =  13
  Text          =  "Text6"
  Top           =  1680
  Width         =  1695
End
Begin VB.CommandButton Command2
  Cancel        =  -1  'True
  Caption       =  "Cancel"
```

```
  Height        =  735
  Left          =  1800
  TabIndex      =  11
  Top           =  5040
  Width         =  1095
End
Begin VB.CommandButton Command1
  Caption       =  "OK"
  Height        =  735
  Left          =  120
  TabIndex      =  10
  Top           =  5040
  Width         =  1095
End
Begin VB.TextBox Text5
  Height        =  285
  Index         =  0
  Left          =  1680
  TabIndex      =  9
  Text          =  "Text5"
  Top           =  1320
  Width         =  1695
End
Begin VB.TextBox Text4
  Height        =  285
  Left          =  1680
  TabIndex      =  7
  Text          =  "Text4"
  Top           =  960
  Width         =  1695
End
Begin VB.TextBox Text3
  BackColor     =  &H00C0C0C0&
  Enabled       =  0  'False
  Height        =  285
  Left          =  5400
  Locked        =  -1  'True
  TabIndex      =  5
  Text          =  "Text3"
  Top           =  360
  Width         =  1095
```

```
End
Begin VB.TextBox Text2
  BackColor      =  &H00C0C0C0&
  Enabled        =  0  'False
  Height         =  285
  Left           =  2760
  Locked         =  -1  'True
  TabIndex       =  3
  Text           =  "Text2"
  Top            =  360
  Width          =  1095
End
Begin VB.TextBox Text1
  BackColor      =  &H00C0C0C0&
  Enabled        =  0  'False
  Height         =  285
  Left           =  480
  Locked         =  -1  'True
  TabIndex       =  0
  Text           =  "Text1"
  Top            =  360
  Width          =  1095
End
Begin VB.Label Label11
  Alignment      =  1  'Right Justify
  Caption        =  "Time for data start (sec)"
  Height         =  255
  Left           =  3720
  TabIndex       =  22
  Top            =  1320
  Width          =  1695
End
Begin VB.Label Label10
  Alignment      =  1  'Right Justify
  Caption        =  "Time for data start(sec)"
  Height         =  255
  Left           =  3480
  TabIndex       =  19
  Top            =  4200
  Width          =  1935
End
```

```
Begin VB.Label Label9
  Alignment      =  1  'Right Justify
  Caption        =  "Following methods"
  Height         =  255
  Left           =  3600
  TabIndex       =  18
  Top            =  3840
  Width          =  1815
End
Begin VB.Label Label8
  Alignment      =  1  'Right Justify
  Caption        =  "First method in sequence"
  Height         =  255
  Left           =  3480
  TabIndex       =  16
  Top            =  960
  Width          =  1935
End
Begin VB.Label Label6
  Alignment      =  1  'Right Justify
  Caption        =  "# of runs in sequence"
  Height         =  255
  Left           =  0
  TabIndex       =  12
  Top            =  1680
  Width          =  1575
End
Begin VB.Label Label5
  Alignment      =  1  'Right Justify
  Caption        =  "Run time (sec)"
  Height         =  255
  Left           =  480
  TabIndex       =  8
  Top            =  1320
  Width          =  1095
End
Begin VB.Label Label4
  Alignment      =  1  'Right Justify
  Caption        =  "Directory Name"
  Height         =  255
  Left           =  360
```

```
    TabIndex      = 6
    Top           = 960
    Width         = 1215
  End
  Begin VB.Label Label3
    Alignment     = 1 'Right Justify
    Caption       = "Last Pixel"
    Height        = 255
    Left          = 5520
    TabIndex      = 4
    Top           = 120
    Width         = 735
  End
  Begin VB.Label Label2
    Alignment     = 1 'Right Justify
    Caption       = "First Pixel"
    Height        = 255
    Left          = 2760
    TabIndex      = 2
    Top           = 120
    Width         = 855
  End
  Begin VB.Label Label1
    Alignment     = 1 'Right Justify
    Caption       = "Integration time (ms)"
    Height        = 255
    Left          = 240
    TabIndex      = 1
    Top           = 120
    Width         = 1455
  End
End
Attribute VB_Name = "Form1"
Attribute VB_Creatable = False
Attribute VB_Exposed = False

Private Sub Command1_Click()

Directoryname = Text4.Text

runtime = Val(Text5(0).Text)
```

```
runnum = Val(Text6.Text)

first = Text8.Text
methods = Text9.Text
datastart = Val(Text10.Text)
datastart1 = Val(Text11.Text)

C.btnMultiple.Enabled = True

Form1.Visible = False
Form1.Enabled = False
Unload Form1

End Sub


Private Sub Command2_Click()
Form1.Enabled = False
Form1.Visible = False
Unload Form1
End Sub


Private Sub Dir1_Change()
 'Drive1.Drive = Dir1.Path
 'File1.Path = Dir1.Path
End Sub

Private Sub Drive1_Change()
 Dir1.Path = Drive1.Drive
End Sub

Private Sub Form_Load()
Text1.Text = dint
Text2.Text = startpixel
Text3.Text = endpixel
Text4.Text = Directoryname
Text5(0).Text = runtime
Text6.Text = runnum

Text8.Text = first
```

```
Text9.Text = methods
Text10.Text = datastart
Text11.Text = datastart1
Dir1.Path = "c:\chroma"
End Sub
```

Form2.Frm

```
VERSION 4.00
Begin VB.Form Form2
  BorderStyle    =  3  'Fixed Dialog
  ClientHeight   =  2280
  ClientLeft     =  195
  ClientTop      =  6135
  ClientWidth    =  3780
  ControlBox     =  0  'False
  Height         =  2685
  Left           =  135
  LinkTopic      =  "Form2"
  MaxButton      =  0  'False
  MinButton      =  0  'False
  ScaleHeight    =  2280
  ScaleWidth     =  3780
  ShowInTaskbar  =  0  'False
  Top            =  5790
  Width          =  3900
  Begin VB.CommandButton Command2
    Cancel       =  -1  'True
    Caption      =  "Cancel"
    Height       =  615
    Left         =  1920
    TabIndex     =  1
    Top          =  1200
    Width        =  1335
  End
  Begin VB.CommandButton Command1
    Caption      =  "Yes"
    Height       =  615
```

```
    Left          =  240
    TabIndex      =  0
    Top           =  1200
    Width         =  1335
  End
  Begin VB.Label Label1
    Caption       =  "Abort run without saving data? "
    Height        =  375
    Left          =  240
    TabIndex      =  2
    Top           =  480
    Width         =  2895
  End
End
Attribute VB_Name = "Form2"
Attribute VB_Creatable = False
Attribute VB_Exposed = False

Private Sub Command1_Click()
n = 17
stopscanning = True ' set flag to stop continuous scanning
  C.Command4.Enabled = True
  C.Command3.Enabled = True
Unload Form2
End Sub
Private Sub Command2_Click()
Unload Form2
End Sub
```

Vbsamp32.Frm

```
VERSION 4.00
Begin VB.Form C
  Appearance     =  0  'Flat
  AutoRedraw     =  -1  'True
  BackColor      =  &H00C0C0C0&
  BorderStyle    =  3  'Fixed Dialog
  ClientHeight   =  5925
  ClientLeft     =  2115
  ClientTop      =  2175
  ClientWidth    =  9705
```

```
ControlBox      =  0  'False
BeginProperty Font {0BE35203-8F91-11CE-9DE3-00AA004BB851}
  Name          =  "MS Sans Serif"
  Size          =  8.25
  Charset       =  0
  Weight        =  700
  Underline     =  0  'False
  Italic        =  0  'False
  Strikethrough =  0  'False
EndProperty
ForeColor       =  &H80000008&
Height          =  6330
Left            =  2055
LinkTopic       =  "Form1"
MaxButton       =  0  'False
MinButton       =  0  'False
ScaleHeight     =  5925
ScaleMode       =  0  'User
ScaleWidth      =  9705
ShowInTaskbar   =  0  'False
Top             =  1830
Width           =  9825
Begin VB.CheckBox Pumpstart
  Caption       =  "Pump Start"
  Height        =  195
  Left          =  480
  TabIndex      =  18
  Top           =  5040
  Width         =  2175
End
Begin VB.CommandButton Command6
  Caption       =  "Zero Now"
  Height        =  495
  Left          =  3600
  TabIndex      =  16
  Top           =  5280
  Width         =  975
End
Begin VB.CommandButton Command5
  Caption       =  "Abort"
  Height        =  495
```

```
  Left        =  1800
  TabIndex    =  15
  Top         =  5280
  Width       =  975
End
Begin VB.CommandButton Command4
  Caption     =  "Exit"
  Height      =  495
  Left        =  480
  TabIndex    =  11
  Top         =  5280
  Width       =  1095
End
Begin VB.CommandButton Command3
  Caption     =  "Initialize"
  Height      =  495
  Left        =  8160
  TabIndex    =  10
  Top         =  5280
  Width       =  1095
End
Begin VB.Timer Timer1
  Enabled     =  0  'False
  Interval    =  1000
  Left        =  4800
  Top         =  5280
End
Begin VB.CommandButton Command2
  Caption     =  "apply x scale"
  Height      =  255
  Left        =  6240
  TabIndex    =  9
  Top         =  480
  Width       =  1815
End
Begin VB.CommandButton Command1
  Caption     =  "apply y scale"
  Height      =  255
  Left        =  6240
  TabIndex    =  8
  Top         =  240
```

```
  Width          =  1815
End
Begin VB.TextBox Text2
  Height         =  285
  Left           =  8160
  TabIndex       =  7
  Text           =  "1000"
  Top            =  480
  Width          =  735
End
Begin VB.TextBox Text1
  Height         =  285
  Left           =  8160
  TabIndex       =  6
  Text           =  "1"
  Top            =  240
  Width          =  735
End
Begin VB.PictureBox Picture1
  AutoRedraw     =  -1  'True
  BackColor      =  &H00FFFFFF&
  Height         =  4095
  Left           =  480
  ScaleHeight    =  -0.828
  ScaleMode      =  0  'User
  ScaleTop       =  1
  ScaleWidth     =  973.199
  TabIndex       =  5
  Top            =  840
  Width          =  8775
End
Begin VB.CommandButton btnStop
  Appearance     =  0  'Flat
  BackColor      =  &H80000005&
  Caption        =  "Stop"
  Enabled        =  0  'False
  Height         =  495
  Left           =  1560
  TabIndex       =  0
  Top            =  240
  Width          =  975
```

```
End
Begin VB.CommandButton btnMultiple
  Appearance     =  0  'Flat
  BackColor      =  &H80000005&
  Caption        =  "Start"
  Enabled        =  0  'False
  Height         =  495
  Left           =  480
  TabIndex       =  1
  Top            =  240
  Width          =  975
End
Begin VB.Label Label6
  Appearance     =  0  'Flat
  BackColor      =  &H00C0C0C0&
  BorderStyle    =  1  'Fixed Single
  Caption        =  " "
  ForeColor      =  &H80000008&
  Height         =  255
  Left           =  4320
  TabIndex       =  17
  Top            =  240
  Width          =  1215
End
Begin VB.Label Label5
  Appearance     =  0  'Flat
  BackColor      =  &H00C0C0C0&
  BorderStyle    =  1  'Fixed Single
  ForeColor      =  &H80000008&
  Height         =  255
  Left           =  5520
  TabIndex       =  14
  Top            =  480
  Width          =  615
End
Begin VB.Label Label4
  Appearance     =  0  'Flat
  BackColor      =  &H00C0C0C0&
  BorderStyle    =  1  'Fixed Single
  Caption        =  " "
  ForeColor      =  &H80000008&
```

```
  Height        =  255
  Left          =  5280
  TabIndex      =  13
  Top           =  5520
  Width         =  2775
End
Begin VB.Label Label3
  Appearance    =  0  'Flat
  BackColor     =  &H00C0C0C0&
  BorderStyle   =  1  'Fixed Single
  Caption       =  " "
  ForeColor     =  &H80000008&
  Height        =  255
  Left          =  5280
  TabIndex      =  12
  Top           =  5280
  Width         =  2775
End
Begin VB.Label Label2
  Appearance    =  0  'Flat
  BackColor     =  &H00C0C0C0&
  BorderStyle   =  1  'Fixed Single
  Caption       =  " "
  ForeColor     =  &H80000008&
  Height        =  255
  Left          =  2640
  TabIndex      =  4
  Top           =  480
  Width         =  1695
End
Begin VB.Label Label1
  Appearance    =  0  'Flat
  BackColor     =  &H00C0C0C0&
  BorderStyle   =  1  'Fixed Single
  Caption       =  " "
  ForeColor     =  &H80000008&
  Height        =  255
  Left          =  5520
  TabIndex      =  3
  Top           =  240
  Width         =  615
```

```
  End
  Begin VB.Label labMaster
    Appearance      =  0  'Flat
    BackColor       =  &H00C0C0C0&
    BorderStyle     =  1  'Fixed Single
    Caption         =  " "
    ForeColor       =  &H80000008&
    Height          =  255
    Left            =  2640
    TabIndex        =  2
    Top             =  240
    Width           =  1695
  End
End
Attribute VB_Name = "C"
Attribute VB_Creatable = False
Attribute VB_Exposed = False
Dim sp As SCANPARM ' the only instance of SCANPARM
Dim PixelNumber As Integer ' pixel number from the edit box



Private Sub btnMultiple_Click()

MkDir "c:\chroma\" + Directoryname


filenumb = 0
For runnumb = 1 To runnum
filenumb = filenumb + 1
ReDim datta(runtime + datastart1 - datastart + 1000, 30 To 81)
ReDim ref(30 To 80, 10)
ReDim ref1(30 To 80)

Picture1.Line (0, 0.1 * Val(Text1.Text))-(Val(Text2.Text), 0.1 * Val(Text1.Text)),
RGB(255, 0, 0)


  Dim Response As Single
   ' disabled all buttons except the 'stop' button
  n = 16
```

```
zeroval = 0
btnMultiple.Enabled = False
btnStop.Enabled = True
Command3.Enabled = False
Command4.Enabled = False
stopscanning = False
pumpstart.Enabled = False

  sp.cmd = CMD_NONE ' no specific command
  sp.dsf = dint ' reads sample frequency/integration time
  sp.average = 1 ' reads samples to average
  sp.boxcar = 10 ' reads boxcar width
  sp.chan_ena(0) = 1 ' sees if each channel is enabled
  sp.chan_ena(1) = 0
  sp.chan_ena(2) = 0
  sp.chan_ena(3) = 0
  sp.scan_dark = 0 ' do not scan for dark
  sp.correct_dark = 0 ' see if correct for dark is checked
  sp.extrig = 0 ' do not external trigger

''''''''''''''''''''''''''''''''''''''''''''''''''''''''''''''''''
'''collect 10 spectra for Io for absorbance calc''''
''''''''''''''''''''''''''''''''''''''''''''''''''''''''''''''''''

      For x = 1 To 10

         MousePointer = 11
         Response = OOI_DoScan_32(sp) ' go and get the scan(s)

            For i = 30 To 80
               ref(i, x) = sp.sdat(i * 10, 0)
            Next i

      Next x

       For i = 30 To 80
         For x = 1 To 10
            ref1(i) = ref1(i) + (ref(i, x) / 10)
         Next x
       Next i
```

```
 MousePointer = 0

 '''''''''''''''''''''''''''''''''''''''''''''
 "turn pump on if checkbox is clicked on""
 '''''''''''''''''''''''''''''''''''''''''''''

 If pumpstart.Value = 1 Then
   AppActivate "pump control"
     If runnumb = 1 Then

runtime = runtime + datastart1 - datastart ' set the runtime longer for the first run by
whatever the difference in data start times is

'''''''''''''''''''''''''''''''''''''''''''''
""""  this pauses for about 5 sec,  """"
""""  after each command,           """"
"""" to allow the pump software     """"
""""  to get commands correctly     """"
'''''''''''''''''''''''''''''''''''''''''''''

pause = Now
pausetime = 0
Do While pausetime < 5
pausetime = DateDiff("s", pause, Now)
DoEvents
Loop
          SendKeys "%(od)m"

pause = Now
pausetime = 0
Do While pausetime < 5
pausetime = DateDiff("s", pause, Now)
DoEvents
Loop
         ' pause = Time
         ' Do While Time < pause + 0.0001
         ' DoEvents
         ' Loop

          SendKeys first
          SendKeys "{enter}"
```

```
pause = Now
pausetime = 0
Do While pausetime < 5
pausetime = DateDiff("s", pause, Now)
DoEvents
Loop
            ' pause = Time
            ' Do While Time < pause + 0.0001
            ' DoEvents
            ' Loop

            SendKeys "%(dt)"


''''''''''''''''''''''''''''''''''''''''''''
"""  this pauses for about 9 min      """"
"""  to allow the target pressure     """"
"""  to be reached, and make the      """"
"""  total run time close to 2 hours  """"
"""  midnight problem has been fixed ""
"""  using the datediff function    """"
"""             Mauro Aiello May 01 ""
''''''''''''''''''''''''''''''''''''''''''''
pause = Now
pausetime = 0
Do While pausetime < 540
pausetime = DateDiff("s", pause, Now)
DoEvents
Loop

'             pause = Time
 '            Do While Time < pause + 0.0063
  '           DoEvents
   '          Loop

          AppActivate "pump control"

          SendKeys "%(s){enter}"   'start the run

       Else
```

```
        SendKeys "%(od)m"
pause = Now
pausetime = 0
Do While pausetime < 5
pausetime = DateDiff("s", pause, Now)
DoEvents
Loop

'           pause = Time
 '          Do While Time < pause + 0.0001
  '         DoEvents
   '        Loop


          SendKeys methods
          SendKeys "{enter}"

pause = Now
pausetime = 0
Do While pausetime < 5
pausetime = DateDiff("s", pause, Now)
DoEvents
Loop

'           pause = Time
 '          Do While Time < pause + 0.0001
  '         DoEvents
   '        Loop

          SendKeys "%(dt)"


pause = Now
pausetime = 0
Do While pausetime < 540
pausetime = DateDiff("s", pause, Now)
DoEvents
Loop

 '          pause = Time
  '         Do While Time < pause + 0.0063
```

```
'          DoEvents
'          Loop

        AppActivate "pump control"

        SendKeys "%(s){enter}"

    End If

Beep
End If


starttime = Time
Label3.Caption = starttime

          '''''''''''''''''
          "start scanning"
          '''''''''''''''''

While stopscanning = False And n < runtime ' until user presses the stop button

  '''''''''''''''''''''''''''''''''''''''''''''''''''''
  " reset Io value when datastart time is reached "
  " datastart1 is used for the first run, since   "
  " the timing is different                       "
  '''''''''''''''''''''''''''''''''''''''''''''''''''''

If runnumb = 1 Then

  If n = datastart1 Then
     ReDim ref(30 To 80, 10)
     ReDim ref1(30 To 80)

     For y = 1 To 10
        n = n + 1
        MousePointer = 11
        Response = OOI_DoScan_32(sp) ' go and get the scan(s)

           For q = 30 To 80
              ref(q, y) = sp.sdat(q * 10, 0)
```

```
            Next q

        Next y

        For z = 30 To 80
            For w = 1 To 10
                ref1(z) = ref1(z) + (ref(z, w) / 10)
            Next w
        Next z

    End If

End If
If runnumb > 1 Then
If n = datastart Then
        ReDim ref(30 To 80, 10)
        ReDim ref1(30 To 80)

        For y = 1 To 10
            n = n + 1
            MousePointer = 11
            Response = OOI_DoScan_32(sp) ' go and get the scan(s)

                For q = 30 To 80
                    ref(q, y) = sp.sdat(q * 10, 0)
                Next q

        Next y

        For z = 30 To 80
            For w = 1 To 10
                ref1(z) = ref1(z) + (ref(z, w) / 10)
            Next w
        Next z

    End If
    End If
     MousePointer = 0

    Response = OOI_DoScan_32(sp) ' go and get the scan(s)
    If Response <> 0 Then ' if OOI_DoScan returns an error
```

```
    MsgBox ("OOI_DoScan returned " + Str(Response)) ' display error
    Exit Sub ' exit subroutine
   End If
   Call UpdateScreen 'if success, update the value(s)
   DoEvents ' check for user events
  Wend ' end continuous loop

  If pumpstart.Value = 1 Then
  AppActivate "pump control"
  SendKeys "%(o)"
  End If

  stoptime = Time
  Label4.Caption = stoptime

  btnStop.Enabled = False

''''''''''''''''''''''''''''''''''''''''''''''''''
'' output all data after the datastart time      ''
'' chosen in the initialization screen           ''
'' .txt is total absorbance                      ''
'' .ssp is absorbance for each group of 10 diodes''
''  both are comma delimited ascii text files    ''
''''''''''''''''''''''''''''''''''''''''''''''''''


outfile = Str(filenumb)

  Open "c:\chroma\" + Directoryname + "\run" + outfile + ".txt" For Output As #1
  Open "c:\chroma\" + Directoryname + "\run" + outfile + ".ssp" For Output As #2
MousePointer = 11

If runnumb = 1 Then
runtime = runtime - datastart1 + datastart ' reset the runtime to the value selected
initially

For i = datastart1 To n
  DoEvents
  Print #1, datta(i, 81)
Next i
```

```
 Close #1

   For i = datastart1 To n
      For x = 30 To 80
         Print #2, datta(i, x); ",";
      DoEvents
   Next x
Print #2,
 DoEvents
Next i

Close #2

Else

For i = datastart To n
  DoEvents
  Print #1, datta(i, 81)


Next i

  Close #1

    For i = datastart To n
       For x = 30 To 80
          Print #2, datta(i, x); ",";
       DoEvents
    Next x
Print #2,
 DoEvents
Next i

Close #2

End If
  MousePointer = 0

Next runnumb

Command3.Enabled = True
```

```
Command4.Enabled = True
pumpstart.Enabled = True

End Sub

Private Sub btnStop_Click()
  stopscanning = True ' set flag to stop continuous scanning
  runnumb = runnum
  Command4.Enabled = True
  Command3.Enabled = True
End Sub

Private Sub UpdateScreen()
Dim standdev As Single
aveg = 0
Sum = 0
n = n + 1
 For i = 30 To 80
  datta(n, i) = -Log(sp.sdat(i * 10, 0) / ref1(i)) / (Log(10))
 Next i

datta(n, 81) = 0

 For i = 30 To 80
  datta(n, 81) = (datta(n, 81) + (datta(n, i) / 51))
 Next i

  Picture1.PSet (n, datta(n, 81) + 0.1 * Val(Text1.Text) - zeroval)

For i = n - 15 To n
  aveg = aveg + (datta(i, 81) / 16)
Next i

For i = n - 15 To n
  Sum = Sum + ((datta(i, 81)) - aveg) ^ 2
Next i



 standdev = (Sum / 16) ^ 0.5
```

```
label2.Caption = standdev


labMaster.Caption = datta(n, 81)
Label1.Caption = n - 17
Label4.Caption = Time
Label5.Caption = DateDiff("s", starttime, Time)
Label6.Caption = sp.sdat(543, 0)
End Sub
Private Sub Command1_Click()
x = 1
yscal = Val(Text1.Text)
Picture1.Cls
Picture1.ScaleTop = yscal
Picture1.ScaleHeight = -yscal
Timer1.Enabled = True
Timer1.Interval = dint
Picture1.Line (0, 0.1 * yscal)-(Val(Text2.Text), 0.1 * yscal), RGB(255, 0, 0)
End Sub


Private Sub Command2_Click()
x = 1
xscal = Val(Text2.Text)
Picture1.Cls
Picture1.ScaleWidth = xscal
Timer1.Enabled = True
Timer1.Interval = dint
Picture1.Line (0, 0.1 * yscal)-(Val(Text2.Text), 0.1 * yscal), RGB(255, 0, 0)

End Sub



Private Sub exit_Click()
Unload C
End
End Sub

Private Sub Command3_Click()
Form1.Enabled = True
```

```
Form1.Visible = True
End Sub

Private Sub Command4_Click()
Unload C
End
End Sub

Private Sub Command5_Click()
Form2.Enabled = True
Form2.Visible = True
End Sub

Private Sub Command6_Click()
x = 1
Picture1.Cls
zeroval = datta(n, Int(endpixel / 10) + 1)
Picture1.Line (0, 0.1 * yscal)-(Val(Text2.Text), 0.1 * yscal), RGB(255, 0, 0)

Timer1.Enabled = True
Timer1.Interval = dint
End Sub

Private Sub Form_Load()
C.Caption = ""
dint = 976
endpixel = 800
startpixel = 300
runtime = 6350
Directoryname = "test"
runnum = 80
x = 1
datastart = 2700
datastart1 = 2700
first = "blank.flo"
methods = "cont.flo"
End Sub

Private Sub Timer1_Timer()

If x < n Then
```

```
For i = x To x + Int(dint / 10)
 If datta(i, Int(endpixel / 10 + 1)) <> 0 Then
 Picture1.PSet (i, datta(i, Int(endpixel / 10) + 1) + 0.1 * Val(Text1.Text) - zeroval)
 End If
Next i

End If
x = x + Int(dint / 10)
If x > n Then
Timer1.Enabled = False
End If
End Sub
```